

## Sustainable Life Cycles of Natural-Precursor-Derived Nanocarbons

Kateryna Bazaka,<sup>†,‡,§</sup> Mohan V. Jacob,<sup>‡</sup> and Kostya (Ken) Ostrikov<sup>\*,†,§,||</sup>

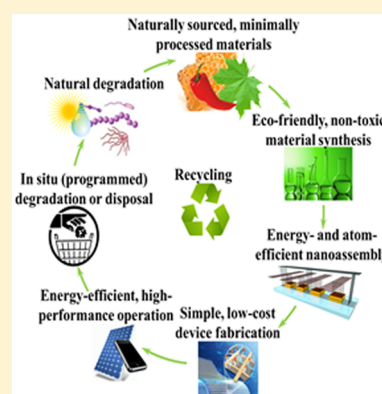
<sup>†</sup>Institute for Future Environments, School of Chemistry, Physics and Mechanical Engineering, Queensland University of Technology, Brisbane, Queensland 4000, Australia

<sup>‡</sup>Electronics Materials Lab, College of Science, Technology and Engineering, James Cook University, Townsville, Queensland 4811, Australia

<sup>§</sup>CSIRO–QUT Joint Sustainable Materials and Devices Laboratory, Commonwealth Scientific and Industrial Research Organization, P.O. Box 218, Lindfield, New South Wales 2070, Australia

<sup>||</sup>School of Physics, The University of Sydney, Sydney, New South Wales 2006, Australia

**ABSTRACT:** Sustainable societal and economic development relies on novel nanotechnologies that offer maximum efficiency at minimal environmental cost. Yet, it is very challenging to apply green chemistry approaches across the entire life cycle of nanotech products, from design and nanomaterial synthesis to utilization and disposal. Recently, novel, efficient methods based on nonequilibrium reactive plasma chemistries that minimize the process steps and dramatically reduce the use of expensive and hazardous reagents have been applied to low-cost natural and waste sources to produce value-added nanomaterials with a wide range of applications. This review discusses the distinctive effects of nonequilibrium reactive chemistries and how these effects can aid and advance the integration of sustainable chemistry into each stage of nanotech product life. Examples of the use of enabling plasma-based technologies in sustainable production and degradation of nanotech products are discussed—from selection of precursors derived from natural resources and their conversion into functional building units, to methods for green synthesis of useful naturally degradable carbon-based nanomaterials, to device operation and eventual disintegration into naturally degradable yet potentially reusable byproducts.



### CONTENTS

1. Introduction	164	7. Controlling Surface Organization of Nanostructures: Case of CNTs	184
1.1. Article Rationale and Focus	167	8. Effect of Precursor Chemistry on CNT Synthesis	187
1.1.1. Focus on Zero-, One-, and Two-Dimensional Carbon Nanomaterials	167	9. CNT Synthesis Using Raw Materials	188
1.1.2. Focus on Process-Driven Synthesis	168	9.1. Coal	188
1.1.3. Focus on Plasma-Enabled Process-Driven Synthesis	168	9.2. Natural Gas	189
1.2. Article Organization	168	9.3. Deoiled Asphalt	189
1.3. Article Scope	169	9.4. Carbon from Biomass	189
2. Salient Features of Plasma Processing	170	9.5. Waste Materials	190
2.1. Green Chemistry Attributes	170	10. Natural-Product-Derived Catalysts and Supports	190
2.2. Chemical Reactivity of Plasma Environment	171	11. Precursor-Driven Synthesis: Organic Polymers and Small Molecules	191
3. Plasma-Enabled Fast Processing: The Case of Carbon Nanodots	174	11.1. Natural Semiconducting and Electrode Materials	193
4. Plasma-Enabled Reduced-Temperature Graphene Synthesis	174	11.2. Low-Cost Synthetic Semiconductors	193
5. Plasma-Enabled Process-Driven Synthesis: The Case of Graphenes	177	11.3. Dielectric, Encapsulation, and Substrate Materials	194
5.1. Continuous Substrate- and Catalyst-Free Synthesis of Freestanding Graphenes	177	12. Plasma-Enabled Precursor-Driven Synthesis: Organic Polymer Films	194
5.2. Nonprecursor-Specific Synthesis of Surface-Supported Graphenes	179	13. Naturally Degradable Devices	197
5.3. Intentional Defect Creation and Functionalization	180	14. Natural Degradation of 1D, 2D, and Hybrid Nanostructures	198
6. Synthesis of 3D and Hybrid Nanostructures	181	15. Plasma-Enabled Degradation of Materials	200

Received: September 24, 2015

Published: December 30, 2015

16. Conclusion and Perspectives	201
Author Information	202
Corresponding Author	202
Notes	202
Biographies	202
Acknowledgments	202
References	202

## 1. INTRODUCTION

Recent times have seen a significant penetration of nanotechnology, including nanofabrication, nanoscale processing, and nanomaterials, leading to substantial advances in diverse fields spanning from health care and medicine to agriculture and manufacturing. Nanomaterials and nanoscale processing have become the cornerstone of modern low-cost high-tech devices and a key enabler for device miniaturization and the ever-increasing scale of integration, where novel materials synthesis, inspection and metrology capabilities, and device patterning techniques advance device scaling. Indeed, presently available silicon electronics offers a good combination of performance, stability in applications, and low cost.<sup>1</sup> Some of these devices consume less energy than their predecessors and can be used to produce energy in a more environmentally friendly manner.

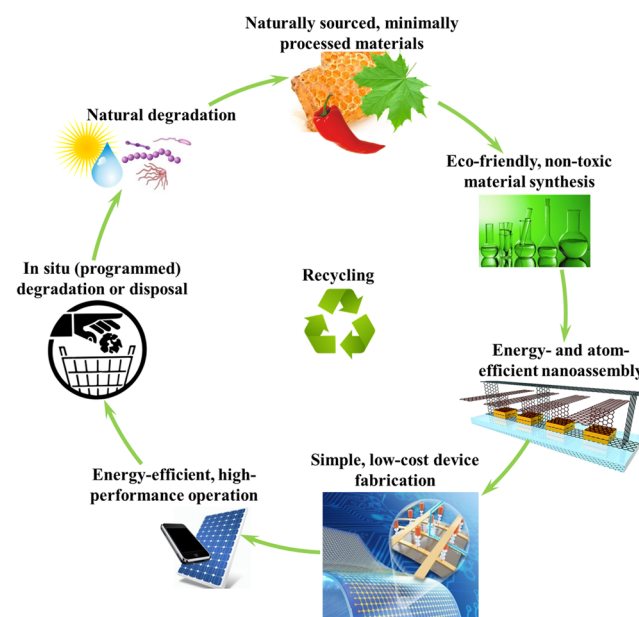
However, operating at nanoscale comes at a cost. Properties that arise at nanoscale are sensitive to the presence of defects, be it chemical impurities within the material, thickness variation or the presence of pinholes across the thin film, or the quality of the interface between the device layers.<sup>2</sup> Such precision requires large energy expenditure and the use of highly purified, often toxic precursors. Using exceedingly integrated nanoscale materials also makes traditional recycling virtually impossible, as more complex, expensive, and resource-consuming processes are required to decompose or extract specific chemicals and/or components. Designed to maintain stability over time and under varied environmental conditions, most nanomaterials and nanodevices do not degrade readily in the landfill or require postprocessing to initiate their decomposition.

Yet, in nature, abundant, renewable carbon-based molecules can be organized into highly complex, efficient molecular and nanoscale assemblies that amply perform their designated function and then naturally degrade into basic units that can be reorganized into a new structure. While at this stage it may not be possible to match the natural world in sophistication, it is nonetheless reasonable to attempt to imitate its guiding principles: (i) the cyclic approach to resource utilization; (ii) energy and material efficiency across the product life cycle; (iii) sustainability, whereby present and future needs are met with minimal harm to the environment or human health. The principles of *green chemistry* and *green engineering* broadly reflect these ideas and provide practical guidance on how nature-inspired sustainable life cycles may be integrated into modern technology.<sup>3–5</sup> Defined by Anastas and Warner,<sup>3,6</sup> the 12 principles of green chemistry focus on atom economy, safer chemical syntheses and chemicals, preferably through utilization of raw, renewable material sources, energy and process efficiency, and waste prevention by minimizing unnecessary derivatization and by designing inherently degradable materials.

These concepts have also been at the foundation of a transformational United Nations' 2030 Agenda for Sustainable Development adopted in September 2015, where one of the key goals and targets is to protect the planet from degradation

while ensuring prosperity.<sup>7</sup> Implied in the Agenda is the necessity to drastically change the way in which companies do business, with an emphasis on respectful treatment of nature and shared responsibility. Central to this approach is corporate transformation led by the integration of ecological, social, and economic values into every strategy, product development, or business model. Indeed, the Agenda explicitly points to integral thinking as the principle enabler for global sustainable development, which echoes the holistic approach to product design discussed in this review. Even more specifically, the Agenda places an important emphasis on green energy, pollution reduction, use of renewable resources, and biological degradability of goods sold to the consumer. While sustainability thinking that permeates through the corporate value chain may necessitate significant innovation in each stage of product life cycle and some investment, the costs are likely to be offset by new product and market opportunities, and financial gains from more efficient operation models.

Figure 1 conceptualizes potential application of green chemistry principles and sustainable resource utilization in

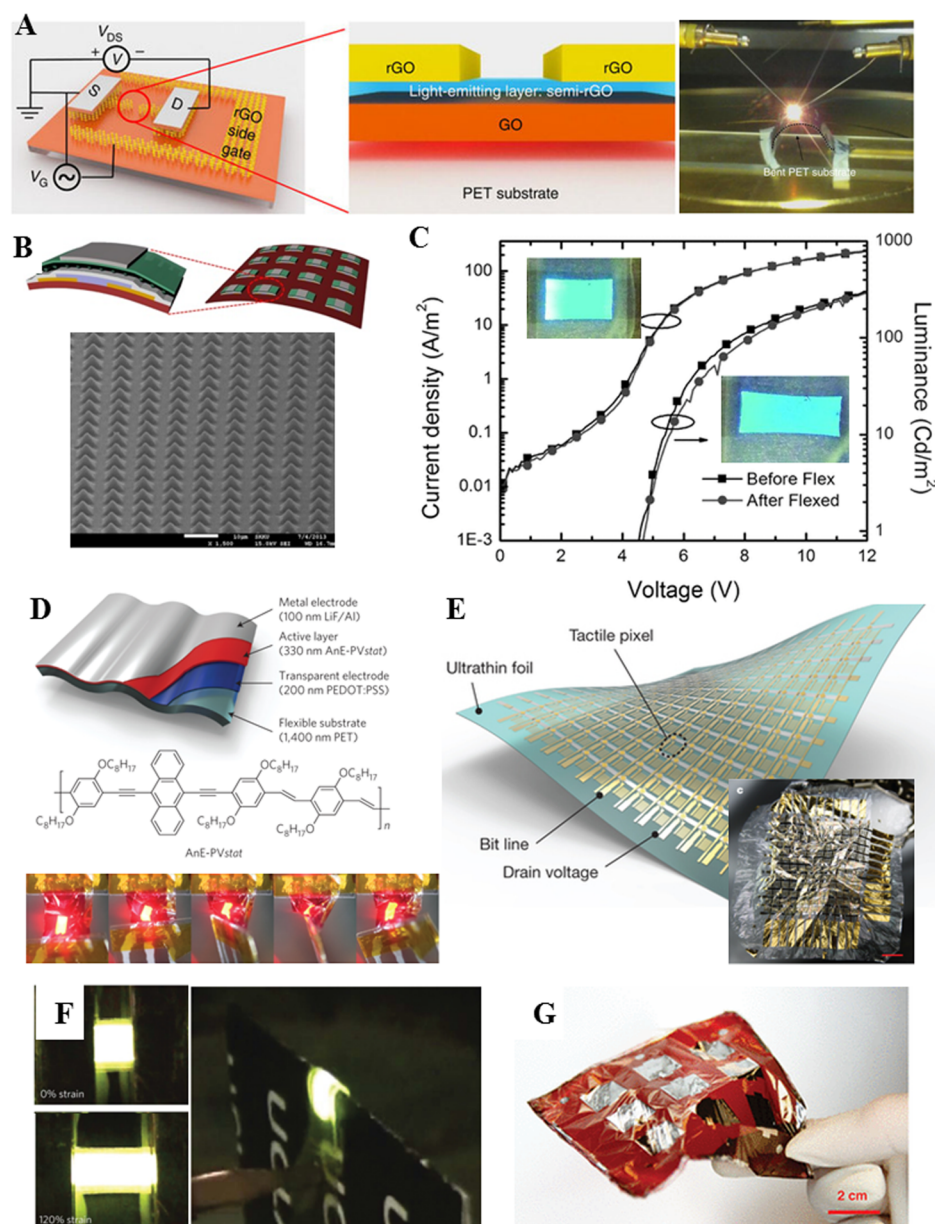


**Figure 1.** Sustainable life cycles of carbon-based devices for electronics and energy applications.

high-tech devices, with communication devices and energy harvesting taken as representative examples. Readily available low-value materials are converted into functional nanomaterials using facile chemical processes that use and generate minimal amounts of hazardous substances. Energy- and atom-efficient processing is then used to assemble and integrate these natural-product-based nanomaterials into electronic devices. At the end of their operational lifespan, the devices are either programmed to decompose in situ or naturally degrade in a landfill, or they can be disintegrated into useful precursors and recycled.

In practice, identifying *materials* that would enable the development of electronic devices that are high-performing, affordable, and sustainable at every stage of their life cycles remains a significant challenge. Currently available high-performance silicon-based electronic devices use a wide variety of expensive, potentially hazardous, highly purified, non-renewable materials, such as rare earth elements, indium,





**Figure 2.** Examples of carbon-based devices, such as stretchable light emitting diodes, displays, and organic solar cells for use in soft robotics. (A) Flexible, all-graphene-based field-effect light emitting diode (LED) on a poly(ethylene terephthalate) (PET) substrate has a bright spectrally tunable electroluminescence from blue ( $\sim 450$  nm) to red ( $\sim 750$  nm). LED size is  $100 \times 100 \mu\text{m}$ ; bending radius is  $\sim 8$  mm. (B) A highly sensitive, pressure-responsive organic field-effect transistor array enabling both rapidly and slowly adapting mechanoreceptors in electronic skin is fabricated from easily deformable, mechanoelectrically coupled, microstructured poly(vinylidene fluoride–trifluoroethylene) ferroelectric gate dielectrics and an pentacene semiconductor channel. (C) LED based on single-walled carbon nanotube–polymer composite electrodes can be linearly stretched up to 45% strain. (D) Freestanding ultrathin polymer LED continue operating as they become crumpled (simultaneously compressed and twisted by  $90^\circ$ ). (E) Thin large-area active-matrix sensor platform ( $12 \times 12$  tactile pixels) that is extremely lightweight ( $3 \text{ g m}^{-2}$ ) and ultraflexible. (F) All-solution-processed elastomeric polymer LED continues to emit light at strains of 120%, e.g. when bent over a sheet of cardboard. (G) Ultralightweight sub- $2\text{-}\mu\text{m}$ -thick organic solar cell with specific weight of  $10 \text{ W/g}$ . Panel A reprinted with permission from ref 23. Copyright 2015 Nature Publishing Group. Panel B reprinted with permission from ref 24. Copyright 2015 Macmillan Publishers Ltd. Panel C reprinted with permission from ref 25. Copyright 2011 Wiley-VCH Verlag GmbH & Co. KGaA. Panel D reprinted with permission from ref 26. Copyright 2013 Nature Publishing Group. Panel F reprinted with permission from ref 27. Copyright 2013 Nature Publishing Group. Panel E reprinted with permission from ref 28. Copyright 2013 Nature Publishing Group. Panel G reprinted with permission from ref 29. Copyright 2013 IEEE.

tantalum,<sup>8</sup> and precursor gases, such as flammable toxic silane ( $\text{SiH}_4$ ), that are derived as a result of a complex, multistage and multienvironment processing. The processing and assembly of device components typically require specific production environments (e.g., high temperature and/or low pressure), significant material (as precursors, catalysts, and auxiliary

substances), water and energy input (to drive the reaction and/or maintain the processing environment), and the use of hazardous auxiliary substances, such as organic solvents and catalysts.<sup>9,10</sup>

Carbon-based nanomaterials, such as organic polymer films, carbon nanotubes, and graphene, have been actively researched

as a more sustainable alternative to inorganic materials and nanostructures.<sup>11</sup> Abundant and chemically diverse, carbon precursors can generally be converted into functional nanomaterials using less energy and at lower cost, with the energy required to produce a high-quality plastic being up to 6 orders of magnitude smaller than that needed to manufacture similar-quality inorganic structures.<sup>9</sup> Postuse, many types of carbon-based materials break down naturally or can be processed to become more readily degradable;<sup>12–15</sup> they can also be reformed into lower-value products<sup>16,17</sup> or become a source of energy.<sup>18</sup>

In terms of their utility in miniaturized devices, carbon-based materials can reversibly withstand extreme mechanical deformation (due to relatively weak bonding between organic molecules), have very low weight, and have large-area coverage.<sup>19,20</sup> These attributes make carbon-based sensors, lighting, displays, and photovoltaics well-suited to the development of soft robots, where amenities for sensing and actuation, data storage, processing and communication, and power generation and storage need to be integrated in the soft materials with compliance that is similar to that of soft biological tissues.<sup>21</sup> The shape-shifting behavior of soft robots prevents the use of most conventional sensing devices; encoders, metal or semiconductor strain gauges, inertial measurement units, and even commercially available piezoelectric-polymer-based bendable sensors fail to meet the requirement of being both bendable and stretchable.<sup>21</sup>

Examples of electronic skin, textiles, and surface conforming foils are presented in Figure 2.<sup>22–29</sup> These devices can be fabricated at low cost using most high-throughput industrial methods, such as inkjet or offset printing, as well as conventional semiconducting processing techniques.<sup>30</sup>

However, many of the currently produced carbon-based materials are nondegradable under mild conditions, presenting a significant waste management and ecological issue.<sup>31</sup> The performance of devices assembled from minimally processed carbon materials using high-throughput methods is lower compared to silicon-based electronics. Conversely, high-quality carbon-based materials are typically produced by multistep processing and/or derivatization of nonrenewable, e.g., petrochemical resources using methods that are complex and energy-demanding, as well as consume and produce hazardous substances. Furthermore, the quantities of electronics-grade carbon nanomaterials that can be produced at present are low. Although significant efforts are devoted to this area of research, it is unlikely that in the near future carbon electronics will achieve the necessary performance or scale to represent a competitive disruptive technology compared to silicon-based electronics; rather, it may be useful for some niche electronic applications.

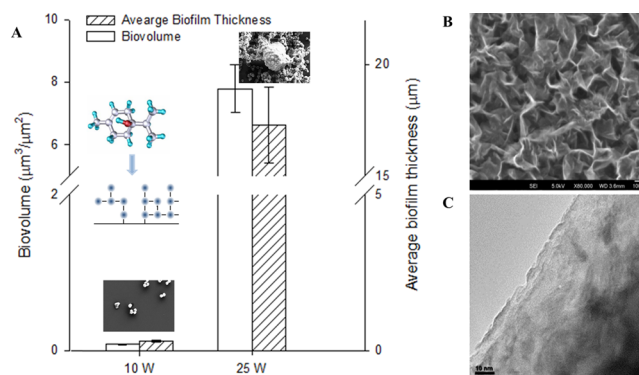
There are a number of promising *processing environments and chemistries* that have the potential to enable simpler, greener synthesis and assembly of carbon materials with the desired properties and level of quality on an industrially relevant scale. Some examples include Leidenfrost drop synthesis for synthesis of porous nanostructures,<sup>32</sup> reversible addition–fragmentation chain-transfer polymerization,<sup>33,34</sup> enzymatic polymer synthesis,<sup>35</sup> low-temperature hydrothermal treatment for synthesis of nanodots,<sup>36</sup> plasma synthesis of nanotubes,<sup>37</sup> biosynthesis of nanoparticles,<sup>38</sup> and many others.

These methods offer a variety of notable benefits over conventional methods of synthesis. However, they are often restrictive with regard to the chemistry and the physical state of

the carbon source. Yet, most raw carbon materials are composed of multiple chemistries with the relative compositions that may vary from batch to batch. Process- and environment-driven synthesis routes, where the nature of the process (more so than precursor chemistry) governs the inherent features of the nanomaterials produced may be more appropriate for the conversion of raw mixed carbon sources.

Low-temperature nonequilibrium plasmas have been demonstrated to afford the level of chemical reactivity and precision necessary to convert organic precursors of different chemical compositions and states into diverse nanomaterials. The plasma environment acts as a catalyst by enabling the new and accelerating the existing reactions or by lowering the energy thresholds (e.g., process temperature) required to initiate and maintain the reactions in both gas and liquid phases.<sup>39–42</sup> Although plasma catalysis is outside the scope of this review, further information about the underlying mechanisms governing the use of plasma as a catalyst in conversion, reforming, synthesis, and degradation of materials can be found in a recent review by Neyts and colleagues, and other relevant works.<sup>41,43,44</sup>

The plasma processing environment is flexible, and it can facilitate a range of synthesis mechanisms, from *precursor-driven* synthesis to *process-driven* synthesis.<sup>42,45,46</sup> At lower energy doses per precursor molecule, the conditions are more conducive to the survival of the original monomer structure in the final product (Figure 3A).<sup>46–48</sup> This can best be



**Figure 3.** Plasma synthesis outcomes are directly affected by the amount of energy that is transferred from the plasma to the precursor and the residence time of the precursor in the plasma. (A) Under low-power conditions (10 W), rf plasma processing of natural essential oil results in the formation of a polymer structure that retains some of the original chemistry and biological activity of terpinen-4-ol. Increasing the power delivered to the reactor from 10 to 25 W results in a complete loss of antibacterial activity characteristic of the monomer. (B, C) Increasing input rf energy to 500 W results in the breakdown of the precursor into smaller molecular, radical, and atomic fragments and its rebuilding into vertically oriented graphene, as confirmed by SEM (B) and TEM (C).<sup>42</sup> Panel A reprinted from ref 46. Copyright 2010 American Chemical Society. Panel A (inset) reprinted with permission from ref 45. Copyright 2011 Elsevier Ltd. Panels B and C reprinted from ref 42. Copyright 2015 American Chemical Society.

observed in lower-power plasmas operated in a pulsed mode, where short (a few microseconds) plasma discharges deliver sufficient energy to generate radicals that can then recombine into a polymer via chemical radical chain reactions during millisecond-long plasma-free periods.<sup>49–51</sup> The resultant materials retain some of the properties of the monomer, such as desirable chemical or biological activity, and electrical and

**Table 1. Molecular Bond Dissociation Energies for  $\text{RH} \rightarrow \text{R} + \text{H}$ : Experimental Bond Enthalpies and Radical Heats of Formation at 298 K (Reprinted from ref 52. Copyright 2003 American Chemical Society.)**

molecule	$\text{DH}_{298}$ (kcal mol <sup>-1</sup> )	$\Delta_f H_{298}(\text{R})$ (kcal mol <sup>-1</sup> )	molecule	$\text{DH}_{298}$ (kcal mol <sup>-1</sup> )	$\Delta_f H_{298}(\text{R})$ (kcal mol <sup>-1</sup> )
Inorganics					
$\text{H}_2$	104.2 ± 0.0	52.1 ± 0.0	$\text{OH}^- \rightarrow \text{O}^- + \text{H}$	110.2 ± 0.1	-33.2 ± 0.1
HF	136.3 ± 0.0	18.8 ± 0.2	$\text{OH}^+ \rightarrow \text{O} + \text{H}^+$	115.2 ± 0.1	59.6 ± 0.0
HCl	103.2 ± 0.0	29.0 ± 0.0	$\text{H}_2\text{S}$	91.2 ± 0.1	34.2 ± 0.2
HBr	87.5 ± 0.1	28.6 ± 0.1	SH	84.1 ± 0.2	66.2 ± 0.3
HI	71.3 ± 0.1	26.0 ± 0.1	H-NO	49.5 ± 0.7	21.8 ± 0.1
H-CN	126.3 ± 0.2	105.0 ± 0.7	H-ONO (trans)	79.1 ± 0.2	8.2 ± 0.1
$\text{NH}_3$	107.6 ± 0.1	44.5 ± 0.1	H-ONO <sub>2</sub>	101.7 ± 0.4	17.6 ± 0.3
$\text{H}_2\text{O}$	118.8 ± 0.1	8.9 ± 0.1	$\text{SiH}_4$	91.7 ± 0.5	47.9 ± 0.6
OH	101.8 ± 0.1	59.6 ± 0.0	$\text{GeH}_4$	83.0 ± 2.0	53.0 ± 2.0
Hydrocarbons					
$\text{CH}_4$	105.0 ± 0.0	35.1 ± 0.1	$\text{CH}_2\text{CH-H}$	110.7 ± 0.6	71.1 ± 0.7
$\text{CH}_3$	110.4 ± 0.2	93.3 ± 0.2	HCC-H	133.3 ± 0.1	135.6 ± 0.2
$\text{CH}_2$	101.3 ± 0.3	142.5 ± 0.2	$\text{C}_6\text{H}_5\text{-H}$	112.9 ± 0.5	80.5 ± 0.5
CH	80.9 ± 0.2	171.3 ± 0.1	$\text{C}_6\text{H}_5 \rightarrow o\text{-C}_6\text{H}_4 + \text{H}$	78.0 ± 3.0	106.0 ± 3.0
$\text{CH}_3\text{CH}_2\text{-H}$	101.1 ± 0.4	29.0 ± 0.4	$\text{C}_6\text{H}_5 \rightarrow m\text{-C}_6\text{H}_4 + \text{H}$	94.0 ± 3.0	122.0 ± 3.0
$(\text{CH}_3)_2\text{CH-H}$	98.6 ± 0.4	21.5 ± 0.4	$\text{C}_6\text{H}_5 \rightarrow p\text{-C}_6\text{H}_4 + \text{H}$	109.0 ± 3.0	138.0 ± 3.0
$\text{CH}_3\text{CH}_2(\text{CH}_3)\text{CH-H}$	98.2 ± 0.5	16.1 ± 0.5	$\text{CH}_2\text{CHCH}_2\text{-H}$	88.8 ± 0.4	41.4 ± 0.4
$(\text{CH}_3)_3\text{C-H}$	96.5 ± 0.4	12.3 ± 0.4	$\text{C}_6\text{H}_5\text{CH}_2\text{-H}$	89.8 ± 0.6	49.7 ± 0.6
Alcohols					
H-CH <sub>2</sub> OH	96.1 ± 0.2	-4.08 ± 0.2	$\text{CH}_3\text{CH}_2\text{O-H}$	104.7 ± 0.8	-3.6 ± 0.8
$\text{CH}_3\text{O-H}$	104.6 ± 0.7	4.3 ± 0.7	$(\text{CH}_3)_2\text{CHO-H}$	105.7 ± 0.7	-11.5 ± 0.7
$\text{CH}_3\text{S-H}$	87.4 ± 0.5	29.8 ± 0.4	$(\text{CH}_3)_3\text{CO-H}$	106.3 ± 0.7	-20.5 ± 0.7
H-CH <sub>2</sub> SH	94.0 ± 2.0	36.0 ± 2.0	$\text{C}_6\text{H}_5\text{O-H}$	90.0 ± 3.0	-58.0 ± 3.0
Peroxides					
HOO-H	87.8 ± 0.5	3.2 ± 0.5	$\text{CH}_3\text{CH}_2\text{OO-H}$	85.0 ± 2.0	-6.8 ± 2.3
$\text{CH}_3\text{OO-H}$	88.0 ± 1.0	4.8 ± 1.2	$(\text{CH}_3)_3\text{COO-H}$	84.0 ± 2.0	-25.2 ± 2.3
Carbonyls					
H-CHO	88.1 ± 0.0	10.1 ± 0.1	H-COOH	≥96.0 ± 1.0	-46.5 ± 0.7
$\text{CH}_3\text{C(O)-H}$	89.4 ± 0.3	-2.4 ± 0.3	$\text{CH}_3\text{COO-H}$	112.0 ± 3.0	-43.0 ± 3.0
H-CH <sub>2</sub> CHO	94.0 ± 2.0	2.5 ± 2.2	$\text{C}_6\text{H}_5\text{COO-H}$	111.0 ± 4.0	-12.0 ± 4.0
HCOO-H	112.0 ± 3.0	-30.0 ± 3.0			

optical characteristics, yet acquire new attributes due to the plasma-driven polymerization. Here, the original chemistry of the precursor largely determines the synthesis pathways and the chemistry of the final nanostructures. Table 1 shows experimentally determined bond enthalpies for a range of organic and inorganic materials.<sup>52</sup> While typical enthalpy values range from 60 to 130 kcal mol<sup>-1</sup>, the bond enthalpy can be affected considerably by the cleavage of ancillary bonds within the molecule, such as the case in reactions where multiple bonds are broken.

When the energy transferred from the plasma greatly exceeds the energy required to dissociate specific bonds in the precursor molecule, even brief exposure of the precursor to the plasma, i.e. very short residence time, results in almost complete monomer dissociation and fragmentation into atoms and smaller molecular and radical fragments. The dissociation is made possible by the comparatively high energy density of plasmas, i.e. high concentration of energy, which leads to highly reactive chemistries, such as energetic charged species and neutral species in excited and metastable states.<sup>53</sup> These fragments and atoms are then rebuilt in a guided fashion into nanostructures that are physicochemically and functionally distinct from the original precursor (Figure 3B). Both the degree of dissociation and subsequent reassembly and organization of the newly created structure are guided by the attributes of the processing environment. Vertically oriented

graphene sheets fabricated from different monomers using low-temperature plasmas demonstrate very similar chemical and physical characteristics regardless of the chemistry of the carbon precursor.<sup>54–56</sup> Here, the processing parameters more so than the chemistry/state of the carbon source define the properties of the final nanostructure; hence the synthesis outcome is largely process-driven.

### 1.1. Article Rationale and Focus

The aim of this article is to critically review recent developments in green nanofabrication that have the potential to facilitate sustainable life cycles of carbon-based electronics and energy devices, focusing specifically on three aspects of the cycle: (i) low and negative value materials; (ii) green synthesis; and (iii) degradation pathways.

**1.1.1. Focus on Zero-, One-, and Two-Dimensional Carbon Nanomaterials.** Carbon forms a basis for the chemistry of life and is abundant in all living systems. For thousands of years, humanity has benefited from a wide range of carbon-based materials, transforming them into a variety of useful products. Carbon itself can take many forms via its different degrees of hybridization (sp, sp<sup>2</sup>, and sp<sup>3</sup>),<sup>57</sup> giving rise to many allotropes, each with a unique and useful set of properties. While the applications for graphite, diamond, and amorphous carbon are well-established, relatively newly discovered buckminsterfullerenes,<sup>58</sup> graphene,<sup>59</sup> nanotubes,<sup>60</sup> nanobuds,<sup>61</sup> nanofibers, lonsdaleite, glassy carbon, carbon



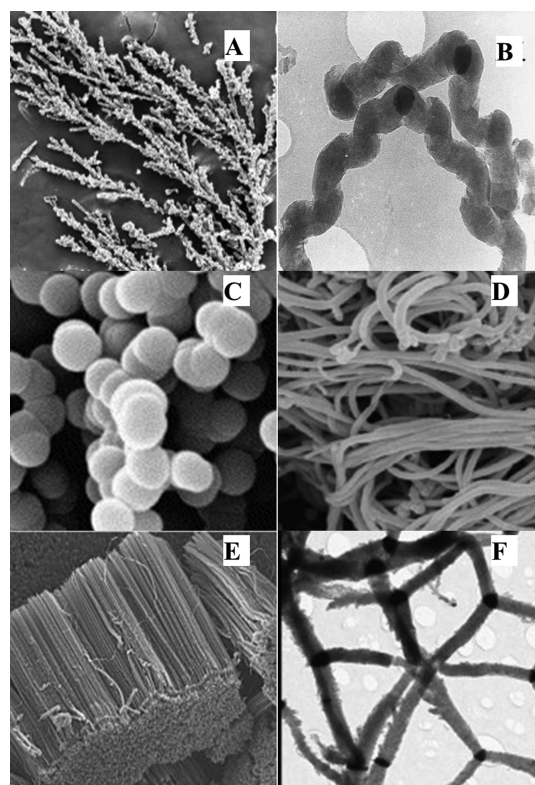
nanof foam,<sup>62</sup> carbide, and some others are yet to reach their full potential in materials science, electronics, and nanotechnology. However, since these materials hold promise in the development of sustainable advanced technologies, their green synthesis will be a focus of this paper.

**1.1.2. Focus on Process-Driven Synthesis.** As briefly discussed in the [Introduction](#), one of the major challenges in integrating these carbon materials into commercially viable products is the cost–quality trade-off: for nanostructures to display their unique and valuable features reliably, they need to be fabricated from high-quality (chemically pure, homogeneous, extensively processed, and often modified) input materials using complex, time- and energy-consuming processing techniques. A closely related issue is the quality–quantity trade-off: nanomaterials produced at the industrially relevant level of throughput do not always display the same level of quality as their lab-scale counterparts because it is difficult to retain the same level of structural quality upon scale-up.

The cost–quality trade-off is a key issue in using raw and waste products because their chemical composition is both complex and difficult to control. While a wide range of synthetic and natural products, e.g. hydrocarbons (saturated, unsaturated, substituted, etc.), polymers (polyethylene, polypropylene, etc.) and natural products (oils, plant fibers) can be successfully converted into a range of carbon nanostructure morphologies ([Figure 4](#)),<sup>63–68</sup> the process of conversion and the resultant product may be more controllable and predictable in the case of simple hydrocarbon sources. The C/H ratio, chemical functionality, structure, and physical attributes of the carbon precursor significantly affect the chemistry and morphology of the resultant nanomaterials.<sup>69</sup> Indeed, in the vast majority of cases the chemistry of the monomer determines both the synthesis method used and the properties of the nanostructures produced (precursor-driven synthesis). [Table 2](#) shows that, even when chemically homogeneous monomers are used, the yield and morphology of nanostructures is affected by the monomer chemistry.<sup>69,70</sup>

While this approach may work well for the synthesis of structures where the chemistry of the carbon source is desirable and to be retained, such as in the case of conducting and semiconducting pigment-based and insulating DNA-based films, it may not suit large-scale reforming of mixed carbon waste into regular nanostructures. Hence, in this article we will primarily focus on processing environments where the characteristics of the process and not the chemistry of the monomer primarily determine the properties of the resultant nanostructures (process-driven synthesis).

**1.1.3. Focus on Plasma-Enabled Process-Driven Synthesis.** Reactive plasma is a process environment that can be controlled to deliver a variety of synthesis outcomes: from largely precursor-driven plasma-enhanced polymerization to virtually precursor-independent process-driven synthesis of graphene-based nanomaterials. Plasma processing also gives rise to unique features that may not be attainable using other methods. This “indiscriminate” nature of some plasma environments with respect to precursor chemistry may help address the cost–quality challenge of green nanofabrication. When used alone or in conjunction with other processes, the catalytic effect of plasmas may also deliver significant environmental and economic benefits, potentially moving toward a solution for the quality–quantity challenge. Hence, this review will use focused examples of the role of the synergy between unique nonequilibrium plasma-enabled chemistry and



**Figure 4.** Examples of different morphologies of carbon nanostructures produced from various carbon sources. (A) Tree-like structures from camphor. (B) Helical fibers from 1,3-butadiene. (C) Spheres from toluene. (D) Tubes and fibers from polypropylene. (E) Aligned CNTs from palm oil. (F) Tripod-like carbon nanofibers from trichloroethylene. Panel A reprinted with permission from ref 63. Copyright 2009 Elsevier Ltd. Panel B reprinted with permission from ref 64. Copyright 2000 Elsevier Ltd. Panel C reprinted with permission from ref 65. Copyright 2005 Elsevier Ltd. Panel D reprinted with permission from ref 66. Copyright 2010 Elsevier Ltd. Panel E reprinted with permission from ref 67. Copyright 2009 Elsevier Ltd. Panel F reprinted with permission from ref 68. Copyright 2012 Elsevier Ltd.

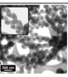
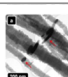
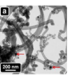
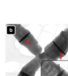


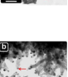
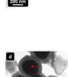
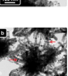

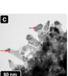
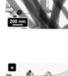


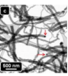

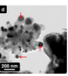
minimally processed renewable resources in the development of carbon-based devices. We will also discuss how these synergies can help in realizing the sustainable product life cycle of the carbon-based nanomaterials.

## 1.2. Article Organization

This article is divided into two parts. The first part opens with [section 2](#), where a brief summary of the plasma attributes and plasma-specific chemical and physical effects that are particularly relevant to sustainable material synthesis and assembly is provided. [Sections 3–12](#) are dedicated to the synthesis of nanomaterials from environmentally sustainable carbon-based precursors, including renewable products, unprocessed fossil fuels, and waste carbon materials. Each section centers on a particular attribute of natural product conversion, which is discussed as a case study focused on specific materials and their microstructures. Cases for precursor-driven and process-driven processes are presented.

Each case begins with a brief description of the nanomaterial, its most desirable attributes and applications, and green processes and precursors most frequently used in the synthesis. The effects of precursor chemistry and state on the properties, assembly, and yield of these materials are emphasized. Potential

**Table 2.** Effect of Chemistry of Carbon Source on Nanostructure Yield and Morphology (Adapted and reprinted with permission from ref 69. Copyright 2012 Elsevier Ltd.)

Alkynes	Yield (%)	Morphology				Alkynes	Yield (%)	Morphology			
		Type of fiber	Growth mode	Diameter (mm)	SEM image			Type of fiber	Growth mode	Diameter (mm)	SEM image
Acetylene	20	Helical	Bidirectional	Helices: 50–100, straight fiber: 100–150		3-Chloroprop-1-yne	13	Solid carbon fibers with roughened edges	Bidirectional	150–220	
2-Butyne	12	Helical, straight, amorphous	Bidirectional, tip growth	Helices: 100–150, straight fibers: 100–200		1-Propyne-3-ol	5	Striated fibers, with tapered ends	Bidirectional	200	
1-Pentyne	7	Small length fibers, and larger more ordered fibers	Tip growth (smaller fibers), bidirectional growth (larger fibers)	50–70 and 100–200		Prop-2-yn-1-amine	2	Stubby fibers	Tip growth	40–80	
2-Pentyne	4	Small length amorphous-like fibers	Tip growth	30–50		3-Bromoprop-1-yne	<1	Fibers, spheres and encapsulated catalyst particles	Tip growth	Variable	
1-Hexyne	9	Straight fibers	Bidirectional	100–150		Ethynyl thiophene <sup>a</sup> , acetylene	9	Straight fibers	Bidirectional	100–150	
2-Hexyne	2	Stubby fibers, with some amorphous carbon deposits	Tip growth	15–35		Ethynyl aniline <sup>a</sup> , acetylene	4	Rough, unstructured carbon fibers	Tip growth	70–150	
3-Hexyne	<1	Amorphous carbon deposits	–	–		Trimethylsilyl acetylene <sup>a</sup> , acetylene	8	Helical, straight, Y-shaped (dominant) fibers	Bidirectional and tri-directional growth	50–150 and 350–500	
1-Heptyne	11	Straight fibers, stacked-like, roughened edges	Bidirectional, tip growth	100–150		Methyl prop-2-ynoate	13	Striated fibers	Bidirectional	200–400	
1-Octyne	<1	No fiber growth, catalyst covered with carbon deposits	–	Variable 20–250							

<sup>a</sup>Used for pretreatment of catalyst only; fibers grown for acetylene after pretreatment.

advantages stemming from the use of plasma-enhanced or plasma-enabled processing in controlled reforming of natural resources into materials intended for electronics and energy applications are then discussed.

The second part of this paper (sections 13–15) introduces potential degradation pathways for carbon-based nanomaterials individually and when integrated into complex devices. This part first gives examples of materials and devices that have been designed to undergo natural degradation under mild degradation conditions into benign degradation products. The section then discusses some mechanisms of natural degradation of one- and two-dimensional carbon nanostructures, and how the knowledge of these mechanisms may be used to design more readily degradable carbon nanomaterials. The plasma environment is discussed as the means to facilitate natural degradation (via modification during the material synthesis stage or postuse treatment) or to decompose the materials into useful building blocks for the synthesis of other functional nanomaterials.

Section 16 concludes the review with the summary of the guiding principles of sustainable product life cycle, and the implications of these principles for enabling technologies used to realize these products. While this paper emphasizes the unique and attractive features of low-temperature plasma environments as the enabling chemistry for the conversion of minimally processed renewable resources into functional

nanomaterials, there are other reactive chemistries that can lead to distinct process-driven (largely precursor-independent) synthesis processes. There are also other non-carbon-based minimally processed abundant low-cost resources that comply with the general principles of the sustainable product life cycle. A brief outlook for the future research in this field concludes this review.

### 1.3. Article Scope

This article provides a broad coverage of the types of nanomaterials that can be produced from carbon-based resources, with a focus on using minimally processed, nontoxic carbon precursors that are abundant and easily isolated from the environment. However, given the very large number of examples of natural precursors and the dielectric, semi-conducting, and conducting nanomaterials in all dimensionalities that can be produced from these precursors, only a relatively small number of focused examples are presented. Similarly, even though there are a vast number of diverse reactive chemistries and synthesis techniques, this review focuses on reactive plasma chemistry in its capacity as a stand-alone unique synthesis process and as a catalyst for the established synthesis reactions.

## 2. SALIENT FEATURES OF PLASMA PROCESSING

Without trying to give an exhaustive review of the properties and attributes of plasma environments and plasma-enabled processing, this section will explain how plasmas can help facilitate low-cost and green synthesis of functional carbon nanostructures from environmentally sustainable carbon-based precursors. It will begin with a statement of the plasma attributes, plasma-specific chemical and physical effects, and process controls that are particularly relevant to sustainable material synthesis and assembly. This will be followed by a more in-depth look at the plasma reactivity as an enabler in the synthesis of nanocarbon materials.

### 2.1. Green Chemistry Attributes

Plasma processing can be used to process and reform matter in liquid, gaseous, and solid states regardless of the chemistry of the material and whether it is chemically pure or a mixed source.<sup>46,55,56,71</sup> This makes plasma processing a promising route for conversion of *low-value raw and waste* carbon-containing materials into value-added industrially viable products. The ability to directly use minimally processed materials *reduces derivatization* and workup chemistry and limits the use of associated auxiliary substances, such as solvents and separation agents, typically associated with other methods of nanoscale synthesis and processing.<sup>71,72</sup>

Plasma processing is one of the cornerstones of silicon semiconductor microfabrication, where it is used for controlled deposition and removal of material.<sup>53,73,74</sup> Being a mature technology, plasma systems are *economically feasible*, easy to scale-up and integrate into existing manufacturing workflow.<sup>75</sup>

Plasma environments are rich in energetic and chemically reactive species that uniquely contribute to dissociation, reforming, and organization of materials.<sup>53</sup> These include electrons, charged species, i.e. ions, photons, and neutral species, i.e. reactive radicals, unfragmented molecules, as well as metastable and excited species.<sup>76</sup> The temperature and chemical reactivity of the plasma species can be very different from one species to another, and dense fluxes of the desired species can be delivered in a controlled manner.

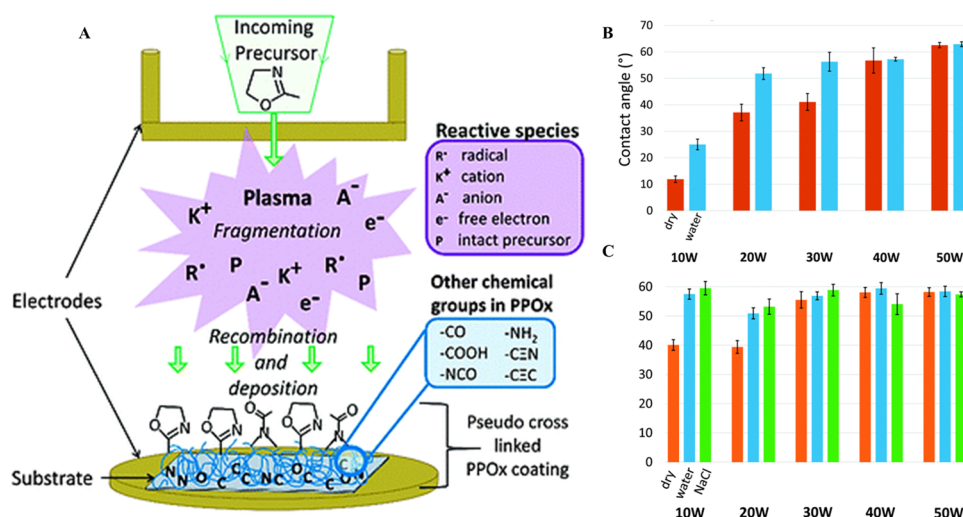
The energetic electrons in the plasma can induce the dissociation of the precursor and the creation of a large number of radical species, which would be very difficult to achieve under normal ground-state conditions.<sup>55,56</sup> Enhanced chemical reactivity of the plasma-generated species compared to species in the gas phase enables similar chemical processes to take place at notably *lower temperatures*, in many cases eliminating the need for external heating and/or catalyst. Thus, plasma processing directly addresses the requirement for *lower energy consumption* of green synthesis. However, when estimating the energy efficiency of plasma-enabled processes, it is important to adequately account for the energy required to initiate and maintain the plasmas. Indeed, certain types of plasmas, such as nonequilibrium nanosecond repetitive pulsed discharges, are significantly more energy efficient per atom incorporated than their continuous-mode counterparts.<sup>75</sup> Here, the relatively short on-periods (approximately nanoseconds) are sufficient to generate the reactive species; the reaction is then allowed to proceed for microseconds to milliseconds during off-periods in the absence of continuous energy supply. This leads to a considerably lower estimated energy per atom incorporated compared to pure thermal and continuous plasma-enhanced or plasma-enabled syntheses.

Furthermore, plasmas are not simply an alternative means for gas heating. The state-of-the-art in plasma research is to create reactive species through nonthermal mechanisms that are different from the conventional thermal process. Of particular interest are nonthermal plasmas, for which the mean electron energy  $\langle \epsilon \rangle$  is significantly higher than the energy of neutral gas particles at atmospheric pressure. Here, relevant building blocks can be produced without the need to heat the entire volume of the gas. Generated plasma chemical species, namely electrons, ions, excited neutral species, and radicals, can serve as vehicles for the specific transfer of energy toward growth processes. These chemical species are typically not found in pure chemical or pure thermal synthesis environments. By utilizing a combination of thermal and nonthermal mechanisms to drive the reaction, energy savings may be achieved.

The nonequilibrium nature of many plasmas is at the core of plasma selectivity. Selectivity of plasma-enabled processes is related to thermal and nonthermal mechanisms of chemical reactions, where heat and chemical species trigger and sustain these reactions. In a typical purely thermal process, energy (as heat) is delivered to the entire volume of the reactor, resulting in uniform gas heating. In nonequilibrium plasmas which are the focus of this review, energy can be delivered to electrons, without activation of all molecules. As such, the gas in the plasma chamber is of lower temperature than that in an otherwise equivalent thermal process where it is extremely difficult, if not impossible, to avoid uniform gas heating. Excited first, the energetic electrons can excite the molecules in a deliberate way—specifically, by exciting their rotational and vibrational degrees of freedom, without increasing the kinetic energy of their motion as a whole. Hence, higher reactivity can be achieved; the reactivity may be sufficient to maintain sufficiently high rates of strongly endothermic reactions at substantially lower temperatures than those required under purely thermal reaction conditions.

Another aspect of plasma selectivity and energy efficiency is associated with plasma effects localized to surfaces and nanoparticles. One interesting example of theoretical elaboration of nanoscale plasma-specific selectivity effects can be found in an article by Ostrikov and Mehdi pour.<sup>37</sup> Depending on the fluxes and energies of plasma-generated species, these effects can lead to sputtering, etching, heating and formation of hot spots, surface charging, deposition, implantation, and photon irradiation, as well as localized nucleation of nanoscale objects such as carbon nanotube caps or graphene sheets. The bombardment by charge carriers, photons, metastable, excited- and ground-state neutrals, heat released from exothermic surface reactions, and locally intense electric fields resulting from the strong local curvature of the nanoparticles provide substantial heating which is localized to the upper surface layer of the substrate. Such localized heating reduces and may even eliminate the need for external heating and significantly lower the overall temperature and energy requirements of the process. Chemical reactions also appear to be different on the surfaces of nanometer-sized particles exposed to the plasma, because of the interplay of the localized heating, ion bombardment effects, modifications of reactivity, and catalytic activity of nanoparticles due to the plasma exposure and several other plasma-specific effects. A substantial amount of literature addresses these phenomena and, although they are outside the scope of this review, we have referred the interested reader to this literature, e.g. the review in *Advances in Physics*<sup>53</sup> and other publications.





**Figure 5.** Synthesis of polyoxazolines from oxazoline monomers is typically carried out via a complex cationic ring opening polymerization method, the cost of which limits industrial applications. (A) Polyoxazoline thin films can be synthesized in a plasma discharge in a single-step process. (B, C) The chemical composition and surface properties of plasma-polymerized polyoxazoline thin films are controlled by the flow rate (B,  $2 \times 10^{-1}$  mbar; C,  $1.1 \times 10^{-1}$  mbar) and input power. Reprinted with permission from ref 84. Copyright 2015 Royal Society of Chemistry.

Lower processing temperatures not only make plasma-assisted synthesis and processing more energy-efficient, they also reduce the amount of material being lost or wasted.<sup>53</sup> At higher temperatures, material deposition is competing against heat-driven evaporation and desorption. Lower temperatures of the plasma processing reduce the rates of material loss from the substrate surface, making the synthesis more matter-efficient.<sup>72,77</sup> This aligns well with the requirement for green synthesis to *minimize waste* and *maximize incorporation of all materials* used in the process into the final product.

The reactivity of the plasma environment also positively contributes to the rates of nanostructure nucleation and growth, leading to more *time-efficient* processing. For instance, compared with similar thermal processes in the same gases and under similar conditions, plasma environment usually increases the growth rates of many common nanostructures, such as single wall carbon nanotubes (SWCNTs).<sup>78,79</sup> Here, plasma-produced carbon atoms reach the catalyst and incorporate into the nanotube walls much faster under the plasma conditions compared to the plasma-free environment. Reactive hydrogen species produced in the plasma are effective in etching amorphous carbon; the etching helps maintain catalytic activity of catalyst nanoparticles longer, resulting in taller SWCNTs.<sup>80</sup>

The ambient temperature and ambient pressure processing of atmospheric pressure plasmas is considered to be even more energy efficient and environmentally benign.<sup>53</sup> Furthermore, low-pressure and most atmospheric-pressure plasma systems employ closed reactor configurations with controlled gas feed and exhaust systems which facilitate the containment of the plasma generated species within the reactor, making it more human-health-friendly to operate.

The attributes of the plasma fit well within the framework of sustainable materials synthesis and nanoscale assembly, which require the process to be low-cost, simple, energy- and material-efficient, and safe to humans and the environment.<sup>75,81</sup> The preference is given to one-step, room-temperature, and atmospheric-pressure processes, provided that the properties and performance of the nanomaterials meet the requirements of the envisaged applications.

## 2.2. Chemical Reactivity of Plasma Environment

Chemical reactivity and stability of plasma discharges depend on the balance of species and energy. Electrons drive the dissociation, ionization, and excitation, and are directly linked to chemical reactivity of the plasma. Ions interact with the surfaces within the plasma environment and, if they are energetic enough, can cause breaking of the chemical bonds, material sputtering, or substantial heating of the substrate. In low-temperature, weakly ionized plasmas, the temperatures of ions and neutral species are much lower than the electron temperature. In thermal plasmas, the temperatures of all species are the same. The heating of the substrate can also be caused by photons; the latter can initiate photochemical reactions, such as chain scission in the plasma-produced polymers.<sup>82</sup> Neutral species contribute to deposition, modification, or etching of the material being processed.

Low-temperature, nonequilibrium plasmas are typically sustained at low pressure and can be generated by electromagnetic energy spanning from direct current (dc) plasmas to radiofrequency (rf) and microwave frequency plasmas. Low-temperature plasmas can also be generated at atmospheric pressures. Examples of atmospheric-pressure nonthermal plasmas include plasma jets and dielectric barrier discharges.

Low-temperature plasmas are well-suited for materials synthesis where preservation of the original chemistry of the precursor is desired, such as synthesis of polymer thin films (Figure 5)<sup>83,84</sup> or functionalization of carbon nanostructures. Such plasmas can catalyze the reaction, or can enhance activation of a solid catalyst if one is used. The chemistry of the process is versatile, while the properties of the final material can be tuned from smooth, defect- and pinhole-free, and chemically homogeneous to rough, porous, and chemically graded structures. This can be achieved by controlling the type of building units (via precursor chemical composition) and the characteristics of the plasma (e.g., power, gas pressure, gas flow, temperature, reactor geometry). Numerous oxidative, reductive, and noble gases and their mixtures can be used as precursors/feedstock.

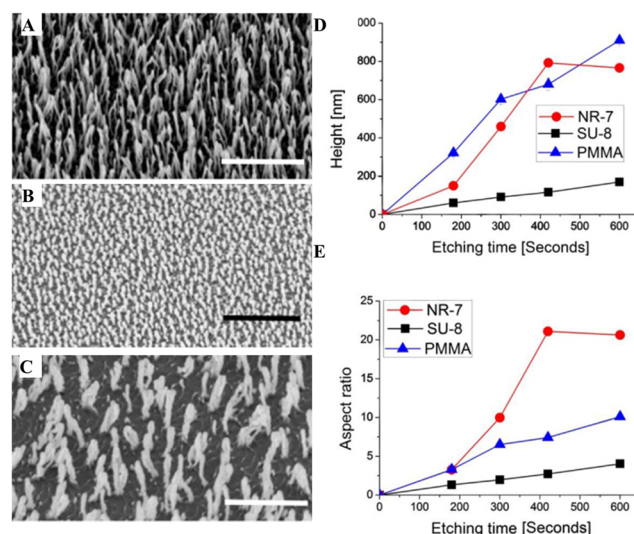
These gases can also serve as a source of elements for the controlled introduction of elemental impurities and structural

defects as a means of fine-tuning the properties of the material, e.g. doping of carbon nanotubes with nitrogen using ammonia gas. Incorporation of impurities, e.g. nitrogen, can induce the formation of vertically aligned carbon nanostructures without the use of catalysts, such as the synthesis of carbon nanorods under rf-plasma-enhanced chemical vapor deposition (CVD) conditions.<sup>85</sup> The type of incorporated carbon–nitrogen bonds, in particular isonitrile functional group bonded to isolated or fused aromatic rings, is crucial for the formation and vertical alignment of the nanorods. Being connected to the graphitic ring through N atom rather than C, the nitrogen atom in this functional group will have a positive charge while C will be negatively charged. The electric field generated by rf plasma in the direction perpendicular to the substrate surface induces aligned deposition and stacking of these polarized bonds which lead to the formation of vertically aligned carbon nanorods containing nitrogen.

Low-pressure plasmas are used extensively for anisotropic, highly selective etching under mild conditions (low temperature, low voltage), which minimizes undesirable heat-related and ion impact-related damage to materials structure.<sup>73,86–88</sup> The anisotropic nature of plasma etching can support high-fidelity transfer of microscopic patterns onto a variety of substrates of mesoscale and larger dimensions. The electric field drives reactive species,<sup>53</sup> e.g. ions, down to the substrate, where they bond with the unmasked atoms, forming volatile compounds that can be extracted (e.g., pumped out) from the etch reactor. The resultant features can have controlled morphologies, ordering, and high aspect ratios and can be used in sensors, energy storage, and optoelectronic devices. Even smaller, closely spaced features can be etched using plasmas; the reactive ions in a plasma have sufficient mobility, high energy, and transport directionality to penetrate deep into the trenches and effectively remove substrate material without substantially damaging the walls of the features.<sup>74</sup> Self-organized arrays of nanostructures can be effectively fabricated at low temperatures over large areas without the use of masks (Figure 6). By treating a layer of polymer photoresist with the plasma in the absence of a mask, polymer nanowires with a diameter of <50 nm and an aspect ratio greater than 20:1 were produced.<sup>89</sup>

In nonthermal plasmas, the difference in the electron and ion velocities leads to the formation of the plasma sheath, a thin region which separates the substrate surface from the plasma bulk. The thickness of the sheath depends on the plasma density, electron temperature, and other factors, and can be used to control the deposition process. The sheath is the result of a large flux of highly mobile electrons arriving at the surface of the substrate well ahead of slower-traveling ions. To balance the negative charge on the substrate surface, the sheath is formed. Electron-depleted ionized atoms and molecules are accelerated toward the surface as they traverse the sheath.<sup>90</sup> For materials synthesis, it is important to balance the speed with which ions arrive at the surface, so as to maximize the speed of materials formation yet minimize excessive ion bombardment which may cause formation of defects or etch newly formed deposits. The electrons play a key role in the generation of radical species in the plasma bulk, within the sheath, and on the substrate surface, whereas plasma-produced ions, atoms, and radicals interact with the surface to induce heating, deposition, etching, recombination, and other processes.

For the growth of nanowires and nanotubes, plasma-enhanced chemical vapor deposition (PECVD) improves the



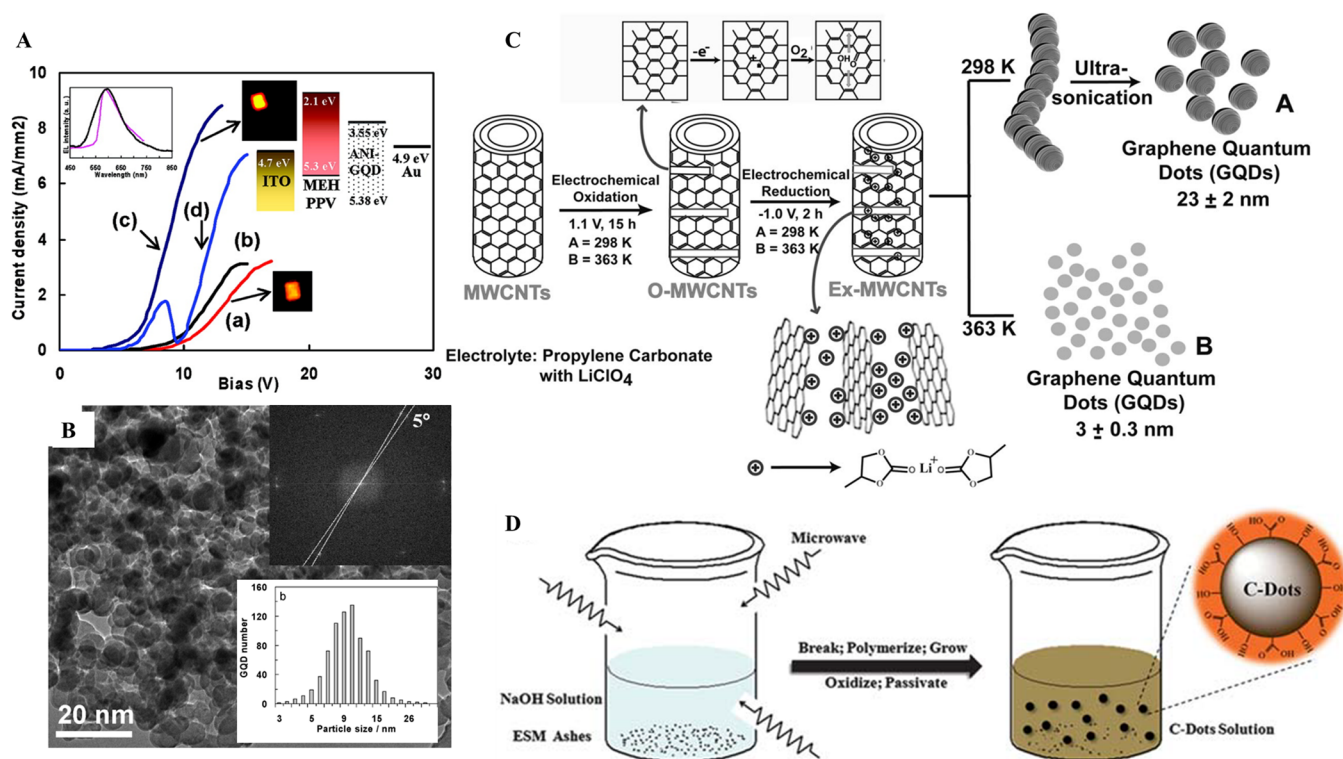
**Figure 6.** Oxygen plasma etching enables maskless synthesis of polymer nanowires. (A–C) Scanning electron microscope (SEM) images of the self-patterned polymer nanowire structures created by etching of NR-7 (A), SU-8 (B), and PMMA (C) films in oxygen plasma for 420 s. The scale bar in each image indicates 1 μm. (D, E) Geometric parameters of the nanowire structures as a function of the etching time. Reprinted with permission from ref 89. Copyright 2014 IOP Publishing.

selectivity and lowers the synthesis temperature, allowing deposition of less dense, thinner, and preferentially ordered nanostructures. In addition to being exploited for the quasi-deterministic assembly of zero-, one-, two-, and three-dimensional (0D, 1D, 2D, and 3D, respectively) nanostructures onto a variety of substrates, including prepatterned substrates,<sup>91</sup> thermal and chemical effects of nonequilibrium plasmas enable synthesis and functionalization of nanoparticles in liquids, where plasmas accelerate electrochemical reactions.<sup>92,93</sup>

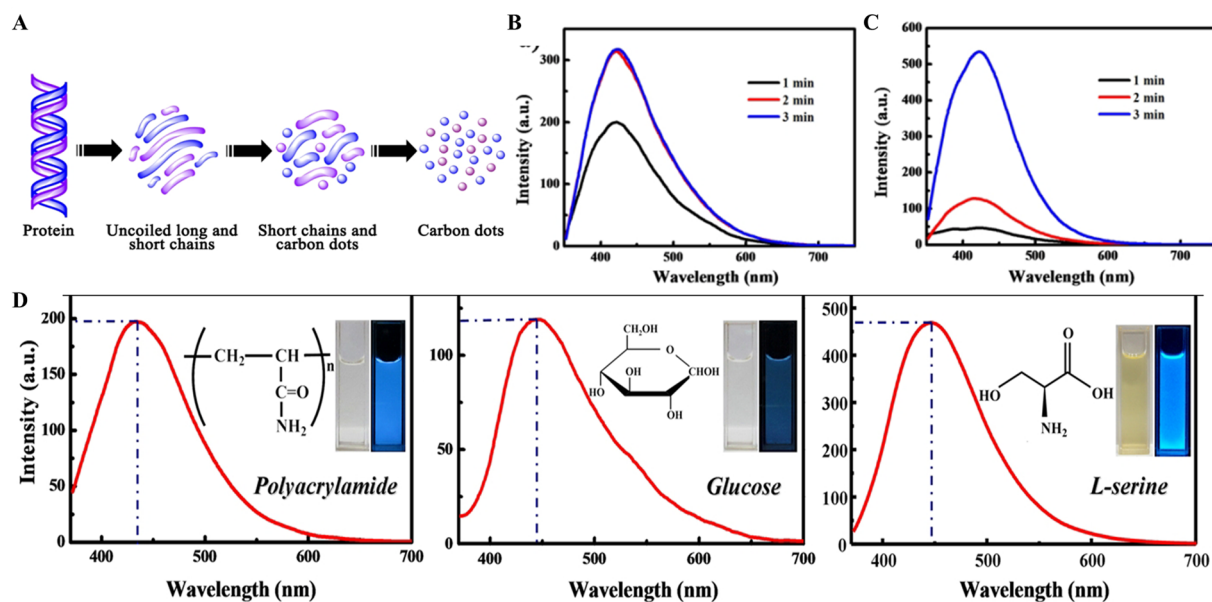
Thermal plasmas are typically created at high pressures by dc or rf arcs, and by inductively coupled torches. High-pressure discharges are characterized by high plasma densities, up to  $10^{17}$  cm<sup>-3</sup> in arcs, and very high rates of collisions. The flow rates of matter and energy are very high in thermal plasmas, making these plasmas ideally suited for the destruction of materials, e.g. for treatment of hazardous waste, or material synthesis where effective atomization of the original precursor is desired, e.g. synthesis of carbon nanotubes. High nanostructure nucleation and growth rates make thermal plasmas attractive for large-scale production of nanomaterials, including carbon nanoparticles.

It is important to note that many currently available plasma processes lack sufficient selectivity and are difficult to control to the extent necessary to produce high-quality carbon nanostructures from natural resources. There still remains a knowledge gap regarding the precise mechanisms and controls that govern the generation and chemical reactivity of species in plasmas. Leading research groups are currently trying to bridge this gap by developing novel plasma systems and complementary instrumentation that can effectively and accurately probe these plasmas. Understanding the nature of selectivity that can arise from a multitude of plasma effects is required to meet the expectations.

The next step is to review the most relevant examples of natural resource-to-nanomaterial conversions and how plasma-specific effects can be used to control them.



**Figure 7.** Photoluminescent C-dots, their synthesis, and application in LEDs. (A) Incorporation of 1% C-dots into poly(2-methoxy-5-(2-ethylhexyloxy)-1,4-phenylenevinylene) polymer increases LED brightness. (B) TEM image and diameter distribution (inset) of C-dots used in the LED device. (C) Schematic representation of various processing stages involved in the preparation of photoluminescent graphene QDs (GQDs) from MWCNTs by electrochemical approach. (D) Synthetic scheme of C-dots from eggshell membrane through a microwave-assisted process. Panels A and B reprinted from ref 97. Copyright 2011 American Chemical Society. Panel C reprinted with permission from ref 99. Copyright 2012 Wiley-VCH Verlag GmbH & Co. KGaA. Panel D reprinted with permission from ref 98. Copyright 2012 Royal Society of Chemistry.



**Figure 8.** Plasma-assisted generation of C-dots from protein. (A) The proposed mechanism involves plasma-generated heating and chemical reactions with the activated species in the plasma, leading to protein denaturation via the breakage of hydrogen bonds and uncoiling of polypeptide chains, partial carbonization, and oxidation of the sample. Continued plasma processing causes the long and short chains of the peptides to break down into shorter chains, and eventually C-dots formation. (B, C) Evolution of PL emission of C-dots produced from egg white (B) and yolk (C) aqueous solution as a function of the plasma exposure time. Longer plasma exposures produce more significant etching effects which lead to higher PL intensities. (D) Effect of precursor chemistry on PL emission spectra of the aqueous solutions of C-dots produced using atmospheric-pressure plasmas. Insets are digital photos under daylight (left) and UV light (right); solution concentration is 1 wt %. Reprinted with permission from ref 71. Copyright 2012 Wiley-VCH Verlag GmbH & Co. KGaA.



### 3. PLASMA-ENABLED FAST PROCESSING: THE CASE OF CARBON NANODOTS

This section will examine the ability of plasmas to significantly reduce the time required for the synthesis of carbon quantum dots (QDs). Carbon QDs (also known as C-dots) are gaining interest as chemically inert and less toxic alternatives to heavy-metal-based semiconducting QDs. C-dots have been widely reported to possess photobleaching-free stable photoluminescence (PL) and excitation-energy-dependent emission spectra,<sup>94–96</sup> with potential applications in optoelectronics, e.g. in light-emitting diodes (LEDs), bioimaging, and biolabeling. C-dot size, presence of defects, oxygen content, and surface termination are key determinants of the photoluminescence and photostability of these nanostructures.<sup>97–99</sup> It is important to note that the issue of photobleaching in C-dots, with reports of fluorescence bleaching caused by photochemical processes, requires further studies.<sup>100,101</sup>

High-quality C-dots are typically synthesized in a top-down approach, e.g. by hydrothermal (chemical) cutting of oxidized graphene sheets,<sup>102</sup> hydrazine hydrate reduction of graphene oxide,<sup>103</sup> electrochemical processing of multiwalled carbon nanotubes (Figure 7C),<sup>104</sup> laser ablation and nitric acid oxidation of graphite,<sup>105</sup> or in a bottom-up approach, from a variety of chemical precursors, such as ethylenediamine-tetraacetic acid salts<sup>106</sup> and citric acid.<sup>107</sup>

Several reports exist on the preparation of C-dots from low-cost natural precursors, e.g. poly(ethylene glycol),<sup>108,109</sup> saccharides (e.g., glucose, fructose, etc.),<sup>110,111</sup> amino acids,<sup>112</sup> ginger juice,<sup>113</sup> paper ash,<sup>114</sup> capsicum,<sup>115,116</sup> watermelon peel,<sup>117</sup> hair,<sup>118</sup> potatoes,<sup>119</sup> guava,<sup>116</sup> peas,<sup>116</sup> tea,<sup>120</sup> spinach,<sup>116</sup> waste frying oil,<sup>121</sup> oilseed press cake,<sup>122</sup> shrimp eggs,<sup>123</sup> and others. Waste materials, such as used plastic bags,<sup>124</sup> candle soot,<sup>125</sup> and tire soot,<sup>126</sup> have also been used as low-cost alternatives to conventional carbon precursors. The common synthesis routes include microwave-mediated pyrolysis,<sup>108,110</sup> Maillard reaction,<sup>112</sup> hydrothermal carbonization,<sup>109,113,115–117,119,122</sup> and wet chemistry.<sup>111,121,126</sup>

Although some of these methods, i.e. Maillard reaction, enable the production of C-dots with bright PL, quantum yield of up to 69%, and ultrahigh photostability,<sup>112</sup> the typical quantum yields are much lower. Furthermore, these methods rely on either prolonged external heating, e.g. 2–5 h in the case of hydrothermal processing,<sup>113,117</sup> specific processing environment, e.g. nitrogen atmosphere,<sup>118</sup> potentially toxic solvents, e.g. sulfuric<sup>121</sup> and nitric acids,<sup>125,126</sup> as well as catalysts, e.g. (*N*-(2-aminoethyl)-3-aminopropyl)tris(2-ethoxy)silane,<sup>127</sup> to drive the reaction.

Recently, amphiphilic C-dots were produced by treating yolk and white fractions of chicken eggs using atmospheric-pressure dielectric barrier discharges (DBDs).<sup>71</sup> The generation of C-dots was a rapid (<3 min) single-step process, where the plasma generated reactive species and plasma-induced heating were driving the reaction (Figure 8A). In this case, the reactive plasma environment served to reform abundant, unprocessed carbon precursor (chicken egg) into relevant hydrocarbon building units under ambient conditions (vacuum-free, solvent-free, and external-heating-free).

Structurally, plasma-produced C-dots are nanocrystalline, being composed of sp<sup>2</sup> hybridized carbon with sp<sup>3</sup> carbon defects. The surfaces of the C-dots produced from egg precursor materials are abundant in oxygen-containing groups, namely C–OH, C–O–C, and C=O. The crystallinity of the

C-dots produced from yolk is higher compared to white-derived structures. This was attributed to the differences in lipid content (33% in yolk, 0.01% in white) and the higher density and viscosity of the yolk. This factors were suggested to enhance electron–ion recombination processes on the surface and thus promote crystallization.<sup>71</sup> With intense blue fluorescence, these nanostructures may be used as fluorescent carbon inks for multicolor luminescent inkjet and screen printing, and in a variety of medical applications.<sup>71</sup> The average lifetime (~6.3 ns), quantum yield (~6–8%), and photostability of plasma-produced egg-based nanodots are comparable to those of luminescent C-dots produced by other methods, e.g. wet chemistry. Furthermore, plasma-processed C-dots are amphiphilic and can be easily dispersed in water and most organic solvents.

The in-plasma passivation of C-dot surfaces can be controlled by changing the rates of reactive species generated in the plasma.<sup>128,129</sup> The degree of C-dot passivation is important, since the emission from unpassivated C-dots is greatly reduced due to the link between the photoluminescence and the presence of energy-trapping sites on the C-dot surface.<sup>130</sup> While passivation of C-dots with polymers can significantly increase the quantum yield,<sup>131</sup> such modification also affects the surface energy and hydrophobicity of the material.

Other types of natural precursors can serve as a carbon precursor in place of egg for the synthesis. The composition of the starting material and the processing conditions determine the properties of C-dots (Figure 8D). Glucose, other simple carbohydrates, and their solutions are easily carbonized and oxidized under the same plasma environment to yield nanodots with a PL emission peak centering at ~450 nm. The properties of the plasma-fabricated glucose-based C-dots are similar to those prepared electrochemically from multiwalled carbon nanotubes.<sup>104</sup> Low molecular weight precursors containing nitrogen functionalities, such as acrylamide, amino acids, and ethylenediamine-tetraacetic acid disodium salt (EDTA-disodium) can also be reformed into luminescent structures using plasma treatment.

However, when polymers, namely poly(methyl methacrylate), polyvinylpyrrolidone, polyacrylamide, poly(vinyl chloride), sodium alginate poly(vinyl alcohol), polystyrene photonic crystals, and poly(ethylene glycol), were subjected to the above treatment conditions, they failed to generate C-dots. Given the high bonding energy in the molecular chains of the solid polymers, higher-energy and/or longer plasma exposure may be necessary to achieve the effect. Interestingly, luminescent C-dots were successfully formed in aqueous solution of polyacrylamide (~3 wt %), suggesting that the liquid state may be conducive to nanodot formation. These results indicate that the mechanisms of C-dot formation in atmospheric-pressure plasmas differ with chemical composition and state of precursor materials, and can thus be precursor-driven. Further in-depth investigations are necessary to elucidate these mechanisms and validate the above conclusion.

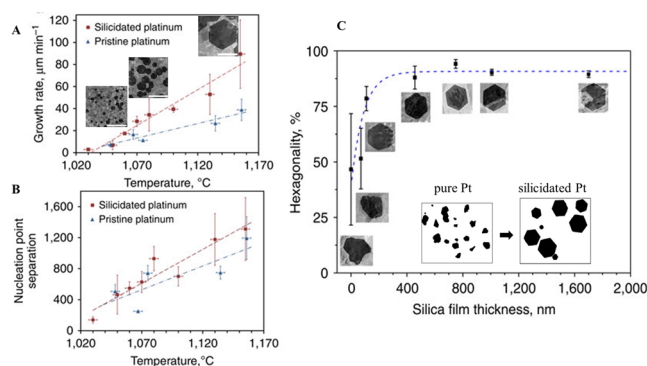
The ability of plasma to accelerate the rate of synthesis can be demonstrated for other carbon nanostructures, e.g. graphene, as discussed below.

### 4. PLASMA-ENABLED REDUCED-TEMPERATURE GRAPHENE SYNTHESIS

This section presents the use of the reactive plasma chemistry to reduce the temperatures for nucleation, growth, and

formation of graphene films. Graphene, the two-dimensional atomic carbon crystal, uniquely combines attractive mechanical, electronic, and thermal properties and catalytic activity.<sup>59,132,133</sup> Properties and applications of graphene have been reviewed extensively by others.<sup>134–139</sup> Briefly, graphene and its bilayer are characterized by extremely low electron–phonon scattering and as such room-temperature electron mobility of  $2.5 \times 10^5 \text{ cm}^2 \text{ V}^{-1} \text{ s}^{-1}$ .<sup>140</sup> A freestanding monolayer graphene membrane displays a Young's modulus of 1 TPa and intrinsic strength of 130 GPa, making it the strongest material ever measured.<sup>141,142</sup> The very high thermal conductivity of above  $3000 \text{ W m}^{-1} \text{ K}^{-1}$  of graphene make this material suitable for thermal management of electronics, where heat removal has become a critical miniaturization-related issue.<sup>143</sup> Due to its unique electronic structure, graphene absorbs a significant fraction of incident white light<sup>144</sup> and can sustain very high densities of electric current. Graphene sheets can be further functionalized to enhance the catalytic activity. Graphene and graphene oxide have been proposed for use as advanced green catalysts.<sup>137,145–147</sup>

Large sheets of graphene can be grown by a variety of chemical and physical vapor deposition methods, confined controlled sublimation, and others.<sup>148,149</sup> Confinement controlled sublimation of silicon carbide, where at sufficiently high temperatures silicon sublimates from the surface and the carbon-rich surface layer transforms to graphene, can yield very high quality, large sheets of graphene; however, the cost of this type of process is relatively high.<sup>148</sup> In vapor deposition methods, metal substrates, such as copper, nickel, iron, cobalt, platinum, and others,<sup>150–153</sup> are typically used to catalyze the formation of mono-, bi-, tri-, or multilayer graphene, with the quality and properties of graphene being intimately linked to the catalyst used in its synthesis (Figure 9).<sup>154</sup> The use of catalyst adds



**Figure 9.** Synthesis temperature and nature of the substrate have a significant effect on the growth rate (A), nucleation point (B), and crystallinity (C) of graphene grown under otherwise identical CVD conditions. Lowest temperature required to initiate graphene formation was above  $1000^{\circ}\text{C}$ , which is typical of purely thermal synthesis methods. Reprinted with permission from ref 154. Copyright 2015 Nature Publishing Group.

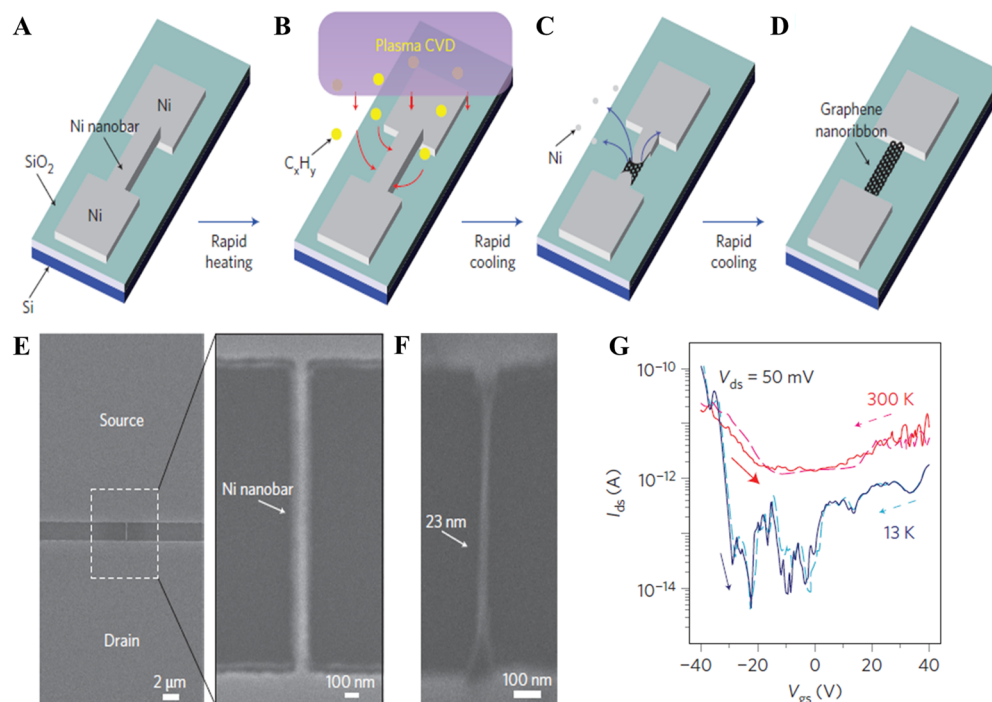
significantly to the overall cost of graphene production. Polycrystalline substrates are more attractive due to their lower cost; however, the uniformity of graphene layer on these surfaces remains an issue. Reusable substrates comprised of silicon wafer topped with a hydrogen-terminated germanium buffer layer have also been proposed, where the weak interaction between graphene and germanium surface enabled the facile etch-free dry transfer of graphene and the recycling of

the germanium substrate for the continual graphene growth.<sup>155</sup> Anisotropic 2-fold symmetry of Ge(110) surface allows unidirectional alignment of multiple graphene seeds, which then join to produce uniform single-crystal graphene with predefined orientation.

As a source of carbon, a variety of gaseous and solid materials, e.g. methane, acetylene, polystyrene, or poly(methyl methacrylate), are used. Large aromatic hydrocarbons, such as benzene and hexachlorobenzene, can be used to lower the temperature of CVD synthesis of monolayer graphene flakes to as low as  $300^{\circ}\text{C}$ .<sup>151,156</sup> However, the toxicity of these highly volatile compounds remains an issue. Synthetic nanographenes can be used as building blocks for bottom-up assembly of transparent thin films.<sup>157,158</sup> Molecules of giant polycyclic aromatic hydrocarbons, such as a superphenalene derivative, have both a large aromatic core and flexible side chains to ensure good solubility for simple solution processing. The molecules are thermally fused together to form larger sheets with properties that enable their use as hole-collecting electrodes in organic solar cells. The efficiency of cells containing poly(3-hexyl)thiophene:phenyl-C61-butyric acid methyl ester and fused graphene sheets as anode was comparable to the highest external quantum efficiency value of 47% for a reference device fabricated with ITO as the anode. In addition to solar cells, these graphene films can be used in the fabrication of flat-panel displays, organic light-emitting diodes, and other modern optoelectronic devices.

Low-temperature plasmas provide a suitable environment for the synthesis of graphene and graphene-based hybrid structures. The advantages of using plasmas for graphene synthesis include controlled, selective production of desired reactive species, reduced energy and material consumption, enhanced catalyst activation or catalyst-free synthesis, shortened operation time, and decreased environmental pollution.<sup>90</sup> These factors satisfy the requirements for quality graphene synthesis as well as time, energy, and cost efficiency. The major challenge for the plasma-assisted growth of graphene is the difficulty to simultaneously deliver small amounts of material to the surface and to enable rapid and uniform monolayer nucleation across the entire surface area without suffering damage to the hexagonal structure from ion bombardment.<sup>53</sup> Remote plasma configurations can provide the means to lower the amount of material delivered to the surface and prevent excessive ion bombardment of the growing carbon structure.<sup>159</sup> At the same time, remote plasmas allow maintaining of relatively low synthesis temperatures, which are typically a couple of hundred degrees lower compared to conventional chemical vapor deposition.

The plasma environment also provides an effective means for graphene doping by incorporation of other elements which modulates the charge transfer properties of the material. For example, exposure to  $\text{NH}_3$  plasmas during synthesis enables fast nitrogen doping of up to  $1.5 \times 10^{13} \text{ cm}^{-2}$  that can be effectively controlled by tuning the time of exposure and the proportion of  $\text{NH}_3$  in the atmosphere.<sup>160</sup> Nitrogen-containing radicals covalently bind to the carbon lattice and maintain stability during postannealing.<sup>161</sup> Plasma doping can also take place postdeposition, providing extra processing flexibility and saving on time and cost associated with multienvironment processes.<sup>162</sup> Oxygen plasma treatment has been shown to significantly alter the band gap of graphene sheets, driving the transition from semimetallic to semiconducting behavior.<sup>163</sup> Exposure to oxygen plasmas was successfully used to induce



**Figure 10.** Schematic of the direct conversion of a Ni nanobar to a graphene nanoribbon by rapid-heating plasma CVD performed using a mixture of methane and hydrogen gases. (A–D) The substrate is rapidly heated to  $\sim 900$  °C for 1 min and plasma CVD is performed. Nucleation of graphene preferentially starts from the Ni nanobar structure during the cooling process, and a graphene nanoribbon is formed. (E, F). Typical SEM image of patterned Ni electrodes and the Ni nanobar before the plasma exposure (E) and graphene nanoribbon converted from 50 nm width Ni nanobars (F). (G) Typical electrical transport properties of graphene nanoribbons. Current–voltage characteristics ( $I_{ds}$ – $V_{gs}$  curves) of a 23-nm-wide graphene nanoribbon device at 300 K confirm ambipolar transport characteristics with an on/off ratio of  $\sim 16$ . At 13 K, the on/off ratio increased to  $1.5 \times 10^4$ . No hysteresis in the curves indicates the clean surfaces of as-grown graphene nanoribbons and/or the suspended structures. Reprinted with permission from ref 175. Copyright 2012 Nature Publishing Group.

strong photoluminescence in single-layer graphene that was spatially uniform across the flakes.<sup>164</sup> A quite similar treatment of graphene multilayers resulted in selective conversion of the topmost layer into photoluminescent material.

On the other hand, exposure to low-density (of  $3.5 \times 10^8$  cm<sup>−3</sup>) Ar plasmas can be used to remove impurities from the surface of graphene with minimal damage to the carbon network.<sup>165</sup> Treatment of silicon-supported graphene sheets with remote hydrogen plasmas revealed strong monolayer selectivity for reactions with the plasma species.<sup>166</sup> In monolayers, isotropic hole formation in the basal plane and etching from the sheet edges were observed, whereas hexagonal pits of uniform size were etched in bilayer or thicker sheets. The etch rate was independent of the substrate morphology, with similar phenomena observed on both silicon and much smoother mica substrates, yet was sensitive to temperature. Faster hydrogenation of bi- and multilayer over monolayer graphene and highly anisotropic etching along specific crystallographic directions were also confirmed.<sup>167–169</sup>

Treatment of graphene with oxygen plasmas is an effective way to convert it to graphene oxide (GO). Conversely, certain plasmas, e.g. remote methane plasma, can be used to reduce the graphene oxide by lowering its oxygen content, which also decreases the band gap of the material. Plasma-enabled reduction of GO to graphene is facilitated by significant defect healing, which positively contributes to the quality of the resultant material.<sup>170</sup> The presence of highly reactive hydrogen atoms and ions reduces the time and temperature required to convert GO to graphene, from  $>1000$  °C for annealing in

alcohol vapor or vacuum to  $<580$  °C for methane plasmas.<sup>170</sup> The temperature is even lower for treatments with atmospheric-pressure plasmas, where sheet resistance of  $\sim 4.8 \times 10^4$  Ω/square was obtained in Ar + H<sub>2</sub> plasmas at only 70 °C.<sup>171</sup> Furthermore, plasma-enabled reduction does not require the use of strong and hazardous chemicals, which limits the environmental impact of the processing as well as minimizes the incidence of impurities or defects being incorporated into the carbon structure.

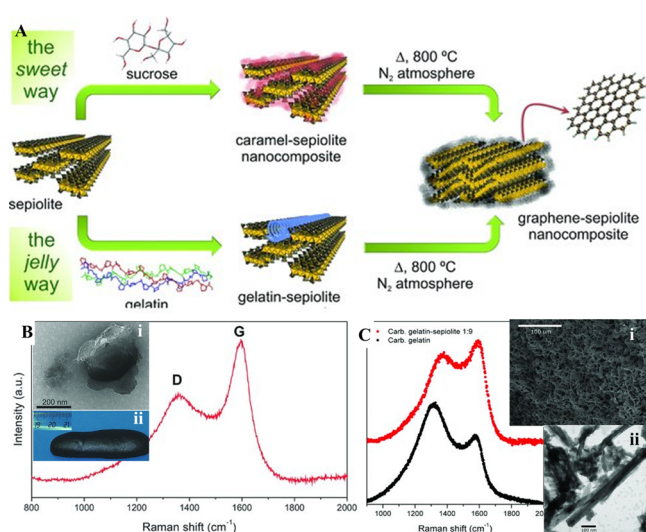
Higher-density plasmas can be employed to unzip carbon nanotubes and thus produce carbon nanoribbons (CNRs),<sup>172</sup> which hold promising applications in molecular electronics as semiconducting materials.<sup>173,174</sup> Nanoribbons combine the unique electronic and spin properties of graphene with a transport gap that arises from quantum confinement and edge effects, making CNRs a promising candidate for the channels of next-generation transistors. Although CNRs can be produced by a variety of methods, control over their surface organization within the device remains a challenge. Rapid-heating plasma CVD of CH<sub>4</sub> and H<sub>2</sub> was used to directly convert nickel nanobars into 23-nm-wide graphene nanoribbons (Figure 10).<sup>175</sup> It was possible to grow CNRs directly between the source and drain electrodes of a field-effect transistor (FET), yielding the FET devices with a clear band gap of 58.5 meV, a high on/off ratio of above  $10^4$ , and no hysteresis (Figure 10G). Certain deposition conditions facilitated synthesis of complex architectures, e.g. parallel and radial arrays of supported and suspended ribbons.



Currently, methane ( $\text{CH}_4$ ) precursor is commonly used in a purified form, and data about its purity are rarely present in the original reports. Although no reports are currently available, graphene synthesis from minimally processed methane is possible in principle. This may affect the level of defects present in the graphene sheets. The relationship between the chemistry of the carbon source and the graphene defect levels will be discussed in more detail in [section 5.3](#).

## 5. PLASMA-ENABLED PROCESS-DRIVEN SYNTHESIS: THE CASE OF GRAPHENES

Although the majority of commonly used carbon sources represent highly purified chemicals, there is growing interest in graphene synthesis from low or negatively valued (waste) raw carbon sources used without purification. Sucrose (table sugar) was successfully converted into single-layer graphene by depositing sucrose powder onto Cu substrate followed by heat treatment at  $800\text{ }^\circ\text{C}$  under  $\text{H}_2/\text{Ar}$  atmosphere.<sup>176</sup> Sucrose was also used as a carbon source for microwave-assisted synthesis of graphene on sepiolite substrate ([Figure 11](#)).<sup>177</sup> Under microwave-assisted heating, sucrose is first converted into caramel, which can then be transformed into graphene with subsequent heating in the absence of oxygen. Using the same method but replacing a carbohydrate with protein, nitrogen-doped graphene can be obtained. Nitrogen doping of



**Figure 11.** Cost-efficient graphene-related materials from natural resources. (A) Schematic routes showing the preparation of graphene supported on the fibrous clay sepiolite prepared from sucrose and gelatin. In the “sweet” way, sucrose is first transformed into caramel in the presence of sepiolite, while the “jelly” way starts with the spontaneous assembly of gelatin into the fibrous silicate. Thermal treatment of both nanocomposites at  $800\text{ }^\circ\text{C}$  in an  $\text{N}_2$  atmosphere results in carbon–clay materials with graphene layers (N doped when derived from the protein) supported on the silicate. (B) Raman spectrum and TEM image (inset, i) of carbon–sepiolite sample prepared from sucrose confirm a graphene-related layer on a silica substrate. Even with a large percentage of insulating mass (the silicate component), silica–graphene low-density monolith (inset, ii) exhibits relatively high electrical conductivity. (C) Raman spectra and TEM (inset, ii) of graphene deposited from gelatin over sepiolite fibers. SEM image (inset, i) of macroporous conducting foam obtained from the carbonization of gelatin–sepiolite colloid after freeze-drying. Reprinted with permission from ref 177. Copyright 2011 Wiley-VCH Verlag GmbH & Co. KGaA.

graphene can also be attained by pyrolysis of a mixture of sugar and urea.<sup>178</sup> A wide range of freestanding monolayers and multilayer graphene structures were obtained by calcination of glucose, where layered graphitic carbon nitride served as a sacrificial template and a source of nitrogen dopant.<sup>179</sup> A thermolytic treatment at  $750\text{ }^\circ\text{C}$  is then used to liberate graphene from the carbon nitride support.

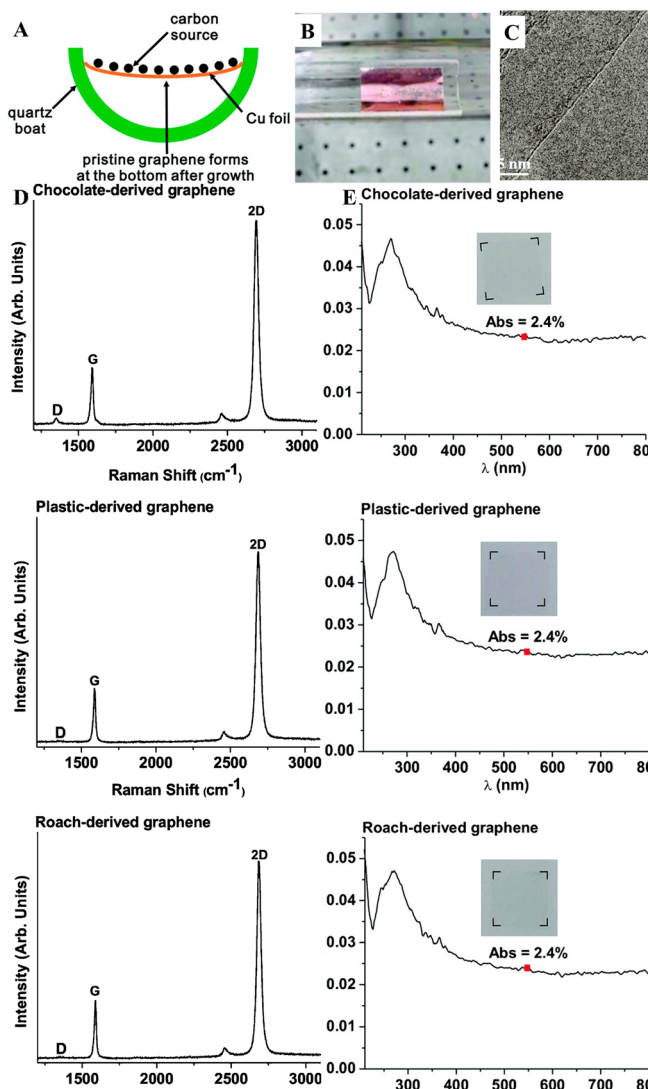
Mixed material sources, including food products, e.g. cookies and chocolate, insect fragments, and waste products, e.g. animal feces, were converted into monolayer graphene.<sup>180</sup> The unpurified carbon materials were placed on the surface of suspended Cu foil and then annealed at  $1050\text{ }^\circ\text{C}$  for 15 min under vacuum and  $\text{Ar}/\text{H}_2$  flow ([Figure 12](#)).<sup>180</sup> As the solid carbon decomposed and carbon atoms diffused across the Cu foil, a layer of graphene formed on the backside of the foil, whereas the original side of the foil retained the elemental residue. Regardless of the carbon source, graphene was of high purity, had few defects, and had  $\sim 97\%$  transparency. Even though precursors were rich in other elements, e.g. oxygen, nitrogen, iron, sulfur, and phosphorus, atoms of other elements were absent from the structure of the graphene, which consisted only of carbon. Used polypropylene plastics were converted into graphene flakes (GFs) with high yield via catalytic carbonization and organically modified montmorillonite catalyst. This catalyst promoted dissociation of waste plastic into light hydrocarbons and aromatics and acted as a catalytic template for carbonization of the light hydrocarbons and aromatics into GFs.<sup>181</sup>

Another extreme example that demonstrates reforming of complex carbon compounds into graphene involves human fingerprint ([Figure 13](#)).<sup>182</sup> A fingerprint consists of a wide array of proteins, amino acids, and lipids, which are distributed nonuniformly across the surface on which the print is made. Nevertheless, annealing of the sample at  $\sim 1000\text{ K}$  for several hours under ultrahigh vacuum yielded graphene which was very similar to that fabricated using pure synthetic precursor carefully distributed onto the surface via liquid precursor deposition. Ex situ liquid precursor deposition is an attractive method of delivering carbon precursors where the substrate has too small or even vanishing sticking coefficients for precursor molecules delivered from the gas phase.

From these examples it is evident that precursor-chemistry-independent graphene synthesis (process-driven synthesis) is achieved under high-temperature processing ( $>1000\text{ K}$ ) and vacuum conditions are necessary. In [section 5.2](#), we will discuss several examples that suggest that under plasma conditions it is possible to achieve process-driven, precursor-independent synthesis at much lower temperatures and much higher pressures.

### 5.1. Continuous Substrate- and Catalyst-Free Synthesis of Freestanding Graphenes

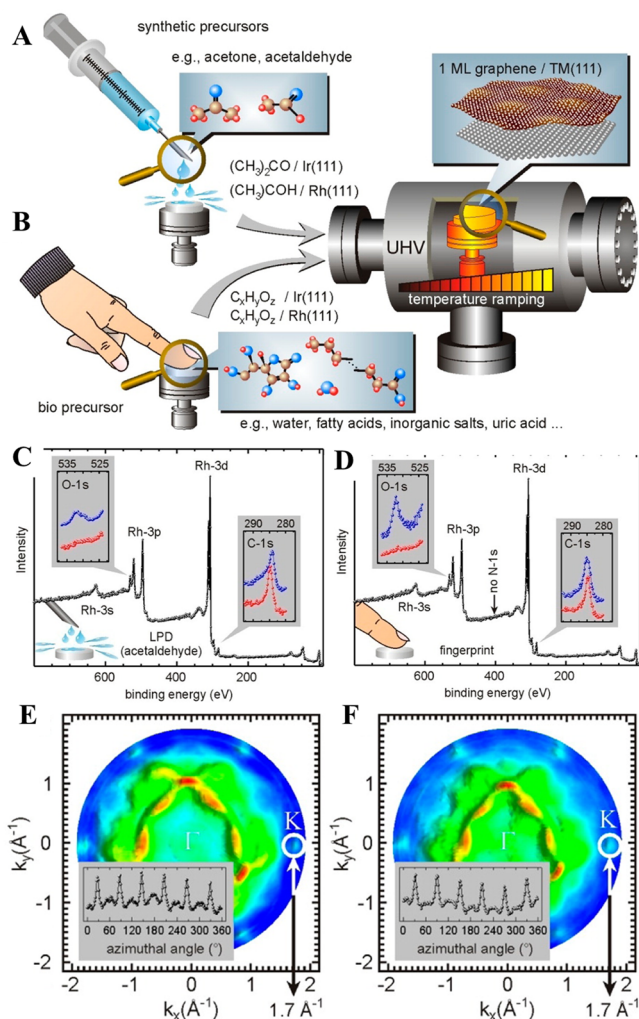
Freestanding graphene has been created without the use of substrates or graphite through gas-phase microwave synthesis at atmospheric pressure,<sup>81,183</sup> providing a potential avenue for the large-scale, continuous synthesis of graphene. Aerosols consisting of liquid ethanol droplets and Ar gas were introduced directly into argon plasmas, where the droplets rapidly ( $\sim 10^{-1}\text{ s}$ ) evaporated and dissociated. Graphene formed in the gas phase exhibited a highly ordered, oxygen-free structure ([Figure 14](#)) that was independent of the applied microwave power. The production rate increased from  $2\text{ mg min}^{-1}$  at  $250\text{ W}$  to  $6\text{ mg min}^{-1}$  at  $1050\text{ W}$ . This suggests that



**Figure 12.** Graphene synthesis from mixed carbon sources using a thermochemical approach. (A) Experimental setup. Cu foil is slightly bent within the quartz boat to contain the carbon precursors. (B) Photograph demonstrating complete transformation of a roach leg into a thin film. (C) TEM images of the edge of monolayer graphene derived from a cookie. (D) Raman spectra of graphene fabricated from three different sources show very similar quality of graphene. (E) UV-vis spectra of graphene were similar, independent of the carbon sources. The absorbance of each monolayer graphene film at 550 nm is approximately  $2.4 \pm 0.1\%$ . Insets show photographs of the monolayer graphene film of  $\sim 1 \text{ cm} \times 1 \text{ cm}$  in size (dashed line) after transfer onto a 1 mm thick quartz slide. Reprinted from ref 180. Copyright 2011 American Chemical Society.

while dissociation of ethanol took place in the plasma glow region and was enhanced at higher power, the formation and growth of graphitic materials occurred in the plasma afterglow where the neutral gas temperature is only moderately affected by the increased microwave power from 3000 K at 350 W to 3400 K at 1100 W.

Decreasing the plasma gas flow rate from 3.4 to 1.7 L/min resulted in the production of 3D graphite sheets and large bulk graphite structures along with graphene sheets.<sup>184</sup> The formation of bulk structures was attributed to the growth, collision, and stacking of individual graphene layers during the prolonged residence time in the reactor, whereas the formation

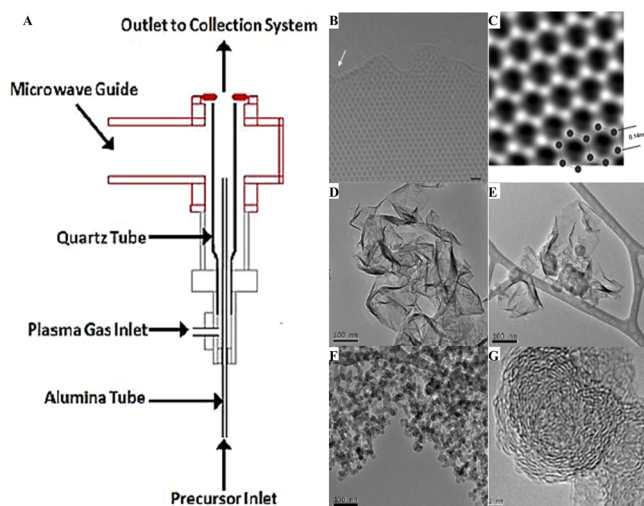


**Figure 13.** Liquid precursor deposition is used to produce graphene on a transition metal surface (e.g., Rh or Ir) from synthetic precursors (e.g., acetone, acetaldehyde) and mixed carbon sources (e.g., human fingerprint). (A, B) Schematics of the synthesis routes for (A) acetone and (B) fingerprint. Synthesis requires temperatures of  $\sim 1000 \text{ K}$  and ultrahigh vacuum. (C, D) XPS data (Al  $K\alpha$  excitation,  $\hbar\omega = 1486.6 \text{ eV}$ , normal emission) after graphene formation on a Rh(111) surface from (C) acetone and (D) fingerprint and degassing. Insets: high-resolution C 1s and O 1s spectra after deposition and degassing of the precursor (blue) and after graphene formation (red). (E, F) Fermi surface maps by angle-resolved ultraviolet photoelectron spectroscopy of graphene from (E) acetone and (F) fingerprint are very similar and display distinct spots at the K points characteristic of graphene. Reprinted from ref 182. Copyright 2014 American Chemical Society.

of graphitic particles arose as a result of the curving and closure of graphite sheets. At longer residence times, an increased number of collisions between the aromatic nuclei created via the dissociation of ethanol may have led to the formation of carbonaceous clusters, which underwent subsequent growth by coagulation and surface reactions and rapid-cooling-induced graphitization in the postplasma region.

Under equivalent synthesis conditions, changing the carbon precursor from ethanol to liquid methanol failed to yield solid matter, whereas liquid isopropyl alcohol resulted in dark, spherical carbonaceous particles of  $<100 \text{ nm}$  in diameter. These particles were fused together into large aggregates, and consisted of randomly oriented stacks of graphene planes and amorphous domains. It is possible that an adjustment in the





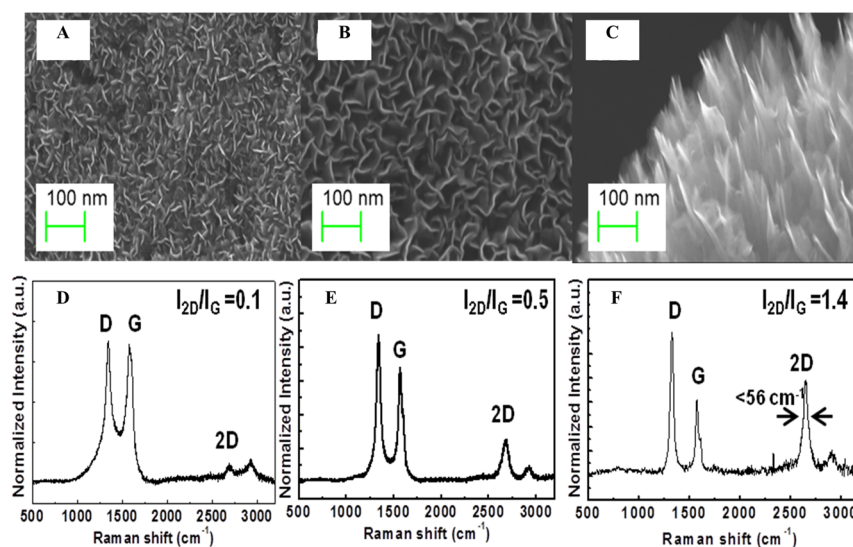
**Figure 14.** (A) Atmospheric-pressure plasma system used for substrate-free graphene synthesis. (B–G). TEM images of gas-phase synthesized graphene: (B, C) high-quality graphene produced from ethanol; (D, E) effect of reducing the plasma gas flow rate on the structure of graphene (at 350 W); (F, G) graphene produced from isopropyl alcohol at 1100 W. Panels A and D–G reprinted with permission from ref 184. Copyright 2010 IOP Publishing. Panels B and C reprinted with permission from ref 183. Copyright 2009 Royal Society of Chemistry.

residence time, specifically increased plasma gas flow rate in the case of isopropyl alcohol and decreased rate for methanol, may enable or substantially improve the quality of graphene produced. Similarly, the approach can be extended to other natural organic, synthetic, and mixed sources in liquid or gas state. We emphasize that the examples considered above are precursor-driven even at relatively high input power and process pressure. In the following, we will present examples of precursor-independent, process-driven synthesis of graphene from a variety of natural precursors.

## 5.2. Nonprecursor-Specific Synthesis of Surface-Supported Graphenes

A single-step, plasma-enabled, catalyst-free synthesis was demonstrated to convert a range of pure and mixed natural precursors, including milk, honey, butter, sugar, and methane, into a few-layer vertical graphenes directly onto Si/SiO<sub>2</sub> substrates.<sup>55,56,72,185</sup> Also known as carbon/graphene nanowalls, nanosheets, nanoflakes, and nanoflowers, vertically oriented graphene structures (VGSs) are a class of nanomaterials where “graphenic” platelets are arranged into typically vertically oriented networks on a substrate.<sup>54,55</sup> The vertical and lateral dimensions of individual nanosheets typically range from 0.1 μm to tens of micrometers, with nanosheet thicknesses of a few nanometers or less.<sup>54,186</sup> Structurally, TEM studies have shown each nanosheet to consist of few-layer (1–10 layers) graphene with an interlayer spacing of 0.34–0.37 nm.<sup>54,186</sup> When produced in the presence of plasmas, these VGS networks typically display vertical orientation in relation to the substrate, nonagglomerated three-dimensional internetworked morphology, controlled intersheet connectivity, and exposed ultrathin and ultralong edges. The VGS structures should not be confused with planar graphene films produced by CVD or mechanically exfoliated platelets which typically have quite different structural and morphological features in terms of defect level, arrangement, or atomic planes and other characteristics.

Although for some electronics applications continuous, defect-free, and reasonably large area films with large single-layer graphene domains are required to attain the desired superior physical, chemical, electrical, and thermal properties of graphene, the unique morphological and structural features of vertically oriented graphene flakes, e.g. readily accessible large surface areas and surface functionalization, may be of advantage for emerging energy, environmental, and catalysis applications, such as energy storage and conversion, and sensing.<sup>54,186</sup> It is important to note that the structure of vertically aligned graphenes is quite different from planar graphenes especially near the point of contact/integration with the substrate and near the exposed edges which can be closed (terminated) or



**Figure 15.** Plasma-enabled synthesis is rapid, taking less than 9 min to convert raw honey into vertically aligned graphene sheets. SEM images and Raman spectra show the evolution of graphene structure with plasma exposure time: from 3 min (A, D) to 5 min (B, E), to 9 min (C, F). Reprinted with permission from ref 72. Copyright 2013 Elsevier Ltd.



open. The structure of planar graphenes is more reliant on the substrate surface properties such as surface roughness compared to their vertically aligned counterparts. Plasma-enhanced fabrication of planar graphene may potentially be achieved by means of remote plasma, the use of which may eliminate the effects of the plasma electrical field and the ion bombardment on the orientation of the grown graphene films.<sup>159</sup>

Whereas conventional methods of graphene synthesis are mostly precursor-specific, using reactive Ar + H<sub>2</sub> plasmas, very similar structures were obtained irrespective of the state of the precursor, i.e. gaseous, liquid, or solid, or its chemical makeup, i.e. sugar, fat, or protein.<sup>55,56,72,185</sup> Importantly, an equivalent thermal process (gas composition, temperature) failed to produce graphene nanosheets, generating carbon fibers or porous carbon at 450 °C or amorphous carbon at 900 °C.

Plasma-assisted synthesis was also rapid, with the transformation of honey into fundamental building blocks and the formation of VGSs triggered between 1 and 3 min into the plasma treatment (Figure 15). After 5 min of the plasma processing, well-defined VGSs were formed. Longer processing (>9 min) yielded VGSs that were thinner, as reflected by  $I_{2D}/I_G$  ratio of 1.4 which was significantly higher than that obtained after 3 min, and had the best defined morphology of all samples produced. The reduction in graphene thickness was attributed to higher substrate temperature (up to 450 °C) and the reactive plasma etching due to ion and radical bombardment. Excessive bombardment of the graphitic structures by energetic argon, hydrogen, and oxygen radicals and ions may also generate defects in the structure.

The morphology of VGSs produced from honey, sugar, milk, butter, and methane was similar. VGSs from table sugar had the highest edge density of more than 1.7 km cm<sup>-2</sup>, whereas the average length of an edge (415 nm) was the highest for methane-derived VGSs.<sup>56</sup> A similar behavior was observed when VGSs were fabricated on a porous Ni foam substrate, with VGSs from methane precursor having a significantly lower density of thin edge planes compared to those derived from butter. The capacitance of methane-derived VGSs was also lower compared to butter-derived graphenes, with the latter exhibiting specific capacitances of up to 230 F g<sup>-1</sup> at a scan rate of 10 mV s<sup>-1</sup> and >99% capacitance retention after 1500 charge–discharge cycles at a high current density.<sup>55</sup> These results suggest that fatty substances such as butter may be suitable carbon sources for the synthesis of high-performance electrode materials for energy storage devices.

In addition to being shorter and simpler compared to other methods, plasma-enabled synthesis is more energy-efficient and hence cheaper than similar thermal processes. By using minimally processed, commercially available low-cost produce as a carbon source, further savings can be made. Given that honey is an abundant and renewable resource, this method of synthesis of VGSs is also more sustainable compared to thermal processes that rely on purified gaseous precursors.

The mechanism of plasma-assisted conversion into graphenes and the role of natural resource chemistry are yet to be fully elucidated. Plasmas represent a highly complex and dynamic environment. An Ar/H<sub>2</sub> plasma is rich in ionic species, including Ar<sup>+</sup>, ArH<sup>+</sup>, H<sup>+</sup>, H<sub>2</sub><sup>+</sup>, H<sub>3</sub><sup>+</sup>, and others. Water vapors that are released from the organic matter, e.g. honey or milk, as a result of the plasma heating may also undergo ionization and dissociation in the plasma bulk to produce a range of species,

including H<sup>+</sup>, OH<sup>-</sup>, etc., resulting in an even wider range of species.

Collectively, these ionic and radical species may interact with the dehydrated components of the organic precursor to produce carbon atoms that will reform into graphene sheets on the surface of the substrate. The chemistry of the dehydrated components varies with the source material; for example, honey dehydrates to monosaccharides (sucrose and fructose).<sup>72</sup> Dehydration and heating may also convert some of the fructose into hydroxymethylfurfural, a molecule that contains a furan ring as well as aldehyde and alcohol side groups. Plasma-generated species interact with these dehydrated molecules to produce carbon building units from which graphenes are formed.

The properties of VGSs can be controlled by hydrogen concentration and processing pressure. In the case of Ar/H<sub>2</sub> plasma-assisted conversion of honey, hydrogen concentrations outside the range of 30–60% resulted in the amorphous carbon layers rather than VGSs. In the process of butter conversion, a better graphitic ordering in VGSs was obtained at H<sub>2</sub> concentration of 80%. For graphene-based supercapacitor electrodes, VGSs with the sp<sup>2</sup> graphitic structure are preferred due to their enhanced charge storage capability.<sup>151</sup> Even though sp<sup>3</sup>-bonded carbon increases the charge transfer resistance, they also provide the structural disorder required for the electrochemically active materials, by producing a higher surface area for ion adsorption.<sup>55</sup>

H<sub>2</sub> concentration plays an important role in the nucleation and growth of many carbon-based nanostructures. In the plasma-assisted CVD, carbon building units are first extracted from the natural source and then reform into the hexagonal carbon rings of the graphene nanosheets. At a low pressure, H<sub>2</sub> can promote the nucleation and growth of VGS by enhancing the movement of these carbon building units toward the surface. Thus, increasing H<sub>2</sub> concentrations promotes graphitization of VGSs. At a certain concentration point, however, the etching effect of hydrogen species becomes more prominent, leading to the formation of defects and reduction in the VGS growth and graphitic ordering.<sup>53,55</sup>

### 5.3. Intentional Defect Creation and Functionalization

This section demonstrates that intentional in situ introduction of defects, pore creation, and functionalization are very useful and promising ways to attain desirable properties in the synthesized material, and discusses examples of the use of plasmas to achieve these objectives. Graphenes produced using plasma synthesis from natural resources are characterized by the presence of the long reactive edges, typically at ~1 km cm<sup>-2</sup>,<sup>56</sup> that should enhance chemical reactivity of these structures and facilitate graphene functionalization.<sup>187</sup> Ions and reactive radicals generated in the plasma are responsible for the formation of line and point defects in the graphene layers, and the decreasing thickness of the reactive edge as a function of exposure time.<sup>53</sup>

Natural precursors may provide an additional source of desirable defects. For instance, calcium, magnesium, phosphorus, and other elements present in natural honey were retained in the resultant VG structures. Plasmas also provide the means for in situ doping of carbon nanostructures by varying the composition of the gas mixture. By adding N<sub>2</sub> to Ar + H<sub>2</sub> + CH<sub>4</sub> plasmas, it was possible to control structural properties of the VGSs. Increasing the concentration of N<sub>2</sub> to 50% resulted in the loss of crystalline structure (presented by diminishing 2D

Raman peaks), increased degree of disorder (indicated by a broader G-peak), and incomplete graphene coverage of the substrate surface.<sup>188</sup>

We stress that plasma-enhanced synthesis of carbon nanostructures involves concomitant deposition and removal of carbon species from the surface, both of which are controlled by the nature of the species present in the plasma. Nitrogen radicals that form in the plasma as a result of the addition of N<sub>2</sub> to the gas mixture may interact with the substrate, forming a barrier that prevents carbon species from bonding to the surface. Cyanide species that are produced from the reaction between nitrogen and hydrocarbon species can act as an etching agent for graphitic structures, leading to the formation of thinner VGSs. Collectively, these processes affect the growth and structure and thus the properties of the VGSs.

Similar plasma environments can be used to produce graphene nanopetals with ultralong defective edges of up to 10<sup>5</sup> m/g and ultradense lattice vacancies that show robust ferromagnetism with saturation magnetization of up to 2 emu/g at 5 K and 1.2 emu/g at room temperatures (Figure 16).<sup>189,190</sup> The lattice vacancies can generate localized electronic states and magnetic moments due to the hybridization of p<sub>z</sub> orbitals in the  $\pi$ -band, and also induce ferromagnetic ordering and

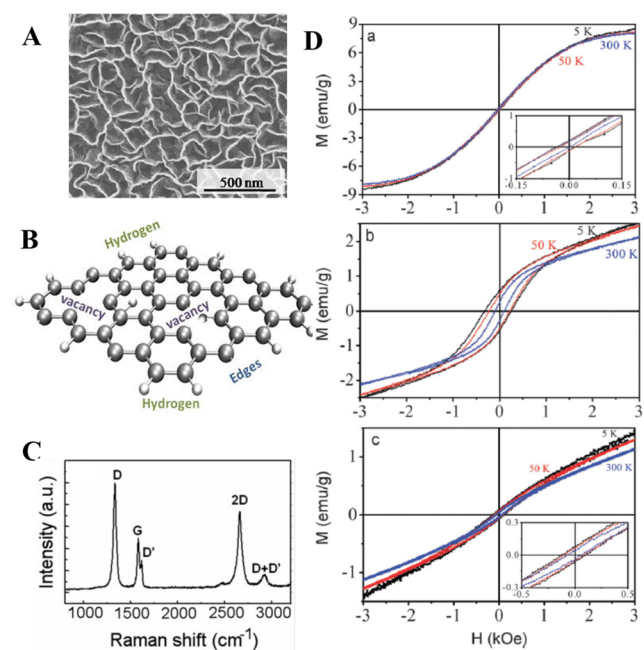
states where sublattice symmetry is broken. Furthermore, exposing the substrate surfaces to hydrogen plasma at high temperature facilitates adsorption of H atoms on the graphene surface, inducing the formation of hydrogen absorption defects on edges and vacancies not just at the surface but also at interlayers. The adsorbed H atoms can generate spontaneous magnetism in graphene via formation of C–H bonds and unpaired electrons.<sup>191</sup> As the stability of the magnetic configurations depends on the distance between H adatoms and the strength of exchange couplings between the defect-induced magnetic moments,<sup>192</sup> strong long-range coupling between local magnetic moments at the same sublattice of graphene petals can maintain room-temperature ferromagnetic ordering against thermal fluctuations. Further, the zigzag edges that along with armchair edges are present in graphene petals can be magnetic due to spin-polarized edge states,<sup>193</sup> where the net spin moment depends on the shape of the petal due to topological frustration of the  $\pi$ -bonds.<sup>189</sup> The chemisorption of H atoms at the ultralong edges of the petals gives rise to the formation of a spin-polarized band at the Fermi level and passivation of the  $\sigma$  dangling bonds, leaving the  $\pi$  orbitals unsaturated and carrying the magnetic moments.<sup>189</sup>

Importantly, ferromagnetic properties of plasma-produced graphenes can be tuned by controlling chemical composition of the carbon source, e.g. by using precursors with a wide range of carbon/oxygen (C/O) ratios.<sup>190</sup> Sucrose present in honey has C/O ratio of ~1:1, whereas palmitic and oleic acids in butter have 8:1 C/O ratios. Graphene nanoflakes produced from butter, milk, and honey were hydrogenated and contained a significant amount of defects: vacancy-type due to ion bombardment and boundary-type due to the presence of the edge plane. However, their magnetic properties differed significantly. Vertically aligned graphenes produced from a precursor with low oxygen content (butter) had saturation magnetic moment of 8 emu g<sup>-1</sup> at 3 kOe and 300 K, with a small ferromagnetic moment, whereas those made from oxygen-rich honey and milk had lower saturation magnetic moments of 2.1 and 1.0 emu g<sup>-1</sup> (at 3 kOe), respectively.<sup>190</sup> Honey-based graphenes had the highest ferromagnetic coercivity at 300 K of all graphene types. In a simple lipid chain, the oxygen is contained mostly as a side chain, leading to the formation of vertical graphenes with zero oxygen content, and hence high saturation magnetic moment and uniform but small ferromagnetic coercivity. On the other hand, oxygen in sucrose is held as a part of the aromatic ring, generating graphenes with moderate graphene oxide content and thus smaller magnetic moments and larger ferromagnetic coercivity.<sup>190</sup>

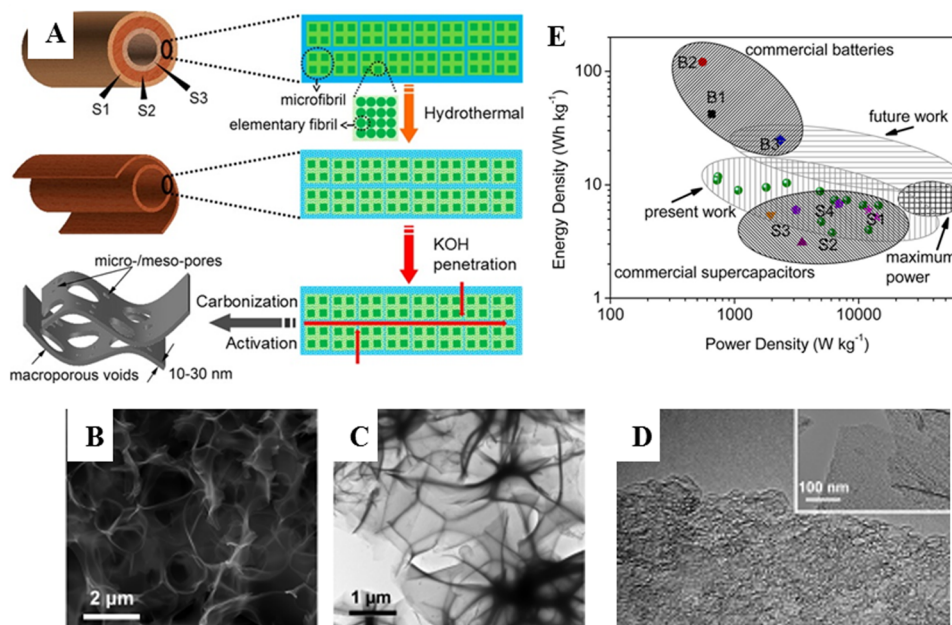
For many applications, 3D and composite/hybrid structures provide better functionality. Several hybrid structures comprising graphene sheets and another electrochemically active materials, such as metal oxides, conductive polymers, or CNTs, have been proposed to overcome limitations or further enhance the properties of surface-supported carbon nanostructures such as nanotubes and vertically aligned graphene flakes.<sup>121,151,194–199</sup>

## 6. SYNTHESIS OF 3D AND HYBRID NANOSTRUCTURES

Nondestructive chemical functionalization of graphene with other carbon nanostructures is important for applications in sensors and transducers. For instance, heterostructures comprised of single-layer graphenes and carbon nanomembranes decorated with functional amino groups form the active



**Figure 16.** Plasma-enabled graphene nanopetals fabricated from methane, and graphene nanoflakes produced from butter, honey, and milk feature a significant number of intentionally introduced defects which lead to ferromagnetic properties. (A) SEM of graphene nanopetals reveals ultralong reactive edges. (B) Proposed atomic structures of the graphene nanopetal with intentionally introduced hydrogen chemisorptions, edge, and lattice vacancy defects. (C) Raman spectrum of the graphenes produced from butter shows presence of a significant number of defects and hydrogenation of the graphene structure. (D) Temperature-dependent magnetic hysteresis loops for graphenes from butter (a), honey (b), and milk (c) suggest that ferromagnetic behavior of vertically oriented graphenes can be controlled by changing the chemistry of the precursor material. Panels A–C reprinted with permission from ref 189. Copyright 2014 AIP Publishing LLC. Panel D reprinted with permission from ref 190. Copyright 2013 Royal Society of Chemistry.



**Figure 17.** Hemp-derived interconnected carbon nanosheets for ultrafast supercapacitors. (A) The synthesis process was strongly influenced by the three different structural layers of the fiber. (B–D) The interconnected, porous, and partially ordered structure of the hemp-derived nanosheets was confirmed by SEM (B) and TEM (C, high-resolution D). (E) Devices fabricated using hemp-derived nanosheets as compared against commercial batteries and supercapacitors (B1, Panasonic NiH(D); B2, Sanyo Li ion; B3, Bolder Pd acid; S1, Maxwell BCAP3000 and BCAP0310; S2, Panasonic 800F; S3, Superfarad 250 F; S4, Saft Gen2 and Gen3); data for hemp-based device is for 20–100 °C temperature range; data for other devices is the maximum energy and power densities. Reprinted from ref 206. Copyright 2013 American Chemical Society.

layer of the field effect transistor.<sup>200</sup> For biochemical and biomedical uses, these hybrid structures offer a favorable combination of physicochemical, mechanical, and optical properties, enabling selective entrapment of various chemical and biological agents while maintaining their activity. Dense forests of long, vertically aligned multiwall carbon nanotubes grown on activated graphite-like carbon film supports provide the means for immobilization of enzymatic biocatalysts while protecting the attached enzymes from shear forces and microbial attacks present in bioreactors.<sup>126</sup> In this case, the enzymes preferentially covalently attach to the underlying carbon film, whereas the layer of CNTs serves as a physical barrier that prevents flow detachment and bacterial colonization of the film surface. For this type of applications, plasma-assisted synthesis not only can be used to lower the cost of synthesis of such well-aligned structures, but also can be used for postsynthesis chemical functionalization of the carbon-based device platforms.

Surface and self-supported 3D all-carbon scaffolds hold potential for applications in the areas of energy storage, electronics, supercapacitors, photovoltaic cells, field emission devices, smart sensors, and medical devices. These scaffolds can comprise a range of nanostructures organized in a patterned or random manner, such as pristine aligned or entangled CNTs, or CNTs and graphene,<sup>201,202</sup> as well as hierarchical and ordered porous carbon nanomaterials.<sup>203</sup> These materials can be produced from a variety of carbon-rich precursors, including polymers, copolymers, biomass-derived polymers, and gaseous precursors.

Currently available methods offer only limited control over the formation of covalent bonds between carbon nanostructures within the scaffold, thus limiting their structural integrity, stability, and electrical conductivity. Addition of a doping agent, e.g. boron, during CVD of CNTs can induce the desirable

localized and topological defects, leading to the formation of covalent bonds between the CNTs, as well as CNT functionalization.<sup>204</sup> Using benzoyl peroxide, MWCNTs can be transformed into an all-carbon macroscopic scaffold with the bulk electrical conductivity of  $2 \times 10^{-1} \text{ S cm}^{-1}$ , which is comparable to or higher than that of thin films of CNTs or graphene with large networks of  $\text{sp}^2$  carbon atoms, and scattered regions of  $\text{sp}^3$  carbon atoms.<sup>205</sup>

Natural materials with complex multilayered structure, such as that of a hemp bast fiber (a waste byproduct of hemp processing) may facilitate the development of 3D structures with interesting architectures and multiscale morphologies (Figure 17).<sup>206</sup> Partially graphitic porous carbon nanosheets prepared from a hemp bast fiber via carbonization, activation, and thermal treatment at 700–800 °C had electrical conductivity of 211–226  $\text{S m}^{-1}$  and promising power–energy characteristics. Consequently, the nanosheets are well-suited for ionic-liquid-based supercapacitor applications.<sup>206</sup> The interconnected two-dimensional nanosheets were 10–30 nm, contained high levels of mesoporosity (~58%), and had high specific surface area of up to 2287  $\text{m}^2 \text{ g}^{-1}$ . The maximum energy density of the assembled supercapacitor device is 12  $\text{Wh kg}^{-1}$ , which is higher compared to some commercially available analogues. Carbon nanosheets were also successfully prepared from a mixture of waste plastics, such as polypropylene, polyethylene, polystyrene, poly(ethylene terephthalate), and poly(vinyl chloride) on organically modified montmorillonite.<sup>207</sup> Although promising, the above-discussed examples required multistep processing (e.g., synthesis of hemp-based nanosheets involved two activation steps, carbonization, filtration, two washing and drying steps, grinding, annealing, etc.), which was lengthy (for the same example, 24 h of carbonization and 12 h oven drying alone) and required the use of acids (e.g., sulfuric acid) and strong bases (e.g., potassium



**Table 3.** Comparative Assessment of the Characteristics of Waste-Derived Carbon Nanomaterials for Their Use in Supercapacitors (Partially adapted from and reproduced with permission from ref 212. Copyright 2013 Royal Society of Chemistry)

material	activating agent	BET surf. area ( $\text{m}^2 \text{g}^{-1}$ )	max capacitance ( $\text{F g}^{-1}$ )	measured at	electrolyte	ref
rice husk	NaOH	1886	210	$0.2 \text{ mA g}^{-1}$	3 M KCl	215
coconut shell	$\text{ZnCl}_2$	1874	268	$1 \text{ A g}^{-1}$	6 M KOH	216
fir wood	$\text{H}_2\text{O}$	1131	140	$25 \text{ mV s}^{-1}$	0.5 M $\text{H}_2\text{SO}_4$	217
pistachio shell	KOH	1096	120	$10 \text{ mV s}^{-1}$	0.5 M $\text{H}_2\text{SO}_4$	218
fir wood	KOH	1064	180	$10 \text{ mV s}^{-1}$	0.5 M $\text{H}_2\text{SO}_4$	218
poplar wood	$\text{HNO}_3$	467	234	$10 \text{ mA cm}^{-2}$	2 M KOH	219
bamboo	KOH	1251	260	$1 \text{ mA cm}^{-2}$	30 wt % $\text{H}_2\text{SO}_4$	220
banana fibers	$\text{ZnCl}_2$	1097	74	$500 \text{ mA g}^{-1}$	1 M $\text{Na}_2\text{SO}_4$	221
corn grains	KOH	3199	257	$1 \text{ mA g}^{-1}$	6 M KOH	222
waste coffee beans	$\text{ZnCl}_2$	1019	368	$50 \text{ mA g}^{-1}$	1 M $\text{H}_2\text{SO}_4$	223
waste newspaper	KOH	416	180	$1 \text{ mA cm}^{-2}$	6 M KOH	224
waste office paper		542		$5 \text{ mV s}^{-1}$	0.1 M KOH	225
recycled filter paper	$\text{ZnCl}_2$	2170	302	$1 \text{ A g}^{-1}$	6 M KOH	226
seaweeds	no activation	746	264	$200 \text{ mA g}^{-1}$	1 M $\text{H}_2\text{SO}_4$	227
sugarcane bagasse	$\text{ZnCl}_2$	1788	300	$250 \text{ mA g}^{-1}$	1 M $\text{H}_2\text{SO}_4$	228
cassava peel waste	KOH	1352	264	—	0.5 M $\text{H}_2\text{SO}_4$	229
sunflower seed shell	KOH	2509	311	$250 \text{ mA g}^{-1}$	30 wt % KOH	230
argan seed shell	KOH/melamine	2062	355	$125 \text{ mA g}^{-1}$	1 M $\text{H}_2\text{SO}_4$	231
<i>Platanus</i> fruit	KOH	1215	216	$1 \text{ A g}^{-1}$	1 M $\text{H}_2\text{SO}_4$	232
neem dead leaves	no activation	1230	400	$500 \text{ mA g}^{-1}$	1 M $\text{H}_2\text{SO}_4$	212
loofah sponge	KOH	1733	304	$1 \text{ A g}^{-1}$	6 M KOH	233
brown seaweed		1080	188	$200 \text{ mA g}^{-1}$	KOH, $\text{Na}_2\text{SO}_4$	234
<i>Enteromorpha</i> sea lettuce	$\text{ZnCl}_2$	1651	103	$400 \text{ mA g}^{-1}$		235

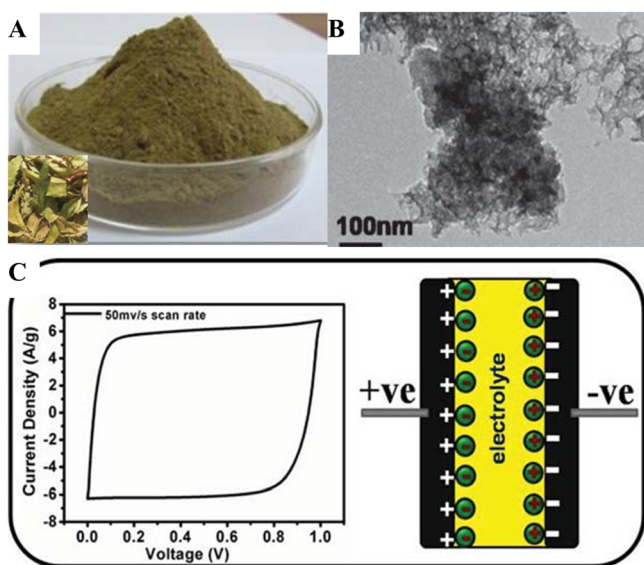
hydroxide). As such, they were less adequately aligned with such principles of green chemistry as energy and process efficiency, and use of safer chemicals. For comparison, plasma-assisted methods for conversion of raw carbon sources into VGSs discussed earlier were single step, lasted for seconds to minutes, and did not employ hazardous chemicals.<sup>42,55,56,72,185</sup>

Other examples of synthesis of 3D nanostructures include electrically conductive hybrid compounds derived from a mixture of sucrose, a fibrous magnesium silicate, and water, using microwave and conventional heating.<sup>208</sup> The resultant graphene-like–clay nanocomposites were characterized by room temperature conductivity of  $10^{-2} \text{ S cm}^{-1}$  and a relatively high specific surface area, making them well-suited for use as electrode and sensor materials.<sup>209</sup> Other sugars, such as glucose, xylose, maltose, sucrose, amylopectin, and starch,<sup>210</sup> can be hydrothermally converted into a range of carbon materials, with the precursor type playing a significant role in deciding the properties of the final material. Interestingly, all of the tested hexose sugars, regardless of their complexity, first converted into hydroxymethyl furfural, and then condensed to form a carbon-like material of similar morphology, and chemical and structural composition. Xylose on the other hand converted into furfural, reacting further to produce a material similar to that synthesized from pure furfural. In addition to pure carbohydrates, proteins and complex biomass sources can also be transformed into useful functionalized and hybrid carbon materials.<sup>211,212</sup> However, in all of these examples, both the process chemistry and the state of the precursor play a decisive role in defining the properties of the resultant material.

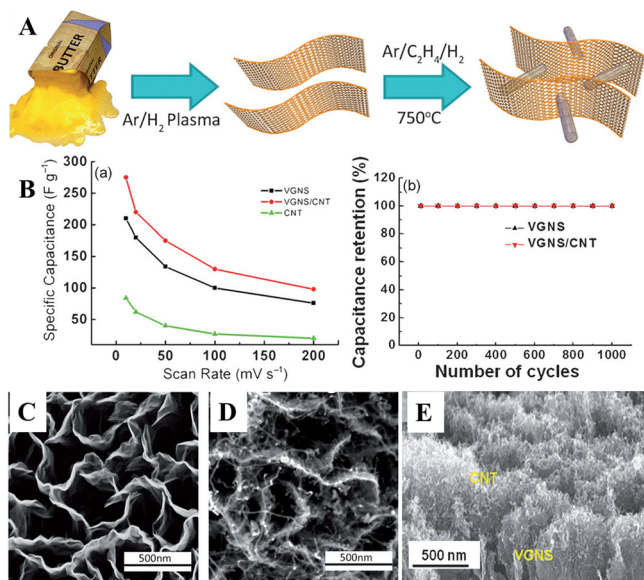
Single-step pyrolysis of raw and waste materials into functional nanomaterials have also been reported (Table 3), however the synthesis was precursor-driven, depending on both the chemistry and the state of the carbon source material.<sup>213</sup> Carbonization of proteins, such as oxygen-rich seaweed-derived

sodium alginate, results in a material with a low specific surface area, high electrical conductivity, and capacitance values due to the oxygen present in the carbon network participating in pseudofaradaic charge-transfer reactions.<sup>214</sup> Waste *Azadirachta indica* leaves have also been successfully reformed into conductive microporous carbon with a high surface area of about  $1230 \text{ m}^2 \text{g}^{-1}$ , a specific capacitance of  $400 \text{ F g}^{-1}$ , and an energy density of  $55 \text{ Wh kg}^{-1}$  (at  $0.5 \text{ A g}^{-1}$  in aqueous 1 M  $\text{H}_2\text{SO}_4$ ) (Figure 18), using single-step pyrolysis.<sup>212</sup> Naturally present in the leaves in trace amounts, metals facilitated chemical activation of the carbons during carbonization; the composition and the constitution (fresh vs dead leaves) of the carbon source affected the conductivity and microporosity properties of the resultant carbonaceous materials, even though high temperatures (up to  $1000^\circ\text{C}$  for 5 h in Ar atmosphere) were used.

Reactive plasma environment provides a pathway for the synthesis of synergistically integrated natural-resource-based vertically oriented graphene nanosheets (VGNSs) and CNTs on different current collectors with a low contact resistance, such as flexible graphite paper. Following the process for the conversion of commercially available low-cost natural precursors, such as butter and honey, VGNSs can be formed on the surface of graphite paper without the need for external heating or catalyst, yielding materials properties that are largely independent of the chemistry and state of the precursor.<sup>55,56,72,188</sup> Strong plasma–surface interactions in the plasma sheath drive the nucleation, formation, and vertical orientation of the VGNSs as opposed to amorphous carbon produced by thermal heating alone. A thermal CVD process is then used to directly grow CNTs on Mo/Co catalyst-loaded VGNSs (Figure 19).<sup>185</sup> The VGNS/CNT hybrid electrode fabricated in this manner possesses a high specific capacitance of  $278 \text{ F g}^{-1}$  at  $10 \text{ mV s}^{-1}$  in a low-concentration aqueous electrolyte, and a



**Figure 18.** (A) Ground powder of dead plant leaves of *Azadirachta indica* (dry waste, inset) is converted into functional microporous conducting carbon by single-step pyrolysis without any activation. (B) HR-TEM images of the carbon derived from dead plant leaves show a highly porous network morphology, with pore size of  $<2$  nm and onion-like  $n$ -layer graphitic character. (C) The synthesized functional carbon exhibits specific capacitance of  $88 \text{ F g}^{-1}$  at a current density of  $2 \text{ A g}^{-1}$  in organic electrolyte. The areal capacitance value is  $32 \mu\text{F cm}^{-2}$ . Reprinted with permission from ref 212. Copyright 2013 Royal Society of Chemistry.



**Figure 19.** Plasma-enabled fusion of VGNSs and CNTs for high-performance supercapacitor electrodes. (A) Schematic for the direct growth of CNTs onto VGNSs. (B) Rate capabilities of pristine VGNS (black), VGNS/CNTs hybrid structures (red), and pure CNT (green); cycle stability of the VGNS and VGNS/CNTs hybrid structures at  $5 \text{ A g}^{-1}$  for 1000 cycles. (C) SEM micrograph of pristine VGNS prior to CNT growth and (D) the final hybrid VGNS/CNTs nanoarchitecture in which the graphene nanosheets were decorated with a high density of CNTs. (E) Cross-sectional SEM images of the VGNS/CNTs hybrid structure. Reprinted with permission from ref 185. Copyright 2014 Wiley-VCH Verlag GmbH & Co. KGaA.

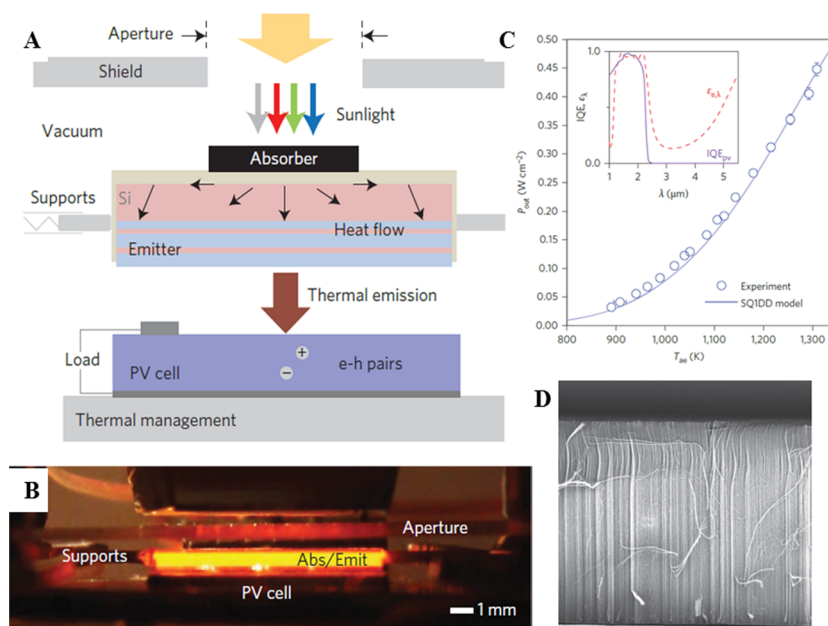
capacitance retention of  $>99\%$  after 8000 charge/discharge cycles. Although currently there are no reports on this matter, it may in principle be possible to use a natural precursor inherently rich in the mineral necessary to catalyze the subsequent growth of CNTs. A similar approach is discussed in section 10.

## 7. CONTROLLING SURFACE ORGANIZATION OF NANOSTRUCTURES: CASE OF CNTS

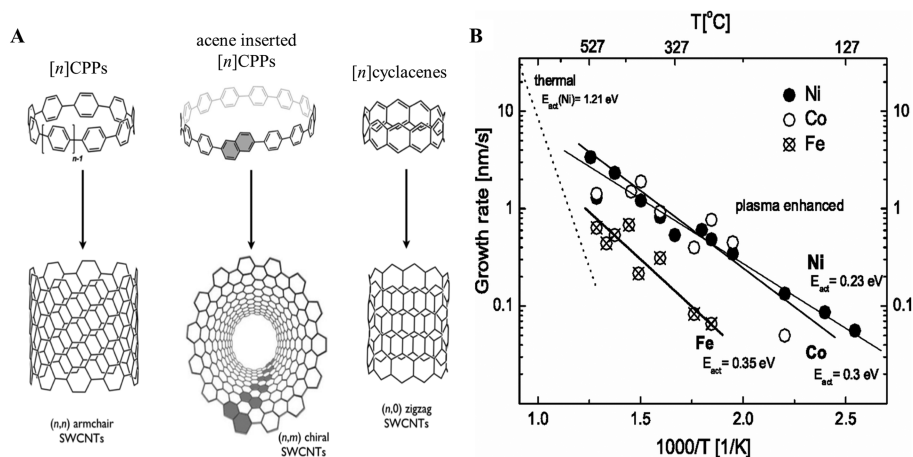
We have already established that there are numerous natural, abundant, and low-cost materials that can replace highly purified carbon precursors, and minimize the number of processing steps used to prepare the catalyst-loaded support. At the same time, in the vast majority of the examples that did not use plasmas, high-temperature, lengthy processing and a variety of processing gases were necessary to enable the synthesis of the carbon nanostructures of suitable quality. In most instances, the structure and surface organization of nanostructures grown using natural materials were difficult to control, particularly under relatively benign processing conditions prescribed by the principles of green synthesis. Surface organization refers to location, orientation/alignment, density, and intertube spacing of CNTs. However, in order to fully realize their potential as materials in microelectronics, sensors, or thermal management surfaces, the production of nanomaterials should not only be low-cost, reliable, and environmentally friendly, but also yield structures with properties that address the stringent requirements imposed by the envisaged applications. For example, if CNTs are to outperform Cu-based interconnects, they need to be grown on conductive supports in the form of high-density vertically aligned forests, in patterned structures (e.g., using predelineated patterns made of particles or holes), and at a maximum tolerance temperature of microelectronic devices which is approximately  $450^\circ\text{C}$ .<sup>236</sup>

In this section, plasma-enabled in situ surface organization of CNTs will be discussed. CNTs offer a favorable combination of high thermal conductivity, mechanical strength, and tunable electrical properties. Electronic transport in metallic SWCNTs and MWCNTs occurs without scattering along the length of the tube, which allows them to carry high currents with minimal heating.<sup>237</sup> Their conductivity, electrical and mechanical stability, and high accessible surface area make CNTs a valuable electrode material for energy storage devices and flexible touchscreens, as their use can enable mechanical flexibility, higher power densities, and faster charge/discharge rates and prolong device lifespan. The high electrical conductivity and accessible surface area allows nanotube-graphene composite materials to achieve high electrical double layer capacitances, which can be further enhanced by pseudocapacitance arising from surface functionalization and using pseudocapacitive materials.<sup>238</sup> If produced at lower cost, using more energy-efficient processes and nontoxic precursors, supercapacitors based on carbon nanostructures may provide an attractive environmentally friendly means for energy storage, particularly for applications where frequent charge and discharge cycles at high current and short duration are required.

For the majority of applications in nanoelectronics and energy devices, CNTs must be organized on the surface, e.g. as horizontally or vertically aligned arrays. For instance, vertically aligned carbon nanotubes are effective solar absorbers, combining high-temperature stability in vacuum, thermal conductivity, and their nearly ideal absorptance of  $>0.99$ , the characteristics required for absorbing highly concentrated



**Figure 20.** Vertically aligned CNTs as effective absorbers for energy harvesting technologies including TPV. (A) Operating principle of TPV devices fabricated using vertically oriented CNTs forests as absorbers. Optical image (B) and operating characteristics (C) of CNT-based TPV. (D) SEM image of the oriented dense CNT forest used as an absorber. Reprinted with permission from ref 239. Copyright 2014 Nature Publishing Group.



**Figure 21.** Properties of CNTs depend on the nature of the carbon precursor and the catalyst, the synthesis temperature and the synthesis method used. (A) In bottom-up synthesis, organic templates can be used to induce specific  $(n,m)$  chirality in SWCNTs, which in turn will determine whether the SWCNTs are metallic or semiconducting. (B) Arrhenius plots for CNT growth rates on different catalysts.  $C_2H_2$  diluted in  $NH_3$  is used as a carbon source. The dotted line is the growth rate variation for Ni thermal CVD. Panel A reprinted with permission from ref 251. Copyright 2015 IOP Publishing Ltd. Panel B reprinted with permission from ref 252. Copyright 2005 American Physical Society.

irradiance at elevated emitter-to-absorber area ratios. With currently reported efficiencies of 3.2%, solar thermophotovoltaic (TPV) devices based on CNT array absorbers may become a viable avenue for energy generation by harnessing the entire solar spectrum, being scalable, compact, and able to store energy in thermal or chemical form (Figure 20).<sup>239</sup> Where spectral selectivity is desired, e.g. when CNTs are used as a solar selective coating, this can be achieved by varying the properties of the CNTs, particularly their length, by varying the density of the CNT array, and by using a suitable tandem absorber beneath the CNT layer.<sup>240</sup>

In electronics, semiconducting CNTs are promising channel materials for extending complementary metal-oxide-semiconductor (CMOS) device performance in very large scale integration (VLSI) technologies.<sup>241,242</sup> Vertically aligned

MWCNTs are promising microelectronic interconnects capable of effectively dissipating heat from sensitive active devices, owing to the low resistance to electron current mostly arising from the contact between the nanotube and the contact material such as the growth substrate.<sup>243</sup> Vertically aligned CNTs are well-suited as electron emitting sources in low-voltage field emission displays due to their high aspect ratios.<sup>244</sup> Narrow single-walled nanotubes have been used as flexible and stretchable nanoscale transistor elements,<sup>245–247</sup> with a rather simple prototype computer built entirely using CNT-based transistors already reported.<sup>248</sup> In the future, digital circuits based on CNT transistors can exceed the energy efficiency (energy–delay product) of silicon-based devices. However, issues associated with CNT fabrication and integration, namely CNT separation, energy cost of CNT production, etc., that



affect the cost of the devices rather than the energy efficiency of operation of these devices should be carefully addressed for this technology to become viable.

It is evident that in situ surface organization of the CNTs may be advantageous, by reducing the number of steps required in the production of aligned (or otherwise organized) nanostructures. However, the challenge of surface organization is not the only challenge in the field of CNT synthesis that requires addressing. First, to be commercially relevant, CNTs should be produced at low cost and at large scale without compromising their quality. Second, CNTs need to be synthesized with the necessary level of selectivity with regard to their chemical structure, morphology, and electronic properties,<sup>249</sup> which is directly linked to the third challenge of understanding (and hence the ability to control) the mechanisms of CNT assembly and organization. Electrical properties of single-walled carbon nanotubes vary between metallic and small-gap semiconducting depending on the way the sheet of graphene is wrapped (represented by  $n$ ,  $m$  indices),<sup>250</sup> which in turn determines the nanotube diameter and chirality (Figure 21).<sup>251</sup> Hence, to enable economically viable large-scale production of future electronics and energy devices that employ highly organized arrays of CNTs, the synthesis at scale may need to rely on cheap and efficient bulk-growth methods coupled with CNT self-assembly or alternatively controlled growth directly on the substrate of choice.<sup>252</sup>

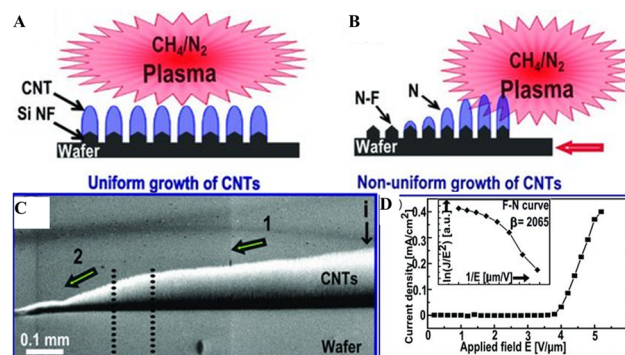
Popular methods to produce CNTs include arc discharge method, laser vaporization, chemical vapor deposition, and spray pyrolysis. In the former, graphite electrodes are evaporated in electric arcs at very high temperatures ( $\sim 4000$  °C) to form well-crystallized, yet impurity-containing CNTs. In laser ablation processes, high-purity graphite (99.99%) targets are evaporated by high-power, expensive lasers in a high-temperature environment, forming CNTs of good purity and temperature-dependent tube diameter. Catalytic CVD is considered as one of the most scalable, low-cost, and efficient processes to produce CNTs, with milder synthesis conditions compared to arc discharge or laser ablation. However, the temperatures are still high to be considered green synthesis.

Plasma environment is known to strongly influence dissociation and recombination processes in the gas phase and at the surface, and thus the kinetics of nucleation, growth, self-organization, and self-assembly of surface-supported nanostructures.<sup>253</sup> In conventional thermal CVD, dissociation of carbon precursors is purely thermal, requiring temperatures above 800 °C. In plasmas, on the other hand, in addition to thermal processes, electron-impact dissociation of precursors in the gas phase is supplemented with ion-assisted dissociation at the catalyst nanoparticle (CNP) surface. Surface recombination of ionic and radical species leads to localized CNP heating, which allows CNP to reach high temperatures without the need for external heating of the substrate. By minimizing or avoiding external substrate heating, CNTs can be produced in a more energy-efficient manner, which aligns well with the energy conservation guiding principle of green synthesis. Furthermore, lower overall temperature of the substrate reduces the rate of evaporation and desorption of building units, leading to better material efficiency of the plasma-assisted processing. The formation of the graphene monolayer from which single-walled nanotubes form also occurs faster in the plasma environment, as it is primarily driven by surface diffusion of carbon on the CNP surface, and not bulk diffusion characteristic of thermal

processes.<sup>53</sup> Reactive hydrogen species produced in plasmas help maintain the catalytic activity of the CNPs by etching amorphous material and preventing catalyst from surface oxidation. Other beneficial contributions of plasmas include ion-enhanced surface mobility and solubility of carbon atoms in CNPs,<sup>254</sup> and prevention of CNP agglomeration.<sup>53</sup>

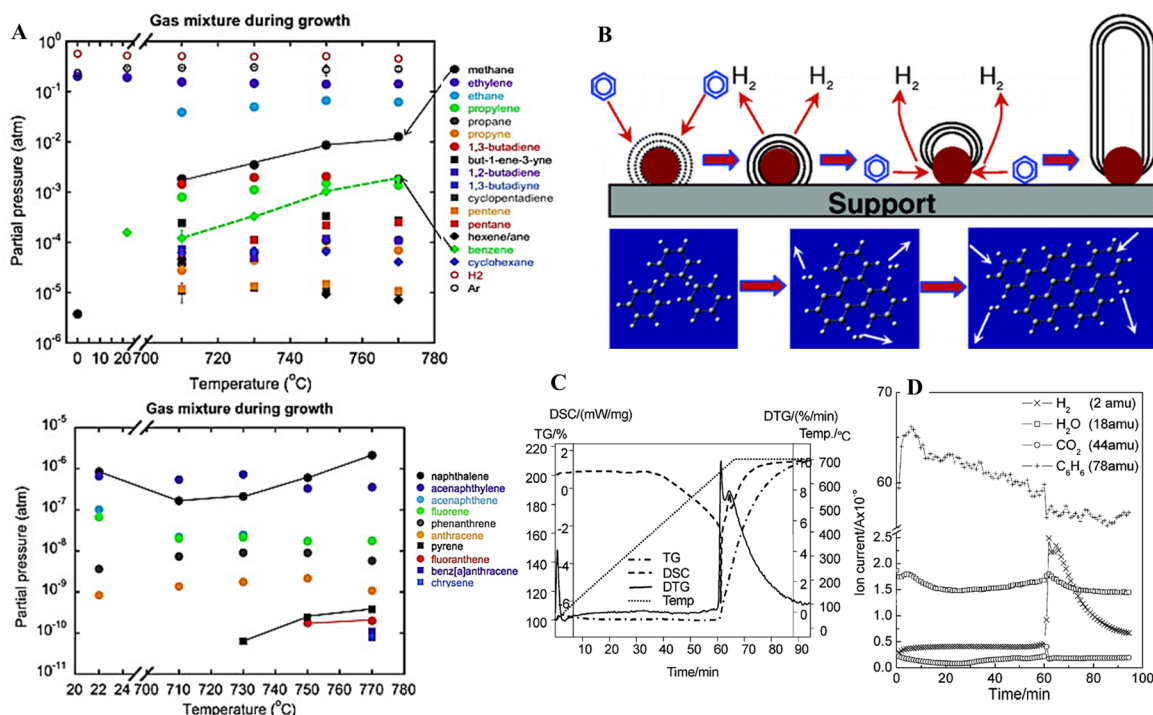
For controlled growth of CNTs directly on the substrate of choice, plasma environments uniquely combine the ability to drive surface organization with the high chemical reactivity that enables catalyst-free synthesis of carbon nanostructures directly on support materials, such as Si. When thin linear features written on a Si wafer are directly exposed to nonuniform methane-based plasmas in the absence of external heating or catalyst, linear and dot arrays of vertically aligned CNTs are produced at high rate.<sup>255</sup> Under similar thermal CVD or remote plasma conditions, the CNT growth is not observed, suggesting that direct exposure of the Si features to the plasma is required. Plasma exposure makes Si catalytic by carbonizing small Si features to produce a segregated SiC nanophase at the tip of the Si nanostructure, which acts as a catalyst for CNT nucleation.<sup>53</sup> This plasma-specific effect makes oxide and metal catalysts redundant, facilitating direct, catalyst-free integration of surface-organized CNTs into Si-based nanodevices. The turn-on field  $E_0$  of these vertically aligned CNTs is  $\approx 4.2$  V  $\mu\text{m}^{-1}$ , indicating the absence of current-blocking oxide layer between the CNTs and the substrate nanofeatures.

In addition to uniform growth of surface-aligned CNTs (Figure 22A),<sup>255</sup> a variety of morphological and structural



**Figure 22.** Plasma-enabled, morphologically graded catalyst-free CNT arrays growth directly on linear Si features. (A, B) Effect of relative positioning of the substrate and the plasma on the synthesis of uniform (a) and length-graded (b) arrays; no nucleation takes place in remote plasmas. Si NF, N, and N-F denote Si nanofeatures, nucleated CNTs, and nucleation-free areas, respectively. (C) SEM image of a length-graded CNT array. (D) Field-emission current density of the CNTs, which were integrated in a standard field-emission device configuration; the calculated field-emission enhancement factor  $\beta$  is shown in the inset. Reprinted with permission from ref 255. Copyright 2012 Wiley-VCH Verlag GmbH & Co. KGaA.

gradients can be achieved by controlling the lengths and orientations of the linear features with respect to the center of the spatially localized plasma discharge. For example, when the substrate was oriented so as to align the linear features with the direction of the plasma density gradient, CNT arrays with gradually decreasing lengths away from the plasma were observed (Figure 22B). The field emission properties of the CNT arrays were comparable to those of bulk CNT forests deposited directly on a metal cathode. Although further efforts are required to lower the temperatures of the plasma-enabled



**Figure 23.** Effect of precursor chemistry on the precursor dissociation and carbon nanostructure reassembly. (A) Ex situ gas chromatography of the exhaust gas. Increasing concentrations of specific volatile organic compounds and polycyclic aromatic hydrocarbons are correlated with the structural transition from synthesis of carbon nanofibers to crystalline CNTs. (B) Proposed mechanisms for the C<sub>6</sub>-based growth mechanism of CNTs with benzene precursor as analyzed by in situ thermal analysis coupled with mass spectroscopy. Benzene molecules adsorbed on catalyst surface are dehydrogenated and aggregate to form graphene sheets on the catalyst surface. CNTs develop through sequential incorporation of the h-C<sub>6</sub> into the graphene layers through surface diffusion. Thermogravimetry–differential scanning calorimetry profiles of the preparation process (C) and the change of the ion currents for certain atomic mass units during the experimental period (D) confirm the reduction of the oxide species of the catalyst, resulting in the formation of H<sub>2</sub>O (18 amu) and CO<sub>2</sub> (44 amu) species. Panel A reprinted with permission from ref 267. Copyright 2011 Elsevier Ltd. Panels B–D reprinted from ref 270. Copyright 2003 American Chemical Society.

CNT syntheses to the temperatures appropriate for processing of heat-sensitive thin film or polymer devices, considerable efforts in this area of research yield promising results for green chemistry.

## 8. EFFECT OF PRECURSOR CHEMISTRY ON CNT SYNTHESIS

In section 7, we already briefly mentioned that, even though CNT synthesis involves extensive decomposition of precursor into carbon atoms and very small fragments, and subsequent reassembly of the carbon-bearing species, the chemical structure, morphology, deposition rate, and yield of the carbon nanostructures is in many cases determined by the chemistry of the precursor. For most synthesis methods, the processing environment (i.e., temperature, pressure, processing gas, substrate, catalyst)<sup>256–258</sup> is determined by the reactivity of the carbon source under these conditions, namely its binding affinity to the catalyst and prevailing dissociation mechanisms.<sup>259–261</sup> While it may complicate high-volume conversion of minimally processed raw and waste materials, the diversity of the natural chemistries suggests that it may be possible to selectively target low-cost, largely homogeneous natural precursors for specific applications. Several reports have highlighted the role of precursor-derived intermediates in the formation of carbon nanotubes and nanofibers.<sup>262</sup> Hence, it may be possible to find precursors that decompose into fragments that can be directly incorporated into the growing CNT structures, and potentially lower the temperature and

time required for the synthesis. In this section, we will consider the examples of precursors, which, when broken down, generate structures that can be directly used in the assembly of CNTs.

Let us first consider the effect of degree of unsaturation in the conventional thermal synthesis of CNTs. In the study by Hernadi et al.,<sup>263</sup> hydrocarbons containing unsaturated bonds in their structures were found to be more reactive toward CNT synthesis than saturated counterparts, and precursors with isolated triple bonds were more reactive than those with isolated double bonds or aromatic structure. Polycyclic molecules, such as naphthalene and anthracene, are more unstable than aromatic compounds, e.g. benzene, and thus the critical temperature for SWNT conversion for these precursors is lower (by ~100 °C) than that for benzene.<sup>259</sup> A difference in a single methyl group, e.g. that between methylacetylene and acetylene, was found to induce significant variations in the yield and the structure of CNTs formed at 720 °C.<sup>264</sup>

Low-temperature (~600 °C) pyrolytic decomposition of xylene, benzene, toluene, and naphthalene resulted in the formation of carbon spheres; although structurally very similar, the spheres fabricated from different precursors differed significantly with regard to their size.<sup>265</sup> An interesting link was found between sp hybridization of the precursors and gas flow rates, where higher flow rates increased the carbon formation from acetylene yet decreased nanostructure synthesis for ethane over a Ni mesh catalyst at 750 °C.<sup>266</sup> Upon heating, acetylene is broken down into H, C<sub>2</sub>H, or CH, whereas ethane

is decomposed into  $\text{C}_2\text{H}_5$  and H radicals.  $\text{C}_2\text{H}_5$  from ethane was found to desorb more readily from the surface of the substrate, leaving it rich in hydrogen and thus not conducive to carbon nanostructure nucleation and growth. On the other hand,  $\text{C}_2\text{H}$  or CH from acetylene was demonstrated to desorb slower than H, with the surface favoring carbon nanostructure growth.

It has already been discussed that synthesis of CNTs at lower temperatures is highly desirable in terms of both minimizing the energy input during the synthesis and enabling direct assembly of the CNTs on the substrates with relatively low temperature tolerance. Remote heating, where the temperature of the precursor delivered to the synthesis chamber is notably (e.g., by  $250^\circ\text{C}$ ) higher than the substrate temperature, may help contribute to their integration into microelectronic devices. By controlling the preheating temperatures of the precursor and the substrate, and by varying the chemistry of the remotely heated precursor gas, a transition from amorphous carbon nanofibers to crystalline CNTs can be induced.<sup>267</sup> Ex situ gas chromatography of the exhaust gas (Figure 23A) confirmed increasing concentrations of specific volatile organic compounds and polycyclic aromatic hydrocarbons during the structural transition. Direct delivery of these molecules in the CVD process may enable selective nanofiber or CNT formation and control of crystallinity at low substrate temperatures, which is a promising development for electronics fabrication.

Heteroatoms (Cl, Br, OH, and  $\text{NH}_2$ ) that may be present in the precursor can impact carbon nanostructure growth and structure,<sup>69,268</sup> which is particularly relevant for processing of mixed carbon resources. For example, the reactivity of trichloroethylene was higher than that of ethylene, and increased even further with temperature, whereas the reactivity of ethylene declines under higher temperature processing.<sup>268</sup> However, the carbon nanomaterials from ethylene were more structured, forming as hollow fibers, while trichloroethylene produced less ordered solid fibers with bamboo-like features. The dynamic relationship between carbon precursor and catalyst morphology also requires consideration. For instance, trichloroethylene precursor can actively engage with the catalyst leading to catalyst restructure into tetrahedral particles capable of supporting the growth of tripod-like carbon fibers.<sup>68,268</sup>

From the above examples, it is evident that the presence of specific chemistries may render the carbon more conducive to the efficient low-temperature synthesis. Let us now consider the role of precursor-derived intermediates in the formation of carbon nanotubes and nanofibers in more detail. Polyaromatic hydrocarbon and free radical condensates, i.e. agglomerations of carbon species with varying hydrogen content, undergo rapid rearrangement at high temperatures, thus serving as building blocks for carbon materials.<sup>262</sup> The nature of the carbon material produced in this process is related to the manner in which hydrogen is abstracted from these intermediate species in the course of radical recombination, with catalyst particles playing a role of a template for nanostructure growth. Another proposed mechanism assumes precursor adsorption onto the surface of the catalyst, where it is dissociated into smaller fragments—the building blocks for the formation of carbon nanostructures (Figure 23). Surface-adsorbed benzene was shown to decompose into dimers and trimers on the Fe–Co/ $\gamma\text{-Al}_2\text{O}_3$  catalyst surface, subsequently reforming into CNTs.<sup>269,270</sup> Dehydrogenated benzene have also been suggested to directly aggregate into graphitic sheets.<sup>269</sup>

These mechanisms suggest that in order to produce carbon nanostructures it may not be necessary to break the precursor down into individual atoms. Further elucidation of these mechanisms and identification of fundamental building blocks may provide an opportunity to selectively produce these building blocks by matching the unique chemistries of the conventional and exotic precursors with appropriate catalyst and temperature to dissociate the carbon–hydrogen bonds, while retaining the carbon–carbon bonds. This may provide alternative pathways for the low-cost, high-volume precursor-driven synthesis of carbon nanostructures. Achievement of the reasonable levels of selectivity in location-specific molecular dissociation processes represents a significant challenge and opportunity for plasma researchers in the future.

## 9. CNT SYNTHESIS USING RAW MATERIALS

In this section, we will continue our examination of how the choice of processing conditions, carbon feedstock, and catalyst determines the morphology (wall number, diameter, length, defect formation, and chirality), functionalization, alignment, and surface organization of CNTs. While CNT production typically relies on high-purity methane, ethylene, acetylene, benzene, xylene, and other purified gases as a source of carbon, the cost of production and workup chemistry may be lowered by employing diverse carbon sources. We will now discuss the properties that arise when CNTs are synthesized using coal, natural gas, petroleum, and waste materials as the carbon source, focusing on specific advantages and challenges that may arise from the use of chemically heterogeneous precursors in nanostructure synthesis.<sup>271</sup>

### 9.1. Coal

Coal is a cheap and abundant *natural source* of carbon that can be used for synthesis of carbon nanotubes and SiC nanowires by arc discharge in a helium atmosphere.<sup>272</sup> In one example, graphite anode packed with a mixture of coal and CuO was used to produce branched CNTs with a Y-type junction.<sup>273</sup> Branched structures stemming from the straight nanotube alter the electronic and mechanical properties of the CNTs. The coal-modified graphite anode carbon source was able to yield CNTs in large quantities with a purity of 70%. Interestingly, the yield from high-purity graphite powder filled anode was significantly lower, suggesting that the macromolecular structure of coal may present certain advantages for branched CNTs (BCNTs) synthesis.

Indeed, the nonpure nature of coal as a carbon source leads to some interesting features that cannot be attained from pure graphite under the same conditions. When graphite is subjected to arc discharge plasmas, it is decomposed into atomic and diatomic carbons, which then reform into fullerenes or CNTs. On the other hand, coal is rich in weakly cross-linked irregular polymerized aromatic hydrocarbon units, such as alkyne and aromatic species that are easily released upon exposure to the arc plasma environment. The temperature distribution in arc discharge plasmas varied greatly between the hot ( $>5000^\circ\text{C}$ ) center and much cooler edge regions. Carbon precursors in the hot region are fully atomized, whereas in the low-temperature fringe regions, the released active carbon species can exist as clusters. These clusters interact with catalyst nanoparticles and give rise to BCNTs, where most of the C–C bonds are distorted from pure  $\text{sp}^2$  bond to partial  $\text{sp}^3$  bond. The process kinetics resembles gas-phase catalytic pyrolysis in a hydrogen arc. In the same manner and using Fe catalyst nanoparticles,



**Table 4.** Chemical Composition of Raw Coal and Coal-Derived Anode (Reprinted with permission from ref 274. Copyright 2007 Elsevier Ltd.)

sample	proximate analysis (wt %)			ultimate analysis (daf, wt %)				
	$M_{ad}$	$A_d$	$V_{daf}$	C	H	N	S	O
Yangquan coal	2.3	11.76	9.62	92.19	3.4	1.48	1.66	1.27
coal anode	2.02	33.43	3.98	94.96	1.31	1.15	1.65	0.93

double-walled CNTs (DWCNTs) with an outer diameter of 1–5 nm and an interlayer spacing of  $\sim 0.41$  nm can be synthesized.<sup>274</sup>

The formation of both BCNTs and DWCNTs is further promoted by organosulfur compounds naturally present in the coal, natural gas, and petroleum (Table 4). Sulfur species can selectively bond to the active sites of the catalyst nanoparticles, suppressing the formation of graphite layers, promoting such features as branching and stabilizing large-diameter nanotubes. The formation of metal–sulfur eutectic potentially leads to higher CNT yields. However, since the yield and the structure of the nanostructures produced are affected by the type of coal used, this presents a potential challenge for the large-scale production of CNTs where reproducibility of quality and yield are paramount. Furthermore, the product is likely to have a significant fraction of impurities, e.g. hollow and fullerene-like NPs, carbons with disordered structures, etc.

## 9.2. Natural Gas

Natural gas, which is a mixture of methane, carbon dioxide, ethane, propane, *n*-butane, isobutene, and dimethyl sulfide, has been suggested as a lower-cost carbon source for CVD processing. Using thermally oxidized garnet powder (as a low-cost catalyst and support) and natural gas as a carbon precursor, pure and highly crystalline relatively well-ordered multiwalled CNTs (MWCNTs) (diameters of 20–50 nm) were grown using CVD at 800 °C.<sup>275</sup> The high density of garnet powder enabled easy separation of the CNTs and garnet sand by means of sonication in a water solution. A number of impurities (e.g.,  $N_2$ ,  $CO_2$ , and  $H_2O$ ) that are present in the natural gas may influence the synthesis process.

In the example of natural gas, hydrogen gas was required during the process to activate the catalyst and control the formation of the nanostructures. The use of hydrogen can be avoided when using low-cost, unpurified liquid petroleum gas (LPG) as the carbon source. The CNT forests formed from LPG in the floating catalyst process showed thinner tubes and lower growth rates compared to the synthesis using conventional carbon sources.<sup>276</sup> Similar to the coal and natural gas cases, the effect was attributed to the presence of organosulfur species. Indeed, as sulfur is an essential element to life, fossil fuels and other biomass-derived products will contain a fraction of organosulfur compounds. It is possible that the effect of sulfur content on the synthesis of CNTs is more profound than the influence of the types of hydrocarbons that constitute the organic precursors. The morphology and alignment of the CNTs grown from LPG were similar to those of CNTs deposited from purified propene, and the purity was high regardless of the catalyst used.<sup>277,278</sup>

## 9.3. Deoiled Asphalt

Another gaseous precursor is deoiled asphalt (DOA), which is a byproduct of the refinement of petroleum. In DOA, carbon is present in the forms of saturated hydrocarbons, partially hydrogenated polycyclic aromatic compounds, high molecular weight phenols, carboxylic acids, and heterocyclic compounds,

with the naphthene and polar aromatics being the dominant components. DOA also contains organosulfur compounds, nickel, and vanadium. Carbon fibers produced from the pyrolysis of DOA and ferrocene were of high purity, with a diameter of 150–200 nm and a maximum length of 10–40  $\mu m$ .<sup>279</sup> Ferrocene-catalyzed thermal decomposition of maltene and asphaltene fractions derived from natural-mined Indonesian asphalt at  $>1100$  °C resulted in the formation of CNTs with a yield between 11 and 26% CNTs.<sup>280</sup>

## 9.4. Carbon from Biomass

In an alternative approach to using fossil fuels, CNTs can be synthesized directly from renewable natural materials, such as leaves, grasses, and oils. The micro- and nanoscale morphological features of natural surfaces, such as regularly distributed dumbbell-shaped idioblasts, prickly hairs, and arrays of papillae, may be used to control surface organization and alignment of carbon nanostructures.<sup>281</sup> For example, in addition to serving as a source of carbon, the structural and compositional (e.g., Al content) differences between the top and bottom surfaces of the bamboo leaf were used as a template to control the shape (branched and bamboo shaped on the top and bottom surfaces, respectively), density, and surface organization of the nanowires.<sup>282</sup> The use of raw agricultural material as the carbon source, catalyst support, and source of catalyst significantly reduced the workup processing energy and time.

Botanical volatile hydrocarbons can replace traditional gaseous carbon precursors. For example, camphor was used as a carbon precursor to grow SWCNTs and vertically aligned MWCNTs on quartz and silicon plates, and zeolite supports.<sup>283–289</sup> Extracted from the latex of the *Cinnamomum camphora* tree, camphor is low-cost and abundant; it is used extensively in aromatherapy and is nontoxic. The ability of camphor to sublime at room temperature makes it well-suited to catalytic CVD processing. On Fe–Co-impregnated zeolite catalyst support at atmospheric pressure and temperature of 650 °C, the use of camphor precursor yielded MWCNTs with 88% purity and high growth rate of  $\sim 50\%$ ,<sup>283</sup> which is attractive for the large-volume synthesis.

The aforementioned examples of nanostructure synthesis were precursor-driven, with the structure and morphology of CNTs depending strongly on the type of the plant oil precursor. Spray pyrolysis of neem oil resulted in bundles of well-aligned tightly packed MWCNTs.<sup>290</sup> Similar treatment of eucalyptus and turpentine oils yielded SWCNTs with diameters of 0.79–1.71 nm.<sup>291,292</sup> CNTs grown from turpentine oil for 60 min at 700 °C were 2 orders of magnitude shorter than those grown from eucalyptus oil. However, turpentine-grown CNTs had a higher degree of graphitization, better resolved concentric shells, and fewer defects compared to eucalyptus-grown structures and, as such, notably higher current density and field emission.<sup>293</sup>

Just as the case with nanotube synthesis using conventional carbon sources, doping agents can be used to introduce defects into the structure of the CNTs and thus modify their electrical

and sensing properties.<sup>294</sup> Nitrogen-doped CNTs fabricated from castor oil–ferrocene with ammonia solution by means of spray pyrolysis were characterized by wavy tube morphology and bamboo-shaped structure, with a diameter of 50–80 nm.<sup>295</sup> The specific morphology and structure were attributed to pentagonal (pyridine-like) and heptagonal defects that are introduced into the hexagonal structure.

Carbon from nongaseous carbon sources, such as grass, can be converted into MWCNTs if sufficient heat and oxygen are provided.<sup>296</sup> Grass is rich in carbohydrates, i.e. cellulose, hemicellulose, and lignin, which are present in vast quantities as vascular bundles. Unlike the conventional mechanism of CNT formation, where heat is used to release active carbon atomic species and drive CNT assembly, a rapid heat treatment (at about 600 °C) of tubular cellulose in grass leads to the dehydration of vascular bundles and their transformation into MWCNTs with diameters of 30–50 nm.

Annealing simple precursors, such as sucrose carbon with boron at 2200–2400 °C, also produces MWCNTs.<sup>297</sup> In this case, pentagons present in graphite sheets of sucrose carbon are the defects that allow the sheets to curl up and form nuclei for nanotube or nanoparticle growth. Since the ratio of pentagons to hexagons varies depending on the source of carbon, the efficiency of conversion of these disordered carbons into graphitic nanotubes and nanoparticles would also differ between carbon sources and processing environments. Sucrose can also be converted into close-ended MWCNTs by a pyrolytic technique using mesoporous molecular sieve silicate templates without transition metal catalysts.<sup>298</sup> The dissolution required to remove the silicate substrate may be detrimental to the quality of the tubes. Furthermore, the use of sulfuric acid as a catalyst for the sucrose conversion is not environmentally friendly.

### 9.5. Waste Materials

The use of waste cooking oils as a carbon precursor not only serves as a low-cost carbon source for industrially useful materials, but also alleviates the need for the disposal of these oils into the environment. Used nonpurified mustard, soybean, sesame, and castor oils were converted into carbon nanowhiskers (CNWs) with diameters of 98–191 nm and lengths of under 2  $\mu\text{m}$  via a high-temperature catalytic reaction in a closed system under self-generated pressure.<sup>299</sup> The CNWs consisted of carbon spirals with spacing between two adjacent layers at  $\sim 3.1$  nm and were arranged perpendicular to the whisker axis. Full conversion of the natural oils to CNWs was obtained at 850 °C for 10 h. The aspect ratio was highest for waste mustard oil (13:1).

In addition to CNWs, other carbon-based products, e.g. carbon spheres or carbon-coated nanocrystals, can be produced by varying the chemistry of the carbon source and the processing conditions. For example, in the absence of metallic catalyst, waste oils were converted into 4–6  $\mu\text{m}$  diameter chiseled carbon microspheres. Similarly, a substitution of the waste cooking oil with engine oil yielded  $\sim 4$   $\mu\text{m}$  diameter carbon microspheres even in the presence of catalyst. While waste oils are rich in fatty acids, i.e. oleic, linolenic, linoleic, palmitic, and stearic acids, engine oil consists purely of hydrocarbons. The gaseous pressure from the decomposition of the fatty acids is proposed to be the critical parameter to the formation of the semigraphitic filamentous structures.

A mixture of single and multiwalled vertically aligned CNTs was produced via floating-catalyst thermal chemical vapor

deposition of waste cooking palm oil.<sup>300</sup> The presence of fats and hydrocarbons leached into the oil during its use did not significantly alter the properties of fabricated CNTs. Electron field emission properties from cathodes of vertically aligned CNTs included field enhancement ( $\beta$ ) of 2740, turn-on and threshold electric fields of 2.25 and 3.00 V/ $\mu\text{m}$ , respectively, and maximum current densities of 6 mA/ $\text{cm}^2$ .

Using a high-temperature high-pressure catalytic process, used plastic bags and bottles, such as those made of low-density and high-density polyethylene and polystyrene, were converted into MWCNTs.<sup>301</sup> Pellets fabricated from polyethylene-derived MWCNTs were characterized by conductivities of 43 and 72 S  $\text{m}^{-1}$  at room temperature and 60 °C, respectively. A minimum of 20 wt % CoAc catalyst was required for complete conversion of polyethylene into MWCNTs, while lower catalyst concentrations led to the formation of a mixture of MWCNTs and carbon spheres. Catalyst-free heating of waste polyethylene terephthalate generated mechanically robust, paramagnetic, conducting carbon microspheres with diameters of 2–10  $\mu\text{m}$ .<sup>302</sup> Polypropylene, polyethylene, and poly(vinyl chloride) plastic bottles were converted into vertically aligned CNT arrays by a coupled process of pyrolysis and chemical vapor deposition.<sup>303</sup>

## 10. NATURAL-PRODUCT-DERIVED CATALYSTS AND SUPPORTS

Catalysts contribute greatly to the cost of CNT production. In catalytic CVD, catalyst drives the decomposition of the carbon source and controls the growth kinetics of the tubes/fibers, and typically is a transition metal (e.g., Fe, Co, Ni, Au, Pd, Ag, Pb, Mn, Cr, Ru, Mo, Cu). Catalyst particles are immobilized on a catalyst support, typically MgO, Al<sub>2</sub>O<sub>3</sub>, or SiO<sub>2</sub>, that provides a high surface area for catalytic CVD reaction. Successful CNT syntheses have been reported with nonmetal catalysts, such as SiO<sub>2</sub>, Si, SiC, Ge, Al<sub>2</sub>O<sub>3</sub>, ZrO<sub>2</sub>, ZnO, C<sub>60</sub>, nanodiamond, and CNT.<sup>304</sup> However, finding a lower-cost alternative to metal particles that is suitable for catalytic CVD is not trivial. Consequently, large-volume synthesis of high-quality CNTs at low cost remains a significant challenge.

In this section we consider natural, abundant materials that can be used to replace both the chemically processed catalysts and the support, significantly reducing the costs of presynthesis processing. The first example concerns the use of unprocessed volcanic lavas both as support and as catalyst for CNT synthesis.<sup>305</sup> Lava and tephra materials are abundant, with estimated  $1 \times 10^7$  m<sup>3</sup> of lava produced during 2002–2003 volcanic eruptions alone. Lavas are naturally rich in iron oxide particles (up to 11 wt % Fe<sub>2</sub>O<sub>3</sub>), distributed among silicate phases, which alleviates the need for any wet-chemical processing of the support.<sup>306</sup> Once reduced to metallic Fe by H<sub>2</sub> treatment at 700 °C, crushed lava rocks were used to catalyze the decomposition of carbon precursor gas and formation of CNTs with an inner wall diameter of less than 10 nm. Given that a large number of natural minerals, clays, and soils contain iron oxides, they may also be used as a low-cost catalyst/support system.

When selecting a natural catalyst support, it is important to ensure that metal catalyst sources within this material are likely to produce similarly structured and organized nanostructures. For instance, when natural bentonite mineral, where Fe is present as siderite and armalcolite, was used for production of MWCNTs, there was a significant variation in the wall thickness and outer diameter (6–40 nm) of the formed

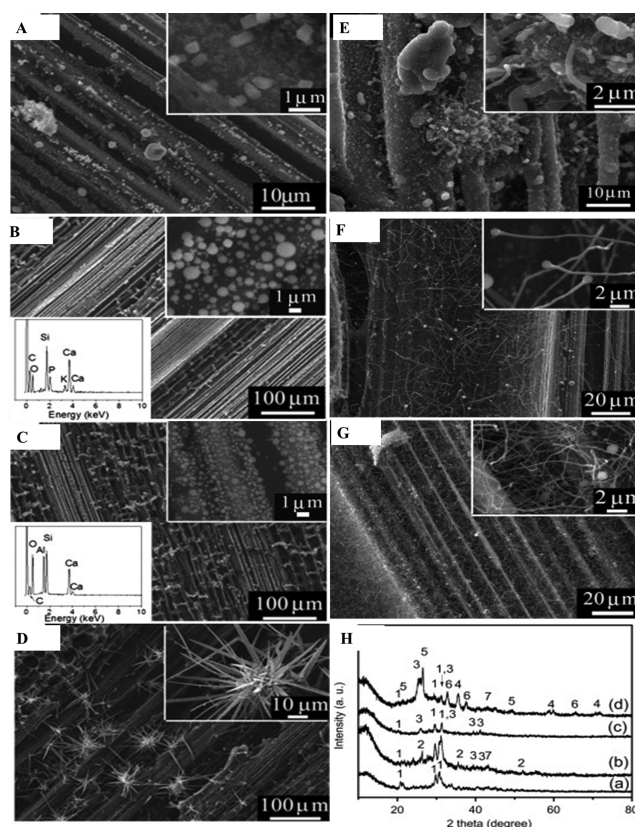
nanotubes. This was attributed to the differences in physical and chemical environments that these two sources presented for nucleation and growth of the nanostructures.<sup>307</sup> Using a fluidized bed reactor, SWCNTs of high quality, few defects, and a high aspect ratio ( $>10^4$ ) were grown on natural sepiolite mineral, with good control over the chirality and diameter distribution.<sup>308</sup> Used in the industrial production of many chemicals and materials, fluidized bed reactors enable the mixing of gas or liquid with powdered catalysts where the catalyst behaves like a fluid, maximizing uniform particle mixing and thus chemical interactions, and maintaining uniform temperature distribution; this system supports continuous withdrawal of the material, enabling high-quantity material synthesis. By using planar surfaces, such as soaked fibrous wollastonite substrates, aligned, highly pure CNT arrays can be produced.<sup>309</sup>

Iron is also an essential element for living organisms; it forms complexes with molecular oxygen in hemoglobin and myoglobin in vertebrates, and is an important constituent of many redox enzymes in plants and animals. It is therefore possible that the ash derived from biomass would contain iron in quantities sufficient to support catalytic synthesis of CNTs. Iron-rich activated carbon (AC) prepared from agricultural waste, namely palm kernel shell, coconut, and wheat straw, supported CVD growth of carbon nanofibers from ethylene and hydrogen mixture.<sup>310</sup> Naturally formed magnesium and calcium silicates in bamboo charcoals were responsible for the nucleation and growth of ethanol-derived MWCNTs (Figure 24, Table 5).<sup>311</sup> In both examples, carbon support was prepared by heating the waste at temperatures of 1000–1500 °C for at least 1 h, followed by the heat-enabled deposition stage at similar temperatures. Pressureless spark plasma sintering where pulsed dc current induces high-rate Joule heating was shown to reduce the processing time during AC fabrication and nanostructure synthesis and favor the formation of highly porous AC supports from biological waste materials.<sup>312</sup>

Although the idea of using iron oxide containing minerals reduces the costs associated with producing catalyst and catalyst supports, CNTs still need to be removed from the support, e.g. by washing with acid. Water dissolvable catalyst supports, such as those based on silicate, carbonate, or chloride, can provide a more environmentally friendly and low-cost alternative. In one example, a catalyst support consisting of  $\text{CaCl}_2$  (matrix), citric acid (foaming agent), and  $\text{Co}(\text{NO}_3)_2$  (catalyst) was used to prepare MWCNTs with 30–150 nm diameter and structures comparable to nanotubes prepared using conventional methods.<sup>313</sup> Interestingly, the synthesis yield was  $>1500\%$  with respect to catalyst weight, which is higher compared to conventional catalytic CVD. The fabricated nanotubes were 94% MWCNTs, with  $\sim 5\%$  impurity, which is on a par with commercially prepared samples.

## 11. PRECURSOR-DRIVEN SYNTHESIS: ORGANIC POLYMERS AND SMALL MOLECULES

To this point in the article, the chemistry of the precursor has been discussed largely as an influencing factor in the breakdown into smaller fragments, reforming, and surface organization of nanocarbon materials. However, there is an equally strong interest in research and industry communities globally in the development of organic polymer materials, where the chemistry of the precursor is crucial to the performance of the polymer. Indeed, organic polymers and small-molecule materials are being actively researched for a variety of electronic applications



**Figure 24.** Pyrolysis of bamboo produces a range of surface chemistries and morphologies. (A–D) SEM images of bamboo samples pyrolyzed at 1200, 1300, 1400, and 1500 °C, respectively, with insets showing respective energy-dispersive X-ray (EDX) spectra. (E–G) SEM images of CNTs grown on bamboo charcoals pyrolyzed at 1200, 1300, and 1400 °C, respectively, in the presence of ethanol vapor. Bamboo sample pyrolyzed at 1500 °C did not produce CNTs. (H) XRD spectra of bamboo samples pyrolyzed at (a) 1000, (b) 1200, (c) 1300, and (d) 1400 °C. 1,  $\text{K}_2\text{SO}_4$ ; 2,  $\text{MgSiO}_3$ ; 3,  $\text{CaSO}_4$ ; 4,  $\text{SiC}$ ; 5,  $\text{SiO}_2$ ; 6,  $\text{CaO}$ ; 7,  $\text{MgO}$ . The nucleation and growth of MWCNTs at 1200–1400 °C was primarily attributed to  $\text{Mg}_2\text{SiO}_4$  and calcium silicate. Reprinted with permission from ref 311. Copyright 2012 Elsevier Ltd.

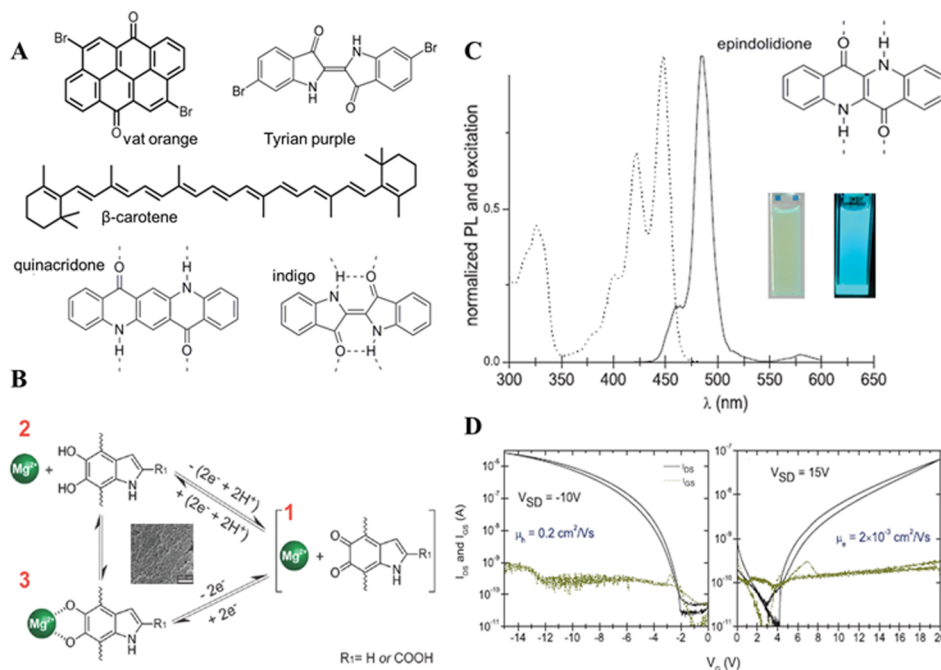
**Table 5. Mineral Composition of Bamboo Charcoal Pyrolyzed at 1000 °C (Reprinted with permission from ref 311. Copyright 2012 Elsevier Ltd.)**

element ( $\text{g kg}^{-1}$ )						
K	Mg	P	S	Si	Ca	Fe
19.6	10.3	8.5	8	7.9	7.1	5.9

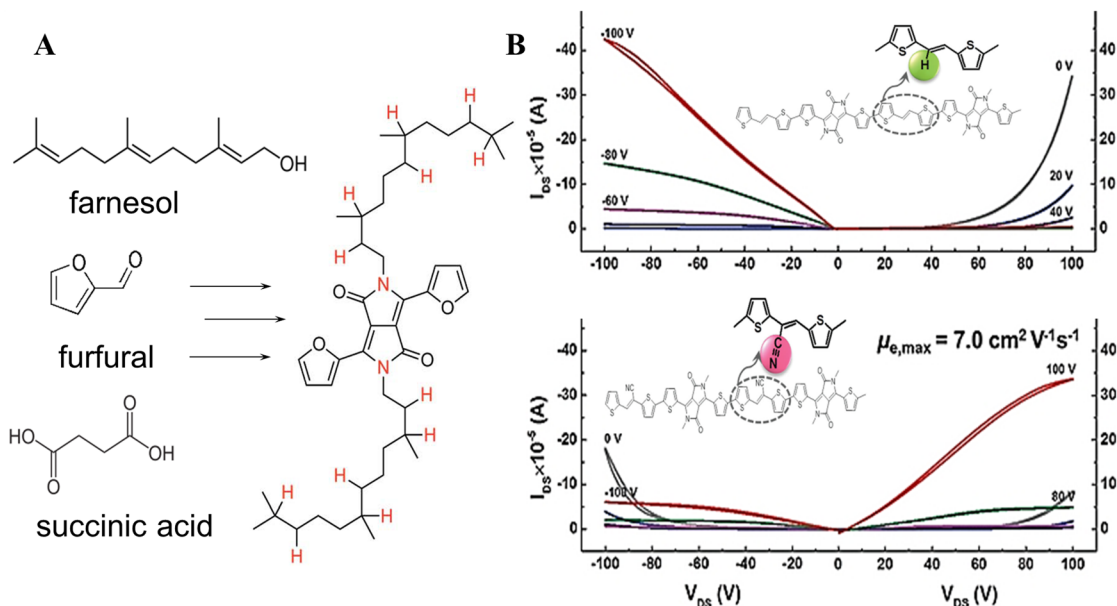
owing to their potential to build devices with mechanical flexibility and stretchability, low toxicity toward biological systems, and low cost.<sup>198,314–317</sup> Within the device, polymers can perform the role of a substrate, an electrode, an active (semiconducting) layer, a dielectric layer, or an encapsulating layer.

In addition to thermochemical polymerization, chemical and physical vapor deposition, and other conventional methods used for precursor-centered material synthesis, plasma environments can be optimized to facilitate the preservation of some of the original chemistry of the precursor in the end material. For example, as demonstrated in Figure 3A in section 1, lower power densities (i.e., energy doses per precursor molecule)





**Figure 25.** Natural semiconductors with good charge transport properties. (A) Chemical structures of promising semiconducting dyes. (B) Natural melanin used as a cathode in Mg ion battery. States 1 and 3 represent reversible insertion (coordinated coupling) and extraction (redox) of  $\text{Mg}^{2+}$  during charging and discharging. (C) Photoluminescence and excitation spectra for epindolidione, a hydrogen-bonded pigment. Epindolidione is a remarkably stable organic solid, with strong low-energy optical emission originating from excimeric states, which coexists with higher-energy fluorescence. (D) Transfer characteristics for low-voltage OFETs fabricated with epindolidione: p-channel with Au source-drain electrodes, and n-channel with Al source-drain electrodes. Epindolidione-based OFETs operate reliably under repeated cyclic tests in different ionic solutions within the pH range 3–10 without degradation. Panel B reprinted with permission from ref 325. Copyright 2014 Wiley-VCH Verlag GmbH & Co. KGaA. Panels C and D reprinted with permission from ref 327. Copyright 2014 Wiley-VCH Verlag GmbH & Co. KGaA.



**Figure 26.** Diketopyrrolopyrrole-based pigments are promising low-cost building blocks for organic semiconducting polymers. (A) Furan-substituted DPP unit alkylated with a farnesol derivative derives 94% of its molecular weight from biomass. All atoms except those labeled in red are derived from natural materials. (B) By the incorporation of only one nitrile group with the electron-withdrawing function in the vinyl link of the DPP-based copolymer, a dramatic inversion of the majority of charge carriers from holes to electrons is achieved. Panel A reprinted with permission from ref 342. Copyright 2013 Royal Society of Chemistry. Panel B reprinted with permission from ref 325. Copyright 2014 Wiley-VCH Verlag GmbH & Co. KGaA.

achieved under low-power, pulse-mode plasmas favor the survival of the original monomer structure since the energy

delivered to the molecules is insufficient for dissociating certain atomic bonds.<sup>46–51</sup>

This section provides a number of examples that use natural or low-cost precursors to fabricate materials for electronics, with the examples being presented according to their potential function in electronic devices.

### 11.1. Natural Semiconducting and Electrode Materials

Animal and plant-derived pigments and dyes that have for centuries been used for textile, cosmetic, and food coloring are now being investigated as sustainable semiconducting materials in organic electronics (Figure 25). Indigoids, such as indigo and Tyrian purple, are among the most widely produced dyes worldwide, in part due to their exceptional degradation stability unlike most other natural-origin dyes.<sup>318</sup> Indigo is synthesized via oxidation from indoxyl extracted from plants of the *Indigofera* and *Isatis* genera, whereas the precursor for Tyrian purple is tyrindoxyl sulfate, a molecule produced by the hypobranchial glands of sea snails of the family Muricidae. Among other natural pigments being investigated are carotenoids, melanin, and pigments extracted from the leaves of teak (*Tectona grandis*), tamarind (*Tamarindus indica*), eucalyptus (*Eucalyptus globulus*), and the flower of the crimson bottle brush (*Callistemon citrinus*).<sup>317,319–322</sup>

Protonic and electronic charge carrier transport was demonstrated in hydrated eumelanin thin films.<sup>323</sup> The electrical response of hydrated eumelanin films is dominated by ionic conduction ( $10^{-4}$ – $10^{-3}$  S cm<sup>-1</sup>), largely attributable to protons, and electrochemical processes. Melanin has also been used as a cathode in secondary Mg<sup>2+</sup> batteries (Figure 25B), where divalent ions improve the volumetric charge storage capacities of electrochemical storage systems compared to those that use monovalent ions.<sup>324,325</sup>

Organic dyes, such as indigo, Tyrian purple, and epindolidione, are ambipolar organic semiconductors with good charge transport properties.<sup>326,327</sup> The dyes can be evaporated to form thin films characterized by a high degree of crystallinity. The ordering of the molecules within the film depends on the nature of the substrate. For instance, the use of aliphatic nonpolar substrate, e.g. low-density polyethylene or tetratetracontane, yields a vertical orientation of the molecules in the film. The long-range ordering and absence of obvious amorphous domains is likely a result of strong intermolecular hydrogen bonding, van der Waals forces, and  $\pi$ – $\pi$  interactions. The hydrogen bonding reinforced  $\pi$ -stacking ensures high mobility and high relative permittivity values of indigoids, at 4.3 and 6.2 for indigo and Tyrian purple, respectively.<sup>328</sup> Indeed, the  $\pi$ -stacking parallel to the substrate is favorable for the effective charge transport in organic field effect transistor (OFET) devices.

Organic semiconductors can be used as an active layer in ambipolar OFETs (Figure 26D).<sup>329–331</sup> The ambipolar behavior is related to the reversible oxidation and reduction electrochemistry.<sup>332</sup> When operated in air, the n-type operation of indigo-containing devices is lost due to the high-lying lowest unoccupied molecular orbital (LUMO) level (3.8 eV) and oxygen acting as an acceptor. Interestingly, the ambipolar operation can be regained when the device is operated in the inert environment, even after prolonged exposure to air. In the case of devices with Tyrian purple layer, the ambipolar operation in air can be maintained for at least 30 min, likely due to the lower lying LUMO level (4 eV) of Tyrian purple. The repeated cycling in air results in a drop in the electron mobility by a factor of 2.

Molecular heterojunction solar cells fabricated using isoindigo/oligothiophene exhibited a power conversion efficiency up to 1.76% with the open circuit voltage  $V_{oc}$  of 0.74 V, short-circuit current  $I_{sc}$  of 6.3 mA/cm<sup>2</sup>, and fill factor FF of 0.38.<sup>333</sup> Solar cells based on terthiophene/isoindigo alternating copolymer and PC<sub>71</sub>BM demonstrated a photoconversion efficiency of 6.3%.<sup>334</sup>

The ambipolarity of indigoids can be favorably exploited in the fabrication of complementary-type circuits. An organic alternative to silicon-based metal-oxide-semiconductor (MOS) integrated circuits typically involves either the use of n- and p-type materials on neighboring transistors or the use of a composite of materials with dominant hole and electron transport. From the fabrication point of view, it would be beneficial to use a single ambipolar material, with a small enough band gap to facilitate the injection of both types of charge carriers from a single electrode material. Indigoids, particularly Tyrian purple, satisfy these requirements, with demonstrated performance of a simple NOT-logic voltage inverter being on a par with the best-performing single materials reported in the literature.

### 11.2. Low-Cost Synthetic Semiconductors

One of the key issues with using natural pigments is that at present they are not produced in sufficiently large quantities. On the other hand, synthetic pigments, such as perylene diimides, Vat Yellow and Vat Orange, and quinacridone, are both abundant and low cost.<sup>335–339</sup> Furthermore, they are relatively environmentally benign during use and degradation, being used for decades in industrial applications.<sup>316</sup> Low toxicity and natural degradability of these semiconductors make them suitable for compostable and biodegradable devices. Unlike natural pigments, however, these semiconductors are not renewable, and their synthesis requires considerable amounts of synthetic and inorganic substances and energy.

Diketopyrrolopyrrole (DPP)-based pigments have been widely used in inks, paints, and plastics for over four decades, and are currently being explored as building blocks for organic semiconducting polymers and small molecules.<sup>340,341</sup> These pigments are synthesized from furfural and dialkylsuccinate (Figure 26). Furfural is derived from biomass and is commercially available in large quantities at low cost. Succinic acid is also cheap and abundant. However, at present it is largely sourced from petrochemical resources, with only a limited portion derived from renewable materials.<sup>342</sup> The alkylating agent used to convert furan-substituted diketopyrrolopyrrole to DPP is also a low-cost and readily available material. One of the key issues with these pigments is balancing the ratio of semiconducting backbone to solubilizing chain. Solubilization of conjugated polymers typically requires branched chains that are both expensive and require high-temperature synthesis. More environmentally friendly alternatives may involve the use of biomass-derived alcohols.

The energy levels of DPP-based pigments can be easily adjusted, affording p-type, n-type, or ambipolar organic semiconductors with highly efficient charge transport properties for OFETs (Figure 26).<sup>325,343</sup> Furthermore, many of the DPP derivatives, especially those flanked by furan rings, have favorable energy levels and band gaps, as well as sufficiently high hole mobility to be used as donor materials for organic photovoltaics (OPVs).<sup>344</sup>

### 11.3. Dielectric, Encapsulation, and Substrate Materials

In addition to conducting and semiconducting elements, organic electronic devices require the use of dielectric, encapsulating, and substrate materials. For many future device applications, these materials are subject to the same requirements including low cost, large scale, reproducibility, environmental friendliness, uniformity of surface organization, flexibility (both bending and stretching), stability in air, and some others. In this section, we present several examples of natural molecules that either display or can be converted into materials that possess the characteristics desirable for dielectric, encapsulating, and substrate materials in OFETs.

There are a number of natural and low-cost minimally processed synthetic materials that can be used as substrates to support the electronics. These include shellac, proteins, such as collagen gelatin and silk, polysaccharides, and such as chitin, chitosan, alginate, dextran, etc.<sup>345–347</sup> Silk is one of the most popular materials, as it is strong and biocompatible.<sup>348,349</sup> Its chemical and mechanical properties and degradation kinetics can be easily modified for the desired application. Furthermore, for biological applications, it can be impregnated with chemical and biological agents that can then undergo controlled release under in vivo or environmental conditions. In addition to therapeutic agents, silk can be loaded with various enzymes that, once released, become active and promote material dissociation.<sup>350</sup> In addition to being used as a substrate/encapsulating layer,<sup>351</sup> silk has been reformed into naturally degradable optical elements.<sup>347</sup> For example, silk was used to prepare freestanding refractive or diffractive devices, with elements that range from microlens arrays and white-light holograms to diffraction gratings and planar photonic crystals with the minimum feature sizes of less than 20 nm.

Gelatin is another natural material that can be readily processed into a variety of shapes. It is biocompatible, and its flexible chemistry allows for fine-tuning of its properties. A natural polyester produced by beetles, shellac resin is readily processed from ethanol solution to form smooth (root-mean-square (rms) roughness < 1 nm) substrates of any shape.<sup>332</sup> Another nontoxic natural material is leather; it is naturally degradable and widely available. It is also highly chemically and mechanically heterogeneous. Paper is also a cheap and abundant substrate for electronic devices.<sup>352–354</sup> Paper is solution-processed from wood, rag, or grass cellulose fibers, and can be readily shaped into very large, flexible thin sheets. Unlike polymer substrates, the surface of paper is rough and porous. Even though paper manufacturing involves multiple steps, it is still regarded as an attractive material for high-throughput fabrication. Smoothing agents may be applied to achieve surface morphology and chemistry required for device assembly.<sup>355</sup> Naturally degradable shape memory thermoplastics that can change their shape or size after implantation is an interesting alternative for implantable electronics applications, where smaller size/simple shape may facilitate less invasive implant placement.<sup>356</sup>

There are many natural proteins that can potentially be used as gate dielectric layers in organic electronic devices (Table 6).<sup>315</sup> Albumen separated directly from fresh chicken egg can be converted into insulating thin films that are flexible and biocompatible.<sup>357</sup> The dielectric layer is produced by the thermal cross-linking.<sup>358</sup> Flexible pentacene and C<sub>60</sub>-based OFETs fabricated with albumen dielectrics demonstrated output currents significantly higher compared to the equivalent devices with poly(methyl methacrylate) (PMMA) dielectric.

**Table 6. Electrical Properties of Several Promising Natural Dielectric Materials (Adapted from and reprinted with permission from ref 315. Copyright 2010 Wiley-VCH Verlag GmbH & Co. KGaA.)**

material	dielectric const (at 1 kHz)	breakdown field (MV cm <sup>-1</sup> )	loss tangent (at 100 mHz)
adenine	~3.85	~1.5	~4 × 10 <sup>-3</sup>
guanine	~4.35	~3.5	~7 × 10 <sup>-3</sup>
glucose	~6.35	~1.5	~5 × 10 <sup>-2</sup>
lactose	~6.55	~4.5	~2 × 10 <sup>-2</sup>
sucrose	N/A	>3	~8 × 10 <sup>-2</sup>
caffeine	~4.1	~2	~9 × 10 <sup>-2</sup>

Pentacene-based OFETs with silk fibroin gate dielectric also exhibited a high field-effect mobility value of 23.2 cm<sup>2</sup> V<sup>-1</sup> s<sup>-1</sup> and a low operating voltage of -3 V.<sup>359</sup> Dielectric layers based on DNA and nucleobases were also tested as they offer an attractive combination of high dielectric breakdown strength and low dielectric losses and leakage currents.<sup>315,360–363</sup> Tetratetracontane, a waxy oligoethylene found in tropical plants, can be vacuum processed into thin dielectric films with aliphatic surfaces.<sup>314,328</sup> These surfaces are well-suited for deposition of indigo and other H-bonded natural semiconductors where orientation anisotropy is critical to semiconducting performance.

For organic electronic and energy devices, it is highly desirable for the insulating layer to be very thin, defect-free, and generally with a high dielectric constant for operating at low voltages. Thin polymer films with a high degree of cross-linking and surface-organized, densely packed self-assembled monolayers are suitable as ultrathin dielectric materials. It is important that the synthesis method used to deposit the dielectric does not undermine the integrity and material properties of the underlying layers, e.g. through the use of excessive temperature or aggressive solvents. We have already mentioned that nonequilibrium environments provide the necessary conditions for low-temperature, substrate-sparing deposition of highly cross-linked, ultrathin, defect-free films. Thermally nonequilibrium plasma environments can also be used for gentle etching of surface features of the substrate, without damaging the integrity of the material, as well as surface functionalization and controlled deposition of surface-organized nanoscale features. These functional groups and nanoscale features can then be used to guide the assembly of ultrathin dielectric monolayers. Surface functionalization can also be used on the dielectric layer itself as the means to enhance device performance. The surface properties, i.e. surface chemistry and morphology of the insulating layer, affect the charge carrier transport in transistor devices, as most of the charge carriers in the active layer are confined to within ~5 nm of the semiconductor layer adjacent to the semiconductor/dielectric interface.<sup>364</sup> Thus, the chemical and physical characteristics of the dielectric surface have a significant effect on the charge carrier transport.

## 12. PLASMA-ENABLED PRECURSOR-DRIVEN SYNTHESIS: ORGANIC POLYMER FILMS

This section will review several examples where the plasma environment was or could potentially be used for synthesis or surface organization of organic polymers. The chemical structure of the organic precursor is important when low-temperature synthesis of polymer and surface functionalization



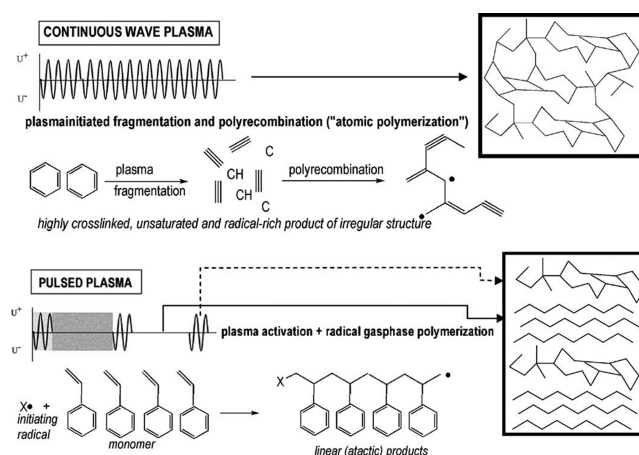
is concerned. This is particularly so for depositions at low power, where only limited dissociation of the original precursor molecule takes place. As power delivered to the reactor increases, stronger monomer fragmentation leads to a major loss of the original precursor chemistry and formation of a highly cross-linked material that is dominated by carbon and hydrogen.<sup>365</sup>

In low-pressure nonthermal plasmas, a large number of mechanisms of plasma polymerization exist.<sup>366</sup> Radical chain growth polymerization is quite similar to conventional polymerization, where linear or regularly structured branched polymers are formed. In this process, radicals that are produced as a result of monomer (M) interactions with the plasma species [ $M + \text{plasma} \rightarrow R^\bullet$ ] interact with unfragmented monomer units to form polymer fragments [ $M + R^\bullet \rightarrow R-M^\bullet \dots \rightarrow R-M^\bullet + M \rightarrow P^\bullet$ ]. Two polymer fragments can then combine to form a polymer chain [ $P^\bullet + P^\bullet \rightarrow P-P$ ]. Linear and branched polymers can also form as a result of ionic chain growth polymerization.

Randomly and irregularly structured materials that bear little resemblance to conventional polymers result from monomer fragmentation–poly recombination process. These materials typically form under continuous plasma regime, and involve plasma-induced fragmentation of the monomer into multiple fragment types, and subsequent random reformation of these fragments into irregular structures. Other processes of interest include ion–molecule reactions, transformation of the monomer into polymer-forming intermediates, fragmentation and recombination reactions involving two or more monomers (in either structured or random manner), and chemical functionalization of surface via grafting. More details on the chemistry of these mechanisms can be found elsewhere.<sup>76</sup>

Precursor structure influences the mechanism of polymer formation, namely through the relative effects of ion and neutral fluxes in the polymer synthesis.<sup>367</sup> For saturated monomers, the deposition rate is directly related to ion flux to the substrate, whereas for unsaturated monomers, the flux of neutral species also contributes to the formation of the polymer. The contribution of the neutral flux decreases as the power of deposition is increased.<sup>367</sup> The material properties of the resultant polymer structures are inherently linked to the chemistry of the precursor, with polymers deposited from saturated monomers characterized by higher elastic moduli, lower solubility, and lower density compared to polymers grown from unsaturated precursors.

The retention of precursor functionality can be further enhanced by using pulsed plasma deposition (Figure 27), where monomer activation and generation of reactive site on the surface occur only during the on-periods (typically microseconds) whereas polymerization takes place during the off-periods (usually milliseconds) in the absence of UV-, ion-, or electron-induced damage to the growing film.<sup>368</sup> Unlike polymers fabricated under continuous low-power plasmas, pulsed plasma-produced polymers show good stability and covalent attachment of the grown film to the substrate at the free radical sites generated during the on-period. Chemical structure, surface morphology, and chemistry of the resultant polymer can be readily tuned by varying the input power,<sup>369</sup> pulsing frequency, and pulse duration.<sup>370,371</sup> The functional units that can be successfully incorporated into polymers using pulsed plasmas include pyridine, anhydride, amine, ester, hydroxyl, sulfonic acid, carboxylic acid, cyano, epoxide, halide, thiol, furan, and many others.<sup>368,372–386</sup>

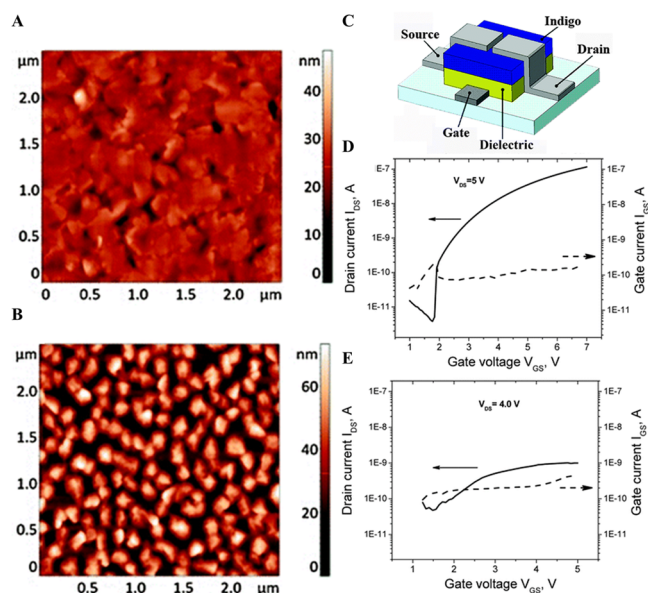


**Figure 27.** Pulsed plasma deposition allows for the synthesis of polymers that consist of more chemically regular products than those fabricated by means of continuous plasma deposition, where predominantly random radical recombination occurs. Reprinted with permission from ref 76. Copyright 2011 Wiley-VCH Verlag GmbH & Co. KGaA.

The use of plasma chemistry in assembly of thin films from naturally occurring semiconductors, such as pigments and dyes, is largely unexplored. Given the ability of plasmas to guide the self-organization and control the structure formation of thin solid film,<sup>53</sup> it may be possible to influence the long-range ordering of dye molecules on a variety of substrates, a behavior currently limited to aliphatic nonpolar substrates. The dependence of mobility on the substrate has been demonstrated in indigoid-containing planar sandwich diodes, where the substrate-induced differences in current–voltage ( $I$ – $V$ ) characteristics reached several orders of magnitude (Figure 28). Since the hopping between the crystallites within the film structure is the mobility-limiting factor, controlling the crystallinity of the growing film is essential.<sup>387</sup>

Low-temperature, weakly ionized plasmas would be appropriate to guide the assembly while preserving the original chemical structure of the monomer. Plasma-assisted etching and modification of the substrate prior to organic semiconductor deposition can also be used, changing the surface chemistry and/or morphology, and thus the surface energy of the material. The micro- and nanoscale patterning of the substrate surface has been demonstrated to influence the growth kinetics of the active layer.<sup>388–390</sup> Plasma environments may be used to tune the chemistry of the thin film during or post deposition by introducing copolymers or feeder gases, with the intent to further lower the LUMO level of the dye and thus improve the n-type operation of the devices.

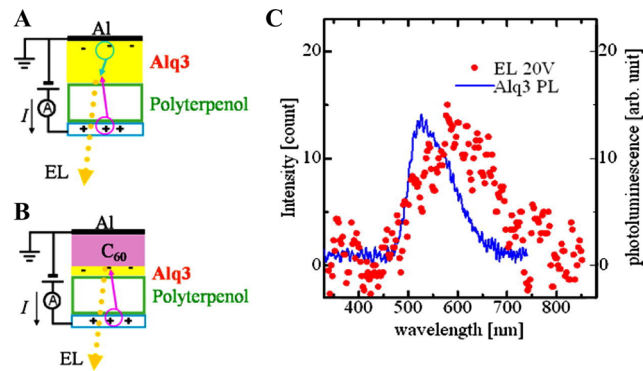
Plasma polymerization is well-suited for the fabrication of dielectric layers from organic precursors. Typical plasma-produced polymers are amorphous and insulating, with good uniformity and adhesion to substrate. Highly cross-linked and branched, plasma-produced polymers are chemically and thermally stable. They are typically fabricated using chemical vapor deposition (CVD) and a gaseous carbon precursor, such as methane, styrene, ethylene, methacrylate, and pyridine. Plasma-produced polymers with a wide variety of other chemical functionalities can be fabricated by using more complex monomer units and/or inorganic gases.<sup>368,372–386</sup> Among natural products, essential oils and their constituents represent suitable sources for plasma-enhanced chemical vapor



**Figure 28.** Effect of morphology of the semiconductor films deposited on different dielectrics on the performance of OFETs. Atomic force microscopy (AFM) images of indigo thin films thermally evaporated on paraffin wax (A) and poly(vinyl alcohol) (B) underlayer dielectrics. Transfer characteristics of indigo-based OFETs (C) fabricated using paraffin wax (D) and poly(vinyl alcohol) (E) as underlayer dielectrics. Reprinted with permission from ref 387. Copyright 2014 Royal Society of Chemistry.

deposition. Essential oils are volatile at room temperature, and thus can be easily delivered to the deposition chamber without the need for additional evaporation. Oils of lavender (*Lavandula angustifolia*), tea tree (*Melaleuca alternifolia*), eucalyptus (*Eucalyptus globulus*), lemongrass (*Cymbopogon nardus*), and their individual components have been successfully polymerized using plasma-enhanced CVD.<sup>391–395</sup> The synthesis of essential-oil-based thin films was plasma-enabled, since no polymer formation was observed under similar conditions in the absence of plasma.

One of the most well studied essential-oil-derived monomers is terpinene-4-ol, a major component of tea tree oil and many other oils. Originally investigated for their biocompatibility, controlled degradation in vivo, and ability to retard bacterial adhesion and biofilm formation,<sup>45,46,48,365</sup> plasma-produced polymers of terpinene-4-ol (polyterpenol) were found to improve the performance of pentacene-based OFET when used as a dielectric interlayer.<sup>396</sup> Incorporation of polyterpenol into OFET shifted the threshold voltage from +20 to −3 V, enhanced the effective mobility from 0.012 to 0.021 cm<sup>2</sup>/(V s), and improved the switching property. Visualization of the carriers within C<sub>60</sub>- and pentacene-based devices using electric field induced optical second harmonic generation revealed the inherent electron blocking hole transport property of polyterpenol.<sup>397–399</sup> This rectifying behavior of polyterpenol is very promising and can be utilized in the fabrication of many organic devices, such as OLEDs (Figure 29). The selective carrier transport in polyterpenol was confirmed using electroluminescent Al/C<sub>60</sub>/tris(8-hydroxyquinoline) aluminum (Alq3)/polyterpenol/indium zinc oxide (IZO) and Al/Alq3/polyterpenol/IZO structures.<sup>398</sup> Interestingly, polymers from linalyl acetate showed hole- and electron-blocking behavior in the same devices.<sup>400</sup> Given that both polyterpenol and poly(linalyl acetate) were produced under the same conditions,



**Figure 29.** Structure and performance of OLEDs with the essential oil derived dielectric layer. Experimental setup and device structure: (A) Al/C<sub>60</sub>/Alq3/polyterpenol/IZO and (B) Al/Alq3/polyterpenol/IZO. (C) Observed electromagnetic radiation as a result of electron–hole recombination in the Alq3 layer. Reprinted with permission from ref 398. Copyright 2012 Elsevier Ltd.

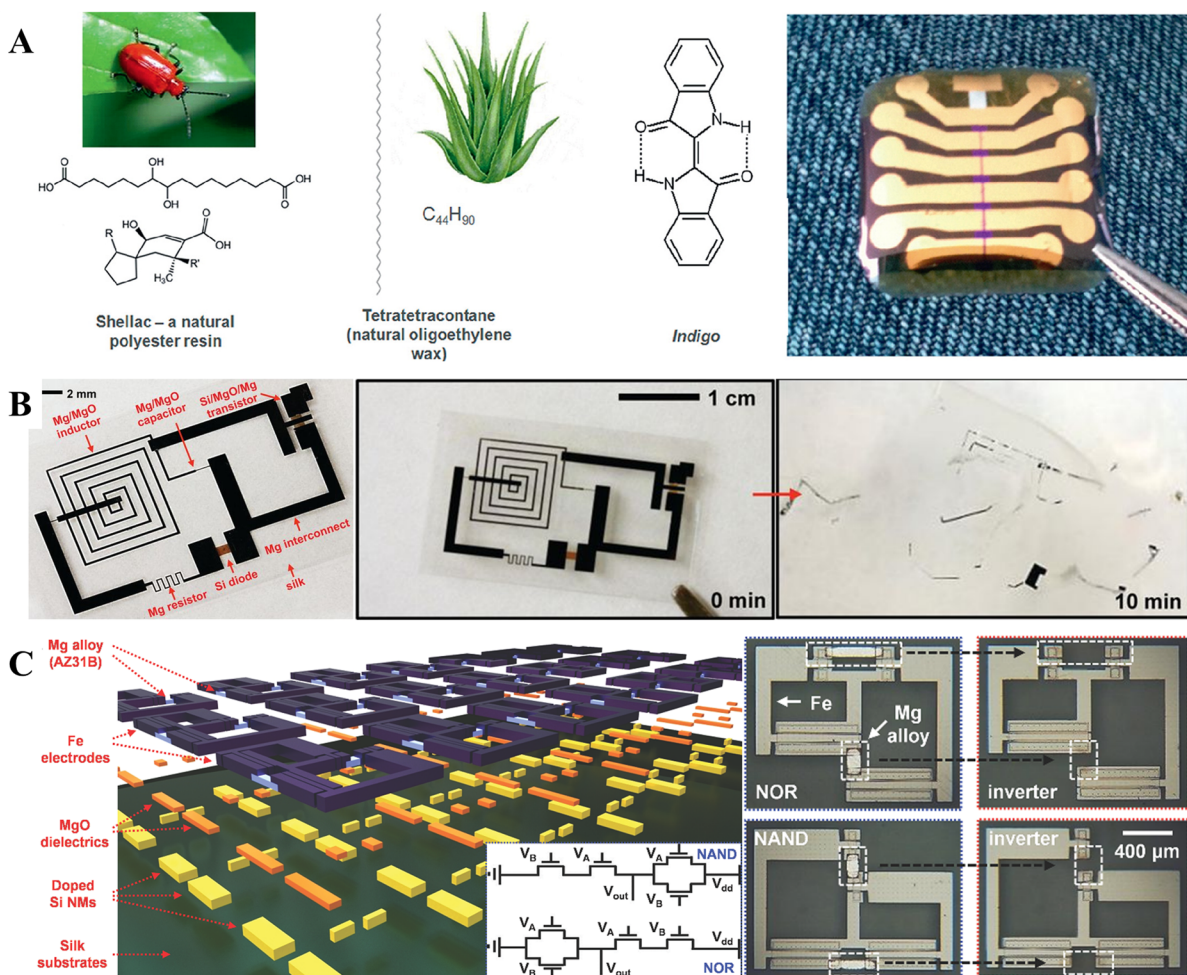
the differences in electrical properties of these polymers arise from the variations in monomer chemistry.

Essential-oil-based plasma-produced polymers were mechanically flexible and adhered well to the substrate, further substantiating their potential as protective barriers to prevent oxygen and water vapor from diffusing into organic electronic devices.<sup>401</sup> Untimely degradation of performance due to degradation of active layers, corrosion of electrodes, and layer delamination is a major issue with most of the currently available organic electronic devices. Unlike many other polymers synthesized with the aid of plasmas, polyterpenol was optically transparent despite being highly cross-linked, even when annealed up to ~200 °C.<sup>402,403</sup> Similar optical properties and thermal stability were also observed for polymers from linalyl acetate, cineol,  $\gamma$ -terpinene, cis- $\beta$ -ocimene, and linalool produced under similar plasma conditions.<sup>394,395,404,405</sup>

Given their chemical and photostability and optical transparency, essential-oil-based plasma-produced polymers are suitable for the encapsulation of organic photovoltaic devices.<sup>406</sup> Encapsulation of the poly[2,6-(4,4-bis(2-ethylhexyl)-4H-cyclopenta[2,1-*b*;3,4-*b'*]dithiophene)-alt-4,7-(2,1,3-benzothiadiazole)]-phenyl C<sub>71</sub>-butyric acid methyl ester (PCPDTBT:PC<sub>70</sub>BM) solar cells with  $\gamma$ -terpinene plasma-produced polymer resulted in a significantly improved performance stability, with the device efficiency slowly decreasing from 3.34 to 2.03% over 80 days. For comparison, the efficiency of the reference device without the encapsulating layer decreased to 1.07% after only 29 days. The short circuit current density, open circuit voltage, and fill factor followed a similar trend, falling markedly in the case of the reference device.

Essential-oil-based plasma-produced polymers are smooth and wettable by many solvents used in solution-based semiconductor processing.<sup>407,408</sup> The surface chemistry and morphology of the dielectric layer are known to influence the optical and morphological characteristics, crystallinity, and charge transport of the semiconducting layers grown on them.<sup>409</sup> Thin films of the n-type, organic semiconductor *N,N'*-bis(*n*-octyl)-1,6-dicyanoperylene-3,4:9,10-bis-(dicarboximide) (PDI-8CN<sub>2</sub>) thermally evaporated on SiO<sub>2</sub> and a linalyl acetate plasma-produced polymer showed variations in morphological and optical properties of the PDI-8CN<sub>2</sub>.<sup>410</sup> Given the flexibility of the plasma enhanced





**Figure 30.** Examples of fully degradable devices. (A) An OFET device utilizing all natural materials. The substrate is shellac foil, produced by drop casting from ethanol solution. An electrochemically grown  $Al_2O_3$  layer passivated with the natural oligoethylene tetratetracontane serves as the gate dielectric. The semiconductor material is indigo. The image on the right shows an array of OFETs on a shellac substrate. These devices showed necessary stability and balanced electron and hole mobilities of  $0.01 \text{ cm}^2/(\text{V s})$ . (B) Demonstration platform for transient electronics, where transistors, diodes, inductors, capacitors, resistors, interconnects, interlayer dielectrics, and silk substrate undergo dissolution in deionized water. (C) By using materials of different types and thicknesses, circuits can be programmed to undergo functional transformation by separation into individual constituent components and also by conversion into equivalent systems but with different operations. In this example, dissolution of Mg alloy segments of the interconnect structure (area marked with dashed line) transforms complementary metal-oxide-semiconductor (CMOS) based NAND and NOR logic gates into inverters. Panel A reprinted with permission from ref 412. Copyright 2012 SPIE. Panel B reprinted with permission from ref 413. Copyright 2012 The American Association for the Advancement of Science. Panel C reprinted with permission from ref 414. Copyright 2014 Wiley-VCH Verlag GmbH & Co. KGaA.

deposition and a wide variety of chemistries offered by natural volatile compounds, the process can be optimized to produce thin layers with the desirable attributes.

### 13. NATURALLY DEGRADABLE DEVICES

Section 1 discussed the potential benefits of electronic devices that, on one hand, can fulfill the needs of conventional, physically stable electronic devices and, on the other hand, degrade under natural or easy-to-control artificial conditions. We have so far considered numerous examples of precursor- and process-driven synthesis of functional nanomaterials for electronic and energy devices, particularly focusing on the areas where salient features of plasmas can give rise to specific benefits, e.g. higher process efficiency, lower cost, and lower environmental impact of the synthesis, as well as better control over the properties and surface organization of carbon nanostructures. This section opens the discussion on the

potential degradation pathways for carbon-based nanomaterials individually and when integrated into complex devices.

In addition to minimizing electronics-associated toxic waste, naturally degradable electronics may enable the development of novel applications, such as nonretrievable environmental and temporary implantable sensors. Irrespective of the selected application, there are some general requirements these devices need to address. First and foremost, the performance of these devices should be reliable, even after extended storage. Second, the cost of fabrication should be comparable to or lower compared to currently available technologies, as it would otherwise impede the market penetration of these devices. Third, their disposal should not involve complicated, energy- or labor-intensive processes. Fourth, the decomposition products that are released from the materials or are formed as a result of chemical reactions between the released species and their environment should not harm the environment. Other



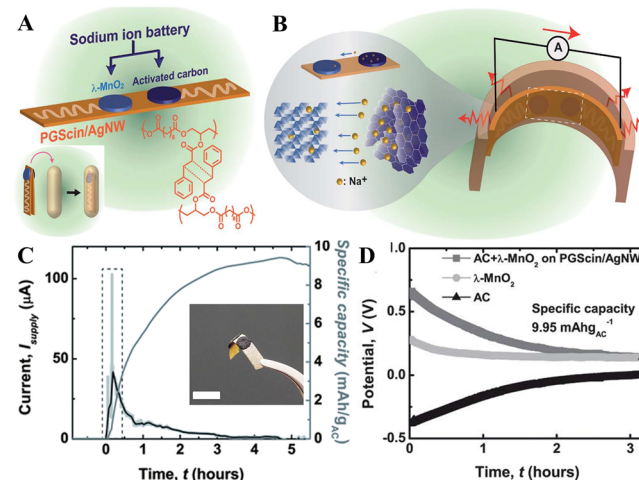
desirable properties include mechanical flexibility, lightweight, small size, favorable biological activity, and some others.<sup>411</sup>

The major challenge in designing naturally degradable devices is to ensure that the byproducts of this degradation process are nontoxic in the own right or when reacted with other chemical substances within and/or outside of the device. Nor should these degradation products accumulate in tissues and organs of humans or other living organisms. Natural degradation is relatively easy to achieve with thin metal layers or soft polymers. Thin metals oxidize readily when exposed to water, and their large surface to volume ratio ensures relatively quick decomposition. In a similar manner, soft polymers and small molecules degrade readily when exposed to water and light. Currently, very few examples of fully naturally degradable electronic devices exist in the literature (Figure 30).<sup>412–414</sup> Furthermore, their current performance, and in particular their stability, is far from the level required for real-world applications. The majority of such examples focus on biomedical applications, as this is the area where most immediate gains are expected.

Magnesium is frequently used for fabrication of conducting elements in naturally degradable devices, with magnesium oxide and silk used as a dielectric material and a substrate/encapsulating layer, respectively.<sup>347</sup> For electrodes and interconnects, in addition to magnesium, other degradable metals, such as iron and zinc, and their alloys are also used.<sup>415</sup> These metals corrode gradually when exposed to humid conditions, dissolving completely into minimally toxic by-products, many of which are essential to many living systems.<sup>416</sup> Figure 30C shows a more sophisticated platform that uses Mg conductors, MgO or SiO<sub>2</sub> dielectrics, monocrystalline Si nanomembranes as semiconductors, and silk as substrate/packaging for fabrication of bioresorbable inductors, capacitors, resistors, diodes, transistors, interconnects, and crossovers.<sup>413</sup> When exposed to deionized water, Mg, MgO, and silk undergo hydrolysis at room temperature, with the rate dependent on the physicochemical properties of the encapsulation layer. Silicon oxides and nitrides also completely dissolve in a controlled fashion with programmable rates that depend on the pH, temperature, and chemical composition of the solution, as well as the specific morphology and chemistry of the films.<sup>417</sup> By using a mix of Fe and Mg conductors, the different dissolution rates of Fe and Mg alloy enable a timed sequence of functional transformations initiated by immersion in water.<sup>414</sup> For example, rapid dissolution of Mg can transform the function from that of CMOS logic gates to CMOS inverters. Sequential degradation can also be achieved by specific patterning of the encapsulation layer.

When developing degradable electronics, it is important to consider potential sources of energy that will power these devices for the intended period of use. Eumelanin pigments derived from *Sepia officinalis* in combination with  $\lambda$ -MnO<sub>2</sub> cathodes, aqueous electrolytes, and sodium ions can be used to fabricate naturally degradable power supplies.<sup>324</sup> The lifetime of a melanin/ $\lambda$ -MnO<sub>2</sub> full cell was estimated to be 5 h when operating at discharge rates of 10  $\mu$ A. Higher energy density of these devices can be obtained by tuning the chemical functionality of protomolecules and enhancing the contact area of the electrode to increase the specific sodium ion loading capacity. Water-activated primary batteries fabricated from Mg foil anodes, Fe, W, or Mo cathodes, phosphate buffered saline electrolyte, and polyanhydride packaging can be multipacked to

achieve energy output sufficient to power LEDs and radio transmitters (Figure 31).<sup>418</sup>

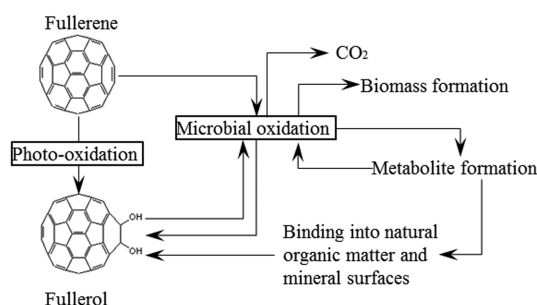


**Figure 31.** Fully degradable, trigger-activated current sources can be used to power temporary electronic devices. (A) A degradable current source consists of flexible composite electrodes and a sodium ion electrochemical cell. The monomers used in this device include glycerol, sebacic acid, cinnamic acid, and  $\alpha$ -truxillic acid. The device is packaged into a degradable capsule for storage and to permit programmable activation. (B) Upon dissolution of the packaging capsule, hydration activates the device by inducing expansion of poly(glycerol-co-sebacate)-cinnamate-silver nanowire (PGScln-AgNW) composite electrodes through reduction of elasticity in mechanically compliant PGScln substrates. Hydration also initiates current flow from the wet electrochemical cell. (C) Supplied current and a total charge delivery gradually decay over time of deployment. (D) Electrochemical potential performance of the current source under a withdrawal current of 10  $\mu$ A. Reprinted with permission from ref 418. Copyright 2013 Royal Society of Chemistry.

#### 14. NATURAL DEGRADATION OF 1D, 2D, AND HYBRID NANOSTRUCTURES

The physicochemical properties of nanocarbon materials are the key determinants of their potential environmental fate, affecting their ability to agglomerate, disperse in aqueous media, photooxidize, undergo microbial oxidation, and react with natural organic and mineral matter. However, under real-world environmental conditions, the movement and degradation of carbon nanomaterials is difficult to assess or predict. For example, in water, unmodified C<sub>60</sub> spontaneously aggregates into  $\sim$ 25–500 nm nanostructures, driven by the hydrophobicity and van der Waals interactions. These nanostructures are stable over a wide range of conditions, and are readily oxidized by water-dissolved ozone to possess carbonyl, vinyl ether, and hydroxyl groups,<sup>419,420</sup> rendering them more water-soluble and susceptible to photooxidation.<sup>421</sup>

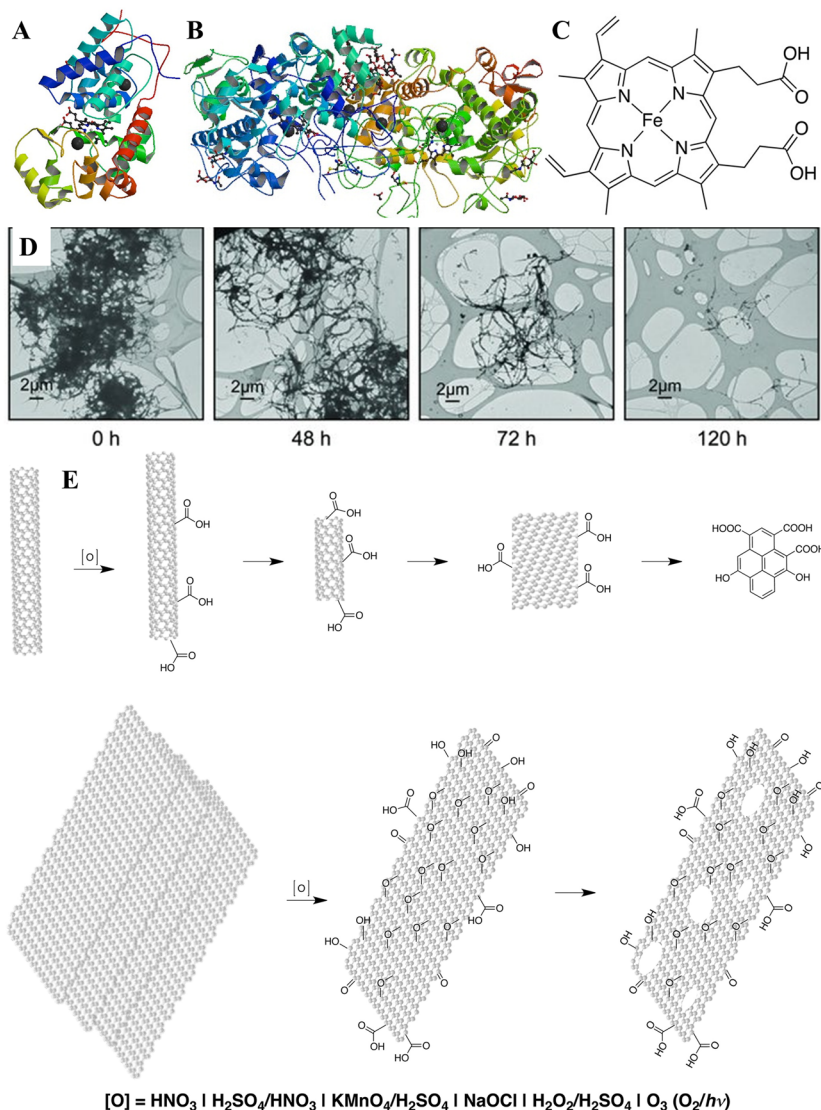
Figure 32 shows an example of the environmental fate of a fullerene as it is oxidized by ozone to fullerol.<sup>422</sup> Widely used to improve specific properties of nanomaterials, surface modifications (functionalization, coating, etc.), derivatization, and complexation may considerably increase the solubility of these particles in water, affecting their ability to penetrate membranes, accumulate, and degrade in living organisms and in the environment.<sup>423</sup> The degradation of carbon nanomaterials also depends on the immediate environment. Soil or water pH, organic carbon and clay content, mineralogy, and cation



**Figure 32.** Potential environmental fates of fullerene. Adapted from and reprinted from ref 422. Copyright 2009 American Chemical Society.

exchange capacity have all been shown to affect the sorption, degradation, and cell/organism uptake of carbon nanomaterials.<sup>12</sup>

Since carbon nanomaterials are readily taken up by plant, microbial, animal, and human cells, cell-mediated degradation is also one of the key mechanisms of environmental transformation of these materials. Many microorganisms have the capacity to decompose highly condensed aromatic hydrocarbons, such as lignin, coal, and biochar.<sup>13–15,424–428</sup> The decay is typically facilitated by extracellular nonspecific enzymes, such as manganese peroxidase, lignin peroxidase, and laccase, which both oxidize and promote polymerization. The latter enables chemical linking of carbon nanostructures to soil and sediment organic matter. White rot basidiomycete fungi (*Phlebia tremellosa* and *Trametes versicolor*) have been



**Figure 33.** Natural degradation of nanocarbon materials. (A, B) Three-dimensional rendering of X-ray crystal structures for (A) horseradish peroxidase isoenzyme C and (B) human leukocyte derived myeloperoxidase. (C) Both enzymes contain an Fe(III) protoporphyrin IX heme group as active sites. (D) Transmission electron microscopy evaluation of in vitro degradation of single-walled CNTs incubated with eosinophil peroxidase. (E) Common pathways for chemical oxidation of carbon nanomaterials. In the presence of H<sub>2</sub>SO<sub>4</sub>, HNO<sub>3</sub>, or another strong oxidant, the sp<sup>2</sup> carbon lattice of unfunctionalized nanostructures is disrupted. Functional groups that contain oxygen are introduced into the structure, with sustained oxidation leading to unzipping and gradual decrease in length (released as CO, CO<sub>2</sub>, aliphatic, and polyaromatic hydrocarbon) of the CNTs. In multilayer graphene, sustained oxidation results in the formation of holes in graphene sheets. Panels A–C and E reprinted from ref 445. Copyright 2012 American Chemical Society. Panel D reprinted with permission from ref 444. Copyright 2013 Wiley-VCH Verlag GmbH & Co. KGaA.

shown to metabolize and degrade an oxygenated C<sub>60</sub> (fullerol) to CO<sub>2</sub>, incorporating minor amounts of the fullerol carbon into lipid biomass.<sup>422</sup>

The evaluation of the interactions between pristine and functionalized carbon nanomaterials with animal cells has demonstrated a wide range of possible impacts, from high cell and organism toxicity to no observable effect.<sup>419,429</sup> In general terms, the nature of cell–nanomaterial interactions is governed by the type of organism or cell line, and the surface chemistry, dimension, and shape of the nanomaterial being investigated.<sup>430–435</sup> Tangled oxidized multiwalled CNTs were observed to agglomerate into large stable complexes in the intercellular space, undergoing minimal degradation,<sup>436</sup> whereas amino-functionalized MWCNTs underwent degradation even at early time points.<sup>437</sup> Interestingly, unmodified, ozone-treated, and aryl-sulfonated CNTs did not degrade under these conditions, indicating that acid carboxylation both introduces carboxyl functionality and also damages the tubular graphenic backbone, providing points for subsequent oxidative attacks.<sup>438</sup> Carboxyl-functionalized 200 nm graphene sheets also agglomerated in tissues into larger 10 μm structures, gradually developing structural disorder from the edges inward.<sup>439</sup> Furthermore, the purity of the nanomaterial may have an effect. Solvents and additives, such as dithio- and diiodooc-tane,<sup>440,441</sup> polydimethylsiloxane,<sup>442</sup> or tetrahydrofuran,<sup>443</sup> frequently used during synthesis or device assembly may be entrapped in the film or agglomerate, potentially affecting the response of the cell to the nanomaterial.<sup>342</sup>

Plant peroxidases, e.g. horseradish peroxidase, and animal peroxidases, e.g. myeloperoxidase, eosinophil peroxidase (Figure 33),<sup>444,445</sup> and lactoperoxidase, have been shown to catalyze the degradation/biodegradation of carbon nanomaterials.<sup>446–448</sup> Strong oxidative activity of horseradish peroxidase (HRP) in the presence of low concentrations of H<sub>2</sub>O<sub>2</sub> is sufficient to initiate biodegradation of carboxylated but not pristine SWCNTs.<sup>449</sup> The latter is degraded readily by chemical oxidants (Figure 33), such as hemin, FeCl<sub>3</sub>, or hypochlorous acid.<sup>450</sup> This observation points toward a heterolytic cleavage of H<sub>2</sub>O<sub>2</sub> with HRP as pristine nanotubes remain intact, and a hemolytic cleavage of H<sub>2</sub>O<sub>2</sub> producing free radicals that oxidize pristine SWCNTs.<sup>451</sup> It is also likely that the state of agglomeration characteristic of hydrophobic pristine CNTs limits access for the enzymes, thus hindering the effective enzyme–tube interactions.

Given the relationship between the surface functionalization and CNT degradation, it is reasonable to attempt to introduce carboxyl, carbonyl, and hydroxyl groups into CNTs (e.g., by strong oxidizing agents) to make them more susceptible to degradation. As carboxyl groups are attached to the graphitic backbone by one bond, this bond is not difficult to cleave, making the carboxylated CNTs more susceptible to oxidation compared to other functionalities. In terms of degradation products, complete disintegration of CNTs would lead to the formation of CO<sub>2</sub> gas. On the other hand, partial degradation will produce a range of oxidized aromatic hydrocarbons. In the case of functionalized MWCNTs, the functional groups would be confined to the outermost layers of the tube; once the external layer is degraded, the pristine internal layer is no longer susceptible to enzymatic oxidation.<sup>452</sup>

Enzymes can be preloaded into naturally degradable components of the device, e.g. substrate or internal encapsulant layer,<sup>453</sup> to be released into the immediate environment of the device in concentrations sufficient for quick degradation of the

nanocarbons with minimal detriment to the surrounding environment.<sup>454</sup> While horseradish peroxidase is commonly used as a model system for enzymatic degradation of CNTs, lower-cost peroxidases from plants or those fabricated using biotechnology can fulfill the need for industrial-scale and environmental applications. Potential limitations of this approach include changes in the properties of the operating environment and premature release of the enzyme from the carrier coating. In the case of the former, introduction of antioxidants may interfere with the oxidative potential of enzymes.<sup>446</sup> For the latter, premature release of the enzyme will alter the properties of the CNTs it comes in contact with, affecting the ability of CNTs to fulfill their purpose. At the same time, some favorable changes can also arise. Treatment of a single layer of graphitic carbon by horseradish peroxidase in the presence of low concentrations of hydrogen peroxide may result in the oxidation of graphene oxide, leading to the formation of holes in its basal plane. The materials produced as a result of the enzymatic reduction demonstrated a p-type semiconducting behavior, with a potential structure of interconnected graphene nanoribbons.<sup>455</sup>

In both enzyme-driven and conventional strong oxidant-based degradation, oxidation and subsequent loss of material from the edges (in the case of CNTs) and across the sheet (through the formation of holes in graphene) play a central role. This opens opportunities for the use of plasmas to accelerate oxidation processes by taking advantage of plasma-specific chemical and physical effects. Furthermore, unlike the enzyme and conventional degradation that relies on wet processing, plasmas can enable high-throughput processing of dry bulk materials, which may be advantageous for single-step decomposition of electronic and energy devices.

## 15. PLASMA-ENABLED DEGRADATION OF MATERIALS

With the knowledge of basic mechanisms that drive biodegradation and chemical degradation of carbon nanomaterials, this section will discuss the plasma environment as the means to facilitate natural degradation (via nanostructure modification at material synthesis stage of the cycle or as postuse treatment) or to decompose the materials into useful building blocks for the synthesis of other functional nanomaterials.

First, let us consider the use of plasmas for waste carbon decomposition. Plasma-assisted technology has established itself in waste management and pollutant control applications, with material recovery and energy generation uses being actively developed. The reactive species in low-temperature plasmas have been used to decompose and remove pollutant molecules, e.g. volatile organic compounds, such as toluene (C<sub>6</sub>H<sub>5</sub>CH<sub>3</sub>), trichloroethane (C<sub>2</sub>H<sub>3</sub>Cl<sub>3</sub>), *n*-heptane (CH<sub>3</sub>(CH<sub>2</sub>)<sub>5</sub>CH<sub>3</sub>), and nitric oxides, and organic particulate matter, such as soot, from gases and liquids.<sup>456,457</sup> The relative ease and speed with which low-temperature plasmas can be adjusted to fluctuating flow volumes and/or contamination levels represents a significant advantage over established methods of waste decomposition, particularly for industrial uses, where both energy efficiency and selectivity are critical. On the industrial scale, plasma-based technologies are frequently coupled with other technologies, with the plasmas primarily acting as an oxidant in the process.<sup>458</sup> The plasma treatment of pollutant-containing gases and liquids typically takes place at ambient temperature and pressure, with dielectric



barrier discharges, corona discharges, and gliding arc discharges typically used as plasma sources.<sup>457</sup> Plasma-generated reactive ions and radicals collide with molecules targeted for degradation, leading to their fast dissociation within 10 ns–1  $\mu$ s time range. Within milliseconds to seconds, the chemical equilibrium is typically reached. There is a potential for plasma-modified pollutants and their products to undergo further conversion to the desired chemicals by means of catalysis at significantly lower energy cost; thus, controlled selective low-temperature and low-energy material decomposition of multi-component solid matter may be achieved.

In addition to directly destroying the waste carbon materials, the effects of the plasma exposure can be more subtle. In section 5.3, examples of the use of plasmas to intentionally introduce defects or functionalize the surface of nanocarbon materials have been discussed. During and postsynthesis, plasma-generated ions and reactive radicals can be used for controlled introduction of line and point defects and creation of pores in the graphene layers, and their chemical functionalization.<sup>53</sup> Certain structural features of materials produced in plasma, such as high accessible surface area and long reactive edges of vertically oriented graphene sheets, are more chemically reactive, and thus potentially more suited to functionalization and degradation.<sup>56,187</sup> Using low-density plasmas, the chemical functionalities can be introduced to or removed from the surface of carbon nanomaterials with minimal damage to the carbon network,<sup>165,166</sup> the integrity of which may be required for some electronics applications. The formation of the defects may be isotropic, e.g. isotropic formation of holes in the basal plane of graphene monolayers, or anisotropic, e.g. formation of uniformly sized hexagonal pits in bi- and multilayer sheets of graphene.<sup>167–169</sup>

By synergistically combining defect-inducing carbon sources, such as those containing minerals,<sup>412</sup> with defect-promoting plasma conditions, such as those with dominant ion bombardment of the surface in contact with the plasma, more readily degradable carbon nanomaterials can be produced. If an appropriate degree of chemical functionalization and/or formation is achieved during the synthesis of the nanocarbon material, this would alleviate the need for postuse treatment of these structures to facilitate their breakdown. This complements the process efficiency, energy and material conservation, and natural degradation design principles of the sustainable nanotech device life cycle described in Figure 1.

Controlled degradation of nanocarbon materials using plasma agitation, functionalization, or postuse treatment briefly discussed above is a relatively new research direction where significant progress is expected in the near future. This expectation is based on the recent progress achieved in the understanding of interactions of plasmas with such materials, and in particular, intentional introduction of defects, holes, chemically reactive sites, etc. which may be regarded as the first step toward controlled degradation under relevant natural or industrial process conditions.

## 16. CONCLUSION AND PERSPECTIVES

The demand for energy and resources involved in the production of silicon electronic and energy devices is expected to double in the next 40 years, with the environmental impacts of production and processing of materials with high embodied energy rapidly becoming critical.<sup>459</sup> In addition to high-quality silicon, manufacturing of modern electronic products consumes a wide variety of minerals, e.g. rare earth elements, indium, and

tantalum, that can both be geologically scarce and/or expensive to process,<sup>460</sup> and for which it is quite difficult to find substitutes.<sup>8</sup> With annual production of 215 and 110 tons, respectively, gallium and indium are expected to last for 20 years before running out completely.<sup>11</sup> In 2010, approximately 70% of globally refined indium was consumed in the fabrication of LCDs, where it is used as a transparent conductive layer.<sup>461</sup> These potential shortages may have a direct limiting effect on the development of thin film photovoltaic modules, where copper–indium diselenide, cadmium telluride, gallium arsenide, and thin film silicon are commonly used.<sup>462,463</sup>

The concept of using minimally processed natural and waste materials in place of conventional highly purified, chemically modified precursors to lower the economic and environmental costs of nanomaterial fabrication is not new. While the interest in using virtually raw renewable organics, e.g. biomass, stems primarily from the desire to address the excessive energy and material consumption associated with the use of inorganic and processed organic compounds, the use of waste carbons also addresses the escalating issue of waste management. Given the ever-increasing volumes and chemical diversity of waste generated globally, consumption of waste carbons, such as food supply chain waste and plastic waste, have also emerged as a significant opportunity to convert the present-day economic and environmental burden into higher-value products.<sup>2</sup> The opportunity is particularly attractive for developing countries, where low-cost materials, such as biomass and coal, are abundant, whereas the opportunities for waste recycling are presently limited.<sup>464–467</sup>

The critical challenge in enabling the convergence of the natural- and waste-derived nanocarbons and high-performance electronic and energy devices lies in finding processes that would enable controlled, reproducible conversion of minimally processed carbon matter into functional materials in a largely *process-driven* manner. These processes should be supported by environmentally benign yet highly efficient chemistries, with the sustainability considerations applied to every stage of the product life cycle: from the synthesis to applications and postuse waste management. There are many promising chemistries that can be effective at low temperatures and atmospheric pressure and rely on human-health-friendly precursor materials. However, many such chemistries are precursor-driven, which significantly limits their ability to convert chemically heterogeneous, batch-to-batch varying carbon resources into nanocarbon materials with the degree of consistency demanded by the industry.

Given the vast diversity of green synthesis methods, it was outside of the scope of this review to provide an exhaustive account of the existing knowledge in the area of sustainable chemical synthesis. It was our intent to highlight the most interesting and promising features of the plasma-enabled synthesis and processing of carbon-based nanostructures for electronics and energy applications. The examples selected for this review suggest that low-temperature reactive plasmas can indeed be employed as a stand-alone tool for green synthesis, surface organization, and postprocessing of diverse nanomaterials, and for their ability to accelerate chemical reactions.

In the area of plasma-enhanced nanofabrication, multiple opportunities for further developments are continuously arising. Although plasma-aided processing is a well-established part of silicon semiconductor fabrication, the examples presented in this review mainly deal with the laboratory-scale synthesis. Furthermore, for many emerging applications, the

energy consumption of the plasma processes used for the synthesis of graphene and CNTs still remain quite significant. It is our deliberate choice to focus on the sustainability aspects of the plasma processes, particularly on reducing the energy and material consumption and several other aspects. On the other hand, the opportunities and challenges associated with the scale-up, translation, and adoption of the relevant technologies for industrial applications are outside the scope of this review.

Nevertheless, being an exciting, rapidly developing topic, major advances in the understanding of the underlying mechanisms and in our ability to control the processes and the outcomes are expected in the near future. Given that the plasma synthesis outcomes are determined by the synergistic contributions of chemical and physical effects, it places the discovery of these mechanisms and potential applications at the interdisciplinary interface. Industrial uptake and adoption of these technologies is an exciting avenue for future development. However, detailed technology assessment involving a multi-disciplinary team of engineers, economists, health, safety, and environmental officers, as well as policy makers is warranted to develop a more overarching picture. We hope that the points raised in this review on aspects of the plasma-enabled sustainable life cycles of natural-precursor-derived nanocarbons will stimulate further advancement of this interesting and rapidly evolving multidisciplinary field.

## AUTHOR INFORMATION

### Corresponding Author

\*E-mail: kostya.ostrikov@qut.edu.au.

### Notes

The authors declare no competing financial interest.

### Biographies

Kateryna Bazaka is an ARC DECRA Fellow with Health and Biomedical Technologies, Queensland University of Technology, Australia. Kateryna is a recipient of the Australian Institute of Nuclear Science and Engineering Postgraduate Award, the Queensland Government Smart Women Smart State Award, the Science and Innovation Awards for Young People in Agriculture Fisheries and Forestry, two Endeavour Research Fellowships, the Inaugural Advanced Manufacturing Cooperative Research Centre Student Prize, an AINSE Gold Medal, and is an author of one monograph and 45 refereed journal papers. Her research focuses on nanoscale processing of materials and living matter for biomedical and electronic applications.

Mohan Jacob is currently an associate professor and the Associate Dean, Research Education, for the College of Science, Technology and Engineering, James Cook University. University of Delhi awarded him a Ph.D. in 1999 in electronic science. He has published over 150 peer-reviewed articles. He developed methods to precisely characterize the dielectric properties of materials at cryogenic temperatures and microwave frequencies. His main research interests also include the development of polymer thin films and graphene from sustainable sources using plasma-enhanced chemical vapor deposition, environmentally friendly biomaterials, and electronic and biomedical devices.

Kostya (Ken) Ostrikov is a professor with Queensland University of Technology and a Science Leader of the Office of Chief Executive with CSIRO, Australia. His achievements include the Pawsey (2008) medal of the Australian Academy of Sciences, the Walter Boas (2010) medal of the Australian Institute of Physics, a Building Future Award (2012), an NSW Science and Engineering Award (2014), election to the

Academy of Europe (2015), six prestigious fellowships in six countries, several patents, three monographs, and more than 470 journal papers. His research on nanoscale control of energy and matter contributes to the solution of the grand challenge of directing energy and matter at the nanoscale, to develop renewable energy and energy-efficient technologies for a sustainable future.

## ACKNOWLEDGMENTS

This work was partially supported by the Australian Research Council (DE130101550, FT100100303, and DP160103116) and CSIRO's Science Leadership Program.

## REFERENCES

- (1) Krishnan, N.; Boyd, S.; Somani, A.; Raoux, S.; Clark, D.; Dornfeld, D. A Hybrid Life Cycle Inventory of Nano-Scale Semiconductor Manufacturing. *Environ. Sci. Technol.* **2008**, *42* (8), 3069–3075.
- (2) Gao, T.; Jelle, B. P.; Sandberg, L. I. C.; Gustavsen, A. Monodisperse Hollow Silica Nanospheres for Nano Insulation Materials: Synthesis, Characterization, and Life Cycle Assessment. *ACS Appl. Mater. Interfaces* **2013**, *5* (3), 761–767.
- (3) Anastas, P. T.; Zimmerman, J. B. Peer Reviewed: Design through the 12 Principles of Green Engineering. *Environ. Sci. Technol.* **2003**, *37* (5), 94A–101A.
- (4) Bergeson, L. L. Sustainable Nanomaterials: Emerging Governance Systems. *ACS Sustainable Chem. Eng.* **2013**, *1* (7), 724–730.
- (5) Abraham, M. A.; Nguyen, N. "Green Engineering: Defining the Principles"—Results from the Sandestin Conference. *Environ. Prog.* **2003**, *22* (4), 233–236.
- (6) Anastas, P. T.; Warner, J. C. *Green Chemistry: Theory and Practice*; Oxford University Press: New York, 1998.
- (7) Leisinger, K. Business Needs to Embrace Sustainability Targets. *Nature* **2015**, *528* (7581), 165.
- (8) Woodhouse, M.; Goodrich, A.; Margolis, R.; James, T.; Dhere, R.; Gessert, T.; Barnes, T.; Eggert, R.; Albin, D. Perspectives on the Pathways for Cadmium Telluride Photovoltaic Module Manufacturers to Address Expected Increases in the Price for Tellurium. *Sol. Energy Mater. Sol. Cells* **2013**, *115*, 199–212.
- (9) Gutowski, T. G.; Branham, M. S.; Dahmus, J. B.; Jones, A. J.; Thiriez, A.; Sekulic, D. P. Thermodynamic Analysis of Resources Used in Manufacturing Processes. *Environ. Sci. Technol.* **2009**, *43* (5), 1584–1590.
- (10) Murphy, C. F.; Kenig, G. A.; Allen, D. T.; Laurent, J.-P.; Dyer, D. E. Development of Parametric Material, Energy, and Emission Inventories for Wafer Fabrication in the Semiconductor Industry. *Environ. Sci. Technol.* **2003**, *37* (23), 5373–5382.
- (11) Irimia-Vladu, M. "Green" Electronics: Biodegradable and Biocompatible Materials and Devices for Sustainable Future. *Chem. Soc. Rev.* **2014**, *43* (2), 588–610.
- (12) Avnasi, R.; Jackson, W. A.; Sherwin, B.; Mudge, J. F.; Anderson, T. A. C60 Fullerene Soil Sorption, Biodegradation, and Plant Uptake. *Environ. Sci. Technol.* **2014**, *48* (5), 2792–2797.
- (13) Dean-Ross, D.; Cerniglia, C. E. Degradation of Pyrene by *Mycobacterium Flavesens*. *Appl. Microbiol. Biotechnol.* **1996**, *46* (3), 307–312.
- (14) Leonowicz, A.; Matuszewska, A.; Luterek, J.; Ziegenhagen, D.; Wojtaś-Wasilewska, M.; Cho, N.-S.; Hofrichter, M.; Rogalski, J. Biodegradation of Lignin by White Rot Fungi. *Fungal Genet. Biol.* **1999**, *27* (2–3), 175–185.
- (15) Márquez-Rocha, F.; Hernández-Rodríguez, V.; Vázquez-Duhalt, R. Biodegradation of Soil-Adsorbed Polycyclic Aromatic Hydrocarbons by the White Rot Fungus *Pleurotus Ostreatus*. *Biotechnol. Lett.* **2000**, *22* (6), 469–472.
- (16) Wei, S.; Zhu, J.; Gu, H.; Wei, H.; Yan, X.; Huang, Y.; Guo, Z. Multifunctional Nanocomposites for Environmental Remediation. In *Nanomaterials for Environmental Protection*; John Wiley & Sons, Inc.: 2014; pp 71–84.

- (17) Bockhorn, H.; Hornung, A.; Hornung, U. Stepwise Pyrolysis for Raw Material Recovery from Plastic Waste. *J. Anal. Appl. Pyrolysis* **1998**, *46* (1), 1–13.
- (18) Burange, A. S.; Gawande, M. B.; Lam, F. L. Y.; Jayaram, R. V.; Luque, R. Heterogeneously Catalyzed Strategies for the Deconstruction of High Density Polyethylene: Plastic Waste Valorisation to Fuels. *Green Chem.* **2015**, *17* (1), 146–156.
- (19) Sekitani, T.; Zschieschang, U.; Klauk, H.; Someya, T. Flexible Organic Transistors and Circuits with Extreme Bending Stability. *Nat. Mater.* **2010**, *9* (12), 1015–1022.
- (20) Yi, H. T.; Payne, M. M.; Anthony, J. E.; Podzorov, V. Ultra-Flexible Solution-Processed Organic Field-Effect Transistors. *Nat. Commun.* **2012**, *3*, 1259.
- (21) Rus, D.; Tolley, M. T. Design, Fabrication and Control of Soft Robots. *Nature* **2015**, *521* (7553), 467–475.
- (22) Kaltenbrunner, M.; White, M. S.; Glowacki, E. D.; Sekitani, T.; Someya, T.; Sariciftci, N. S.; Bauer, S. Ultrathin and Lightweight Organic Solar Cells with High Flexibility. *Nat. Commun.* **2012**, *3*, 770.
- (23) Wang, X.; Tian, H.; Mohammad, M. A.; Li, C.; Wu, C.; Yang, Y.; Ren, T.-L. A Spectrally Tunable All-Graphene-Based Flexible Field-Effect Light-Emitting Device. *Nat. Commun.* **2015**, *6*, 7767.
- (24) Kim, D.-I.; Quang Trung, T.; Hwang, B.-U.; Kim, J.-S.; Jeon, S.; Bae, J.; Park, J.-J.; Lee, N.-E. A Sensor Array Using Multi-Functional Field-Effect Transistors with Ultrahigh Sensitivity and Precision for Bio-Monitoring. *Sci. Rep.* **2015**, *5*, 12705.
- (25) Yu, Z.; Niu, X.; Liu, Z.; Pei, Q. Intrinsically Stretchable Polymer Light-Emitting Devices Using Carbon Nanotube-Polymer Composite Electrodes. *Adv. Mater.* **2011**, *23* (34), 3989–3994.
- (26) White, M. S.; Kaltenbrunner, M.; Glowacki, E. D.; Gutnichenko, K.; Kettlgruber, G.; Graz, I.; Aazou, S.; Ulbricht, C.; Egbe, D. A. M.; Miron, M. C.; Major, Z.; Scharber, M. C.; Sekitani, T.; Someya, T.; Bauer, S.; Sariciftci, N. S. Ultrathin, Highly Flexible and Stretchable Pleds. *Nat. Photonics* **2013**, *7* (10), 811–816.
- (27) Kaltenbrunner, M.; Sekitani, T.; Reeder, J.; Yokota, T.; Kuribara, K.; Tokuhara, T.; Drack, M.; Schwodiauer, R.; Graz, I.; Bauer-Gogonea, S.; Bauer, S.; Someya, T. An Ultra-Lightweight Design for Imperceptible Plastic Electronics. *Nature* **2013**, *499* (7459), 458–463.
- (28) Liang, J.; Li, L.; Niu, X.; Yu, Z.; Pei, Q. Elastomeric Polymer Light-Emitting Devices and Displays. *Nat. Photonics* **2013**, *7* (10), 817–824.
- (29) Kaltenbrunner, M.; White, M. S.; Sekitani, T.; Sariciftci, N. S.; Bauer, S.; Someya, T. Breakthroughs in Photonics 2012: Large-Area Ultrathin Photonics. *IEEE Photonics J.* **2013**, *5* (2), 0700805–0700805.
- (30) Andersen, T. R.; Dam, H. F.; Hosel, M.; Helgesen, M.; Carle, J. E.; Larsen-Olsen, T. T.; Gevorgyan, S. A.; Andreasen, J. W.; Adams, J.; Li, N.; Machui, F.; Spyropoulos, G. D.; Ameri, T.; Lemaitre, N.; Legros, M.; Scheel, A.; Gaiser, D.; Kreul, K.; Berny, S.; Lozman, O. R.; Nordman, S.; Valimaki, M.; Vilkmann, M.; Sondergaard, R. R.; Jorgensen, M.; Brabec, C. J.; Krebs, F. C. Scalable, Ambient Atmosphere Roll-to-Roll Manufacture of Encapsulated Large Area, Flexible Organic Tandem Solar Cell Modules. *Energy Environ. Sci.* **2014**, *7* (9), 2925–2933.
- (31) Jambeck, J. R.; Geyer, R.; Wilcox, C.; Siegler, T. R.; Perryman, M.; Andrady, A.; Narayan, R.; Law, K. L. Plastic Waste Inputs from Land into the Ocean. *Science* **2015**, *347* (6223), 768–771.
- (32) Abdelaziz, R.; Disci-Zayed, D.; Hedayati, M. K.; Pöhls, J.-H.; Zillohu, A. U.; Erkartal, B.; Chakravadhanula, V. S. K.; Duppel, V.; Kienle, L.; Elbahri, M. Green Chemistry and Nanofabrication in a Levitated Leidenfrost Drop. *Nat. Commun.* **2013**, *4*, 2400.
- (33) Semsarilar, M.; Perrier, S. 'Green' Reversible Addition-Fragmentation Chain-Transfer (RAFT) Polymerization. *Nat. Chem.* **2010**, *2* (10), 811–820.
- (34) Keddie, D. J. A Guide to the Synthesis of Block Copolymers Using Reversible-Addition Fragmentation Chain Transfer (RAFT) Polymerization. *Chem. Soc. Rev.* **2014**, *43* (2), 496–505.
- (35) Kobayashi, S.; Makino, A. Enzymatic Polymer Synthesis: An Opportunity for Green Polymer Chemistry. *Chem. Rev.* **2009**, *109* (11), 5288–5353.
- (36) Li, W.; Zhang, Z.; Kong, B.; Feng, S.; Wang, J.; Wang, L.; Yang, J.; Zhang, F.; Wu, P.; Zhao, D. Simple and Green Synthesis of Nitrogen-Doped Photoluminescent Carbonaceous Nanospheres for Bioimaging. *Angew. Chem., Int. Ed.* **2013**, *52* (31), 8151–8155.
- (37) Ostrikov, K.; Mehdipour, H. Nanoscale Plasma Chemistry Enables Fast, Size-Selective Nanotube Nucleation. *J. Am. Chem. Soc.* **2012**, *134* (9), 4303–4312.
- (38) Iravani, S. Green Synthesis of Metal Nanoparticles Using Plants. *Green Chem.* **2011**, *13* (10), 2638–2650.
- (39) Neyts, E. C.; Bogaerts, A. Understanding Plasma Catalysis through Modelling and Simulation—a Review. *J. Phys. D: Appl. Phys.* **2014**, *47* (22), 224010.
- (40) Mutaf-yardimci, O.; Saveliev, A. V.; Fridman, A. A.; Kennedy, L. A. Employing Plasma as Catalyst in Hydrogen Production. *Int. J. Hydrogen Energy* **1998**, *23* (12), 1109–1111.
- (41) Neyts, E. C.; Ostrikov, K. Nanoscale Thermodynamic Aspects of Plasma Catalysis. *Catal. Today* **2015**, *256*, 23–28.
- (42) Jacob, M. V.; Rawat, R. S.; Ouyang, B.; Bazaka, K.; Kumar, D. S.; Taguchi, D.; Iwamoto, M.; Neupane, R.; Varghese, O. K. Catalyst-Free Plasma Enhanced Growth of Graphene from Sustainable Sources. *Nano Lett.* **2015**, *15* (9), 5702–5708.
- (43) Neyts, E. C.; Ostrikov, K.; Sunkara, M. K.; Bogaerts, A. Plasma Catalysis: Synergistic Effects at the Nanoscale. *Chem. Rev.* **2015**, *115*, 13408.
- (44) Chen, H. L.; Lee, H. M.; Chen, S. H.; Chao, Y.; Chang, M. B. Review of Plasma Catalysis on Hydrocarbon Reforming for Hydrogen Production—Interaction, Integration, and Prospects. *Appl. Catal., B* **2008**, *85* (1–2), 1–9.
- (45) Bazaka, K.; Jacob, M. V.; Crawford, R. J.; Ivanova, E. P. Plasma-Assisted Surface Modification of Organic Biopolymers to Prevent Bacterial Attachment. *Acta Biomater.* **2011**, *7* (5), 2015–2028.
- (46) Bazaka, K.; Jacob, M. V.; Truong, V. K.; Wang, F.; Pushpamali, W. A. A.; Wang, J. Y.; Ellis, A. V.; Berndt, C. C.; Crawford, R. J.; Ivanova, E. P. Plasma-Enhanced Synthesis of Bioactive Polymeric Coatings from Monoterpene Alcohols: A Combined Experimental and Theoretical Study. *Biomacromolecules* **2010**, *11* (8), 2016–2026.
- (47) Ahmad, J.; Bazaka, K.; Whittle, J. D.; Michelmore, A.; Jacob, M. V. Structural Characterization of  $\Gamma$ -Terpinene Thin Films Using Mass Spectroscopy and X-Ray Photoelectron Spectroscopy. *Plasma Processes Polym.* **2015**, *12*, 1085.
- (48) Bazaka, K.; Jacob, M.; Truong, V. K.; Crawford, R. J.; Ivanova, E. P. The Effect of Polyterpenol Thin Film Surfaces on Bacterial Viability and Adhesion. *Polymers* **2011**, *3* (1), 388–404.
- (49) Hynes, A. M.; Shenton, M. J.; Badyal, J. P. S. Pulsed Plasma Polymerization of Perfluorocyclohexane. *Macromolecules* **1996**, *29* (12), 4220–4225.
- (50) Ryan, M. E.; Hynes, A. M.; Badyal, J. P. S. Pulsed Plasma Polymerization of Maleic Anhydride. *Chem. Mater.* **1996**, *8* (1), 37–42.
- (51) Bazaka, K.; Jacob, M. V.; Chrzanowski, W.; Ostrikov, K. Anti-Bacterial Surfaces: Natural Agents, Mechanisms of Action, and Plasma Surface Modification. *RSC Adv.* **2015**, *5* (60), 48739–48759.
- (52) Blanksby, S. J.; Ellison, G. B. Bond Dissociation Energies of Organic Molecules. *Acc. Chem. Res.* **2003**, *36* (4), 255–263.
- (53) Ostrikov, K.; Neyts, E. C.; Meyyappan, M. Plasma Nanoscience: From Nano-Solids in Plasmas to Nano-Plasmas in Solids. *Adv. Phys.* **2013**, *62* (2), 113–224.
- (54) Bo, Z.; Yang, Y.; Chen, J.; Yu, K.; Yan, J.; Cen, K. Plasma-Enhanced Chemical Vapor Deposition Synthesis of Vertically Oriented Graphene Nanosheets. *Nanoscale* **2013**, *5* (12), 5180–5204.
- (55) Seo, D. H.; Han, Z. J.; Kumar, S.; Ostrikov, K. Structure-Controlled, Vertical Graphene-Based, Binder-Free Electrodes from Plasma-Reformed Butter Enhance Supercapacitor Performance. *Adv. Energy Mater.* **2013**, *3* (10), 1316–1323.
- (56) Seo, D. H.; Rider, A. E.; Han, Z. J.; Kumar, S.; Ostrikov, K. Plasma Break-Down and Re-Build: Same Functional Vertical Graphenes from Diverse Natural Precursors. *Adv. Mater.* **2013**, *25* (39), 5638–5642.



- (57) Dresselhaus, M. S.; Terrones, M. Carbon-Based Nanomaterials from a Historical Perspective. *Proc. IEEE* **2013**, *101* (7), 1522–1535.
- (58) Kroto, H. W.; Heath, J. R.; O'Brien, S. C.; Curl, R. F.; Smalley, R. E. C<sub>60</sub>: Buckminsterfullerene. *Nature* **1985**, *318* (6042), 162–163.
- (59) Geim, A. K.; Novoselov, K. S. The Rise of Graphene. *Nat. Mater.* **2007**, *6* (3), 183–191.
- (60) Iijima, S. Helical Microtubules of Graphitic Carbon. *Nature* **1991**, *354* (6348), 56.
- (61) Nasibulin, A. G.; Pikhitsa, P. V.; Jiang, H.; Brown, D. P.; Krasheninnikov, A. V.; Anisimov, A. S.; Queipo, P.; Moisala, A.; Gonzalez, D.; Lientschnig, G.; Hassanien, A.; Shandakov, S. D.; Lolli, G.; Resasco, D. E.; Choi, M.; Tomanek, D.; Kauppinen, E. I. A Novel Hybrid Carbon Material. *Nat. Nanotechnol.* **2007**, *2* (3), 156–161.
- (62) Rode, A. V.; Gamaly, E. G.; Christy, A. G.; Fitz Gerald, J. G.; Hyde, S. T.; Elliman, R. G.; Luther-Davies, B.; Veinger, A. I.; Androulakis, J.; Giapintzakis, J. Unconventional Magnetism in All-Carbon Nanofoam. *Phys. Rev. B: Condens. Matter Mater. Phys.* **2004**, *70* (5), 054407.
- (63) Tang, J.; Jin, G.-Q.; Wang, Y.-Y.; Guo, X.-Y. Tree-Like Carbon Grown from Camphor. *Carbon* **2010**, *48* (5), 1545–1551.
- (64) Chesnokov, V. V.; Zaikovskii, V. I.; Buyanov, R. A. Symmetric Twisted Carbon Filaments Formed from Butadiene-1,3 on Ni–Cu/Mgo-Catalyst: Growth Regularities and Mechanism. *J. Mol. Catal. A: Chem.* **2000**, *158* (1), 267–270.
- (65) Jin, Y. Z.; Gao, C.; Hsu, W. K.; Zhu, Y.; Huczko, A.; Bystrzejewski, M.; Roe, M.; Lee, C. Y.; Acquah, S.; Kroto, H.; Walton, D. R. M. Large-Scale Synthesis and Characterization of Carbon Spheres Prepared by Direct Pyrolysis of Hydrocarbons. *Carbon* **2005**, *43* (9), 1944–1953.
- (66) Zhang, J.; Du, J.; Qian, Y.; Xiong, S. Synthesis, Characterization and Properties of Carbon Nanotubes Microspheres from Pyrolysis of Polypropylene and Maleated Polypropylene. *Mater. Res. Bull.* **2010**, *45* (1), 15–20.
- (67) Suriani, A. B.; Azira, A. A.; Nik, S. F.; Md Nor, R.; Rusop, M. Synthesis of Vertically Aligned Carbon Nanotubes Using Natural Palm Oil as Carbon Precursor. *Mater. Lett.* **2009**, *63* (30), 2704–2706.
- (68) Shaikjee, A.; Coville, N. J. Catalyst Restructuring Studies: The Facile Synthesis of Tripod-Like Carbon Fibers by the Decomposition of Trichloroethylene. *Mater. Lett.* **2012**, *68*, 273–276.
- (69) Shaikjee, A.; Coville, N. J. The Effect of Substituted Alkynes on Nickel Catalyst Morphology and Carbon Fiber Growth. *Carbon* **2012**, *50* (3), 1099–1108.
- (70) Shaikjee, A.; Coville, N. J. A Novel Type of Carbon: The Synthesis of Patterned Co-Block Carbon Nanofibers. *Small* **2011**, *7* (18), 2593–2597.
- (71) Wang, J.; Wang, C.-F.; Chen, S. Amphiphilic Egg-Derived Carbon Dots: Rapid Plasma Fabrication, Pyrolysis Process, and Multicolor Printing Patterns. *Angew. Chem., Int. Ed.* **2012**, *51* (37), 9297–9301.
- (72) Seo, D. H.; Rider, A. E.; Kumar, S.; Randeniya, L. K.; Ostrikov, K. Vertical Graphene Gas- and Bio-Sensors Via Catalyst-Free, Reactive Plasma Reforming of Natural Honey. *Carbon* **2013**, *60*, 221–228.
- (73) Di Mundo, R.; Palumbo, F.; Barucca, G.; Sabato, G.; d'Agostino, R. On the “Growth” of Nano-Structures on C-Silicon Via Self-Masked Plasma Etching Processes. *Plasma Processes Polym.* **2013**, *10* (10), 843–849.
- (74) Liu, Z.; Gu, X.; Hwu, J.; Sassolini, S.; Olynick, D. L. Low-Temperature Plasma Etching of High Aspect-Ratio Densely Packed 15 to Sub-10 Nm Silicon Features Derived from Ps-Pdms Block Copolymer Patterns. *Nanotechnology* **2014**, *25* (28), 285301.
- (75) Pai, D. Z.; Ostrikov, K.; Kumar, S.; Lacoste, D. A.; Levchenko, I.; Laux, C. O. Energy Efficiency in Nanoscale Synthesis Using Nanosecond Plasmas. *Sci. Rep.* **2013**, *3*, 1221.
- (76) Friedrich, J. Mechanisms of Plasma Polymerization – Reviewed from a Chemical Point of View. *Plasma Processes Polym.* **2011**, *8* (9), 783–802.
- (77) Kumar, S.; van der Laan, T.; Rider, A. E.; Randeniya, L.; Ostrikov, K. Multifunctional Three-Dimensional T-Junction Graphene Micro-Wells: Energy-Efficient, Plasma-Enabled Growth and Instant Water-Based Transfer for Flexible Device Applications. *Adv. Funct. Mater.* **2014**, *24* (39), 6114–6122.
- (78) Ostrikov, K.; Mehdipour, H. Thin Single-Walled Carbon Nanotubes with Narrow Chirality Distribution: Constructive Interplay of Plasma and Gibbs–Thomson Effects. *ACS Nano* **2011**, *5* (10), 8372–8382.
- (79) Mehdipour, H.; Ostrikov, K. Size- and Orientation-Selective Si Nanowire Growth: Thermokinetic Effects of Nanoscale Plasma Chemistry. *J. Am. Chem. Soc.* **2013**, *135* (5), 1912–1918.
- (80) Tam, E.; Ostrikov, K. Plasma-Controlled Adatom Delivery and (Re)Distribution: Enabling Uninterrupted, Low-Temperature Growth of Ultralong Vertically Aligned Single Walled Carbon Nanotubes. *Appl. Phys. Lett.* **2008**, *93* (26), 261504.
- (81) Dato, A.; Radmilovic, V.; Lee, Z.; Phillips, J.; Frenklach, M. Substrate-Free Gas-Phase Synthesis of Graphene Sheets. *Nano Lett.* **2008**, *8* (7), 2012–2016.
- (82) Bhat, N. V.; Upadhyay, D. J.; Deshmukh, R. R.; Gupta, S. K. Investigation of Plasma-Induced Photochemical Reaction on a Polypropylene Surface. *J. Phys. Chem. B* **2003**, *107* (19), 4550–4559.
- (83) Sedlacek, O.; Monnery, B. D.; Filippov, S. K.; Hoogenboom, R.; Hruby, M. Poly(2-Oxazoline)S – Are They More Advantageous for Biomedical Applications Than Other Polymers? *Macromol. Rapid Commun.* **2012**, *33* (19), 1648–1662.
- (84) Macgregor-Ramiasa, M. N.; Cavallaro, A. A.; Vasilev, K. Properties and Reactivity of Polyoxazoline Plasma Polymer Films. *J. Mater. Chem. B* **2015**, *3* (30), 6327–6337.
- (85) Ritikos, R.; Rahman, S. A.; Gani, S. M. A.; Muhamad, M. R.; Yap, Y. K. Catalyst-Free Formation of Vertically-Aligned Carbon Nanorods as Induced by Nitrogen Incorporation. *Carbon* **2011**, *49* (6), 1842–1848.
- (86) Zeniou, A.; Ellinas, K.; Olziersky, A.; Gogolides, E. Ultra-High Aspect Ratio Si Nanowires Fabricated with Plasma Etching: Plasma Processing, Mechanical Stability Analysis against Adhesion and Capillary Forces and Oleophobicity. *Nanotechnology* **2014**, *25* (3), 035302.
- (87) Song, Y.; Park, G.; Kang, E.; Yeo, C.; Lee, Y. Antireflective Grassy Surface on Glass Substrates with Self-Masked Dry Etching. *Nanoscale Res. Lett.* **2013**, *8*, 505.
- (88) Hsu, C.-H.; Lo, H.-C.; Chen, C.-F.; Wu, C. T.; Hwang, J.-S.; Das, D.; Tsai, J.; Chen, L.-C.; Chen, K.-H. Generally Applicable Self-Masked Dry Etching Technique for Nanotip Array Fabrication. *Nano Lett.* **2004**, *4* (3), 471–475.
- (89) Du, K.; Wathuthanthri, I.; Liu, Y.; Kang, Y. T.; Choi, C.-H. Fabrication of Polymer Nanowires Via Maskless O<sub>2</sub> Plasma Etching. *Nanotechnology* **2014**, *25* (16), 165301.
- (90) Wang, Q.; Wang, X.; Chai, Z.; Hu, W. Low-Temperature Plasma Synthesis of Carbon Nanotubes and Graphene Based Materials and Their Fuel Cell Applications. *Chem. Soc. Rev.* **2013**, *42* (23), 8821–8834.
- (91) Anthony, R. J.; Cheng, K.-Y.; Holman, Z. C.; Holmes, R. J.; Kortshagen, U. R. An All-Gas-Phase Approach for the Fabrication of Silicon Nanocrystal Light-Emitting Devices. *Nano Lett.* **2012**, *12* (6), 2822–2825.
- (92) Huang, X. Z.; Zhong, X. X.; Lu, Y.; Li, Y. S.; Rider, A. E.; Furman, S. A.; Ostrikov, K. Plasmonic Ag Nanoparticles Via Environment-Benign Atmospheric Microplasma Electrochemistry. *Nanotechnology* **2013**, *24* (9), 095604.
- (93) Mariotti, D.; Švrček, V.; Hamilton, J. W. J.; Schmidt, M.; Kondo, M. Silicon Nanocrystals in Liquid Media: Optical Properties and Surface Stabilization by Microplasma-Induced Non-Equilibrium Liquid Chemistry. *Adv. Funct. Mater.* **2012**, *22* (5), 954–964.
- (94) Zhao, Q.-L.; Zhang, Z.-L.; Huang, B.-H.; Peng, J.; Zhang, M.; Pang, D.-W. Facile Preparation of Low Cytotoxicity Fluorescent Carbon Nanocrystals by Electrooxidation of Graphite. *Chem. Commun.* **2008**, *41*, 5116–5118.
- (95) Zhang, X.; Wang, H.; Wang, H.; Zhang, Q.; Xie, J.; Tian, Y.; Wang, J.; Xie, Y. Single-Layered Graphitic-C<sub>3</sub>N<sub>4</sub> Quantum Dots for Two-Photon Fluorescence Imaging of Cellular Nucleus. *Adv. Mater.* **2014**, *26* (26), 4438–4443.

- (96) Peng, H.; Travas-Sejdic, J. Simple Aqueous Solution Route to Luminescent Carbogenic Dots from Carbohydrates. *Chem. Mater.* **2009**, *21* (23), 5563–5565.
- (97) Gupta, V.; Chaudhary, N.; Srivastava, R.; Sharma, G. D.; Bhardwaj, R.; Chand, S. Luminescent Graphene Quantum Dots for Organic Photovoltaic Devices. *J. Am. Chem. Soc.* **2011**, *133* (26), 9960–9963.
- (98) Wang, Q.; Liu, X.; Zhang, L.; Lv, Y. Microwave-Assisted Synthesis of Carbon Nanodots through an Eggshell Membrane and Their Fluorescent Application. *Analyst* **2012**, *137* (22), 5392–5397.
- (99) Shinde, D. B.; Pillai, V. K. Electrochemical Preparation of Luminescent Graphene Quantum Dots from Multiwalled Carbon Nanotubes. *Chem. - Eur. J.* **2012**, *18* (39), 12522–12528.
- (100) Khan, S.; Verma, N. C.; Gupta, A.; Nandi, C. K. Reversible Photoswitching of Carbon Dots. *Sci. Rep.* **2015**, *5*, 11423.
- (101) Wang, W.; Damm, C.; Walter, J.; Nacken, T. J.; Peukert, W. Photobleaching and Stabilization of Carbon Nanodots Produced by Solvothermal Synthesis. *Phys. Chem. Chem. Phys.* **2015**, *18*, 466.
- (102) Pan, D.; Zhang, J.; Li, Z.; Wu, M. Hydrothermal Route for Cutting Graphene Sheets into Blue-Luminescent Graphene Quantum Dots. *Adv. Mater.* **2010**, *22* (6), 734–738.
- (103) Shen, J.; Zhu, Y.; Chen, C.; Yang, X.; Li, C. Facile Preparation and Upconversion Luminescence of Graphene Quantum Dots. *Chem. Commun.* **2011**, *47* (9), 2580–2582.
- (104) Zhou, J.; Booker, C.; Li, R.; Zhou, X.; Sham, T.-K.; Sun, X.; Ding, Z. An Electrochemical Avenue to Blue Luminescent Nanocrystals from Multiwalled Carbon Nanotubes (Mwcnts). *J. Am. Chem. Soc.* **2007**, *129* (4), 744–745.
- (105) Bourlinos, A. B.; Stassinopoulos, A.; Anglos, D.; Zboril, R.; Karakassides, M.; Giannelis, E. P. Surface Functionalized Carbogenic Quantum Dots. *Small* **2008**, *4* (4), 455–458.
- (106) Pan, D.; Zhang, J.; Li, Z.; Wu, C.; Yan, X.; Wu, M. Observation of Ph-, Solvent-, Spin-, and Excitation-Dependent Blue Photoluminescence from Carbon Nanoparticles. *Chem. Commun.* **2010**, *46* (21), 3681–3683.
- (107) Wang, F.; Pang, S.; Wang, L.; Li, Q.; Kreiter, M.; Liu, C.-y. One-Step Synthesis of Highly Luminescent Carbon Dots in Non-coordinating Solvents. *Chem. Mater.* **2010**, *22* (16), 4528–4530.
- (108) Jaiswal, A.; Ghosh, S. S.; Chattopadhyay, A. One Step Synthesis of C-Dots by Microwave Mediated Caramelization of Poly(Ethylene Glycol). *Chem. Commun.* **2012**, *48* (3), 407–409.
- (109) Fan, R.-J.; Sun, Q.; Zhang, L.; Zhang, Y.; Lu, A.-H. Photoluminescent Carbon Dots Directly Derived from Polyethylene Glycol and Their Application for Cellular Imaging. *Carbon* **2014**, *71*, 87–93.
- (110) Zhu, H.; Wang, X.; Li, Y.; Wang, Z.; Yang, F.; Yang, X. Microwave Synthesis of Fluorescent Carbon Nanoparticles with Electrochemiluminescence Properties. *Chem. Commun.* **2009**, *34*, 5118–5120.
- (111) Li, Y.; Zhong, X.; Rider, A. E.; Furman, S. A.; Ostrikov, K. Fast, Energy-Efficient Synthesis of Luminescent Carbon Quantum Dots. *Green Chem.* **2014**, *16* (5), 2566–2570.
- (112) Wei, W.; Xu, C.; Wu, L.; Wang, J.; Ren, J.; Qu, X. Non-Enzymatic-Browning-Reaction: A Versatile Route for Production of Nitrogen-Doped Carbon Dots with Tunable Multicolor Luminescent Display. *Sci. Rep.* **2014**, *4*, 3564.
- (113) Li, C.-L.; Ou, C.-M.; Huang, C.-C.; Wu, W.-C.; Chen, Y.-P.; Lin, T.-E.; Ho, L.-C.; Wang, C.-W.; Shih, C.-C.; Zhou, H.-C.; Lee, Y.-C.; Tzeng, W.-F.; Chiou, T.-J.; Chu, S.-T.; Cang, J.; Chang, H.-T. Carbon Dots Prepared from Ginger Exhibiting Efficient Inhibition of Human Hepatocellular Carcinoma Cells. *J. Mater. Chem. B* **2014**, *2* (28), 4564–4571.
- (114) Wei, J.; Shen, J.; Zhang, X.; Guo, S.; Pan, J.; Hou, X.; Zhang, H.; Wang, L.; Feng, B. Simple One-Step Synthesis of Water-Soluble Fluorescent Carbon Dots Derived from Paper Ash. *RSC Adv.* **2013**, *3* (32), 13119–13122.
- (115) Yin, B.; Deng, J.; Peng, X.; Long, Q.; Zhao, J.; Lu, Q.; Chen, Q.; Li, H.; Tang, H.; Zhang, Y.; Yao, S. Green Synthesis of Carbon Dots with Down- and up-Conversion Fluorescent Properties for Sensitive Detection of Hypochlorite with a Dual-Readout Assay. *Analyst* **2013**, *138* (21), 6551–6557.
- (116) Wang, J.; Ng, Y. H.; Lim, Y.-F.; Ho, G. W. Vegetable-Extracted Carbon Dots and Their Nanocomposites for Enhanced Photocatalytic H<sub>2</sub> Production. *RSC Adv.* **2014**, *4* (83), 44117–44123.
- (117) Zhou, J.; Sheng, Z.; Han, H.; Zou, M.; Li, C. Facile Synthesis of Fluorescent Carbon Dots Using Watermelon Peel as a Carbon Source. *Mater. Lett.* **2012**, *66* (1), 222–224.
- (118) Liu, S.-S.; Wang, C.-F.; Li, C.-X.; Wang, J.; Mao, L.-H.; Chen, S. Hair-Derived Carbon Dots toward Versatile Multidimensional Fluorescent Materials. *J. Mater. Chem. C* **2014**, *2* (32), 6477–6483.
- (119) Xu, J.; Zhou, Y.; Liu, S.; Dong, M.; Huang, C. Low-Cost Synthesis of Carbon Nanodots from Natural Products Used as a Fluorescent Probe for the Detection of Ferrum(III) Ions in Lake Water. *Anal. Methods* **2014**, *6* (7), 2086–2090.
- (120) Konwar, A.; Gogoi, N.; Majumdar, G.; Chowdhury, D. Green Chitosan–Carbon Dots Nanocomposite Hydrogel Film with Superior Properties. *Carbohydr. Polym.* **2015**, *115*, 238–245.
- (121) Wu, Z.-S.; Feng, X.; Cheng, H.-M. Recent Advances in Graphene-Based Planar Micro-Supercapacitors for on-Chip Energy Storage. *National Science Review* **2014**, *1* (2), 277–292.
- (122) Das Purkayastha, M.; Manhar, A. K.; Das, V. K.; Borah, A.; Mandal, M.; Thakur, A. J.; Mahanta, C. L. Antioxidative, Hemocompatible, Fluorescent Carbon Nanodots from an “End-of-Pipe” Agricultural Waste: Exploring Its New Horizon in the Food-Packaging Domain. *J. Agric. Food Chem.* **2014**, *62* (20), 4509–4520.
- (123) Yang, X.; Cheng, C.; Wang, Y.; Qiu, L.; Li, D. Liquid-Mediated Dense Integration of Graphene Materials for Compact Capacitive Energy Storage. *Science* **2013**, *341* (6145), 534–537.
- (124) Hu, Y.; Yang, J.; Tian, J.; Jia, L.; Yu, J.-S. Green and Size-Controllable Synthesis of Photoluminescent Carbon Nanoparticles from Waste Plastic Bags. *RSC Adv.* **2014**, *4* (88), 47169–47176.
- (125) Liu, H.; Ye, T.; Mao, C. Fluorescent Carbon Nanoparticles Derived from Candle Soot. *Angew. Chem., Int. Ed.* **2007**, *46* (34), 6473–6475.
- (126) Kondyurin, A.; Levchenko, I.; Han, Z. J.; Yick, S.; Mai-Prochnow, A.; Fang, J.; Ostrikov, K.; Bilek, M. M. M. Hybrid Graphite Film–Carbon Nanotube Platform for Enzyme Immobilization and Protection. *Carbon* **2013**, *65*, 287–295.
- (127) Huang, J. J.; Zhong, Z. F.; Rong, M. Z.; Zhou, X.; Chen, X. D.; Zhang, M. Q. An Easy Approach of Preparing Strongly Luminescent Carbon Dots and Their Polymer Based Composites for Enhancing Solar Cell Efficiency. *Carbon* **2014**, *70*, 190–198.
- (128) Khare, B. N.; Meyyappan, M.; Cassell, A. M.; Nguyen, C. V.; Han, J. Functionalization of Carbon Nanotubes Using Atomic Hydrogen from a Glow Discharge. *Nano Lett.* **2002**, *2* (1), 73–77.
- (129) Perrin, J.; Shiratani, M.; Kae-Nune, P.; Videlot, H.; Jolly, J.; Guillon, J. Surface Reaction Probabilities and Kinetics of H, SiH<sub>3</sub>, Si<sub>2</sub>H<sub>5</sub>, CH<sub>3</sub>, and C<sub>2</sub>H<sub>5</sub> During Deposition of a-Si:H and a-C:H from H<sub>2</sub>, SiH<sub>4</sub>, and CH<sub>4</sub> Discharges. *J. Vac. Sci. Technol., A* **1998**, *16* (1), 278–289.
- (130) Baker, S. N.; Baker, G. A. Luminescent Carbon Nanodots: Emergent Nanolights. *Angew. Chem., Int. Ed.* **2010**, *49* (38), 6726–6744.
- (131) Sun, Y.-P.; Zhou, B.; Lin, Y.; Wang, W.; Fernando, K. A. S.; Pathak, P.; Mezziani, M. J.; Harruff, B. A.; Wang, X.; Wang, H.; Luo, P. G.; Yang, H.; Kose, M. E.; Chen, B.; Veca, L. M.; Xie, S.-Y. Quantum-Sized Carbon Dots for Bright and Colorful Photoluminescence. *J. Am. Chem. Soc.* **2006**, *128* (24), 7756–7757.
- (132) Novoselov, K. S.; Falko, V. I.; Colombo, L.; Gellert, P. R.; Schwab, M. G.; Kim, K. A Roadmap for Graphene. *Nature* **2012**, *490* (7419), 192–200.
- (133) Bunch, J. S.; Verbridge, S. S.; Alden, J. S.; van der Zande, A. M.; Parpia, J. M.; Craighead, H. G.; McEuen, P. L. Impermeable Atomic Membranes from Graphene Sheets. *Nano Lett.* **2008**, *8* (8), 2458–2462.
- (134) Ambrosi, A.; Chua, C. K.; Bonanni, A.; Pumera, M. Electrochemistry of Graphene and Related Materials. *Chem. Rev.* **2014**, *114* (14), 7150–7188.

- (135) Li, Z.; Liu, Z.; Sun, H.; Gao, C. Superstructured Assembly of Nanocarbons: Fullerenes, Nanotubes, and Graphene. *Chem. Rev.* **2015**, *115* (15), 7046–7117.
- (136) Roy-Mayhew, J. D.; Aksay, I. A. Graphene Materials and Their Use in Dye-Sensitized Solar Cells. *Chem. Rev.* **2014**, *114* (12), 6323–6348.
- (137) Su, D. S.; Perathoner, S.; Centi, G. Nanocarbons for the Development of Advanced Catalysts. *Chem. Rev.* **2013**, *113* (8), 5782–5816.
- (138) Xu, M.; Liang, T.; Shi, M.; Chen, H. Graphene-Like Two-Dimensional Materials. *Chem. Rev.* **2013**, *113* (5), 3766–3798.
- (139) Mao, H. Y.; Laurent, S.; Chen, W.; Akhavan, O.; Imani, M.; Ashkarran, A. A.; Mahmoudi, M. Graphene: Promises, Facts, Opportunities, and Challenges in Nanomedicine. *Chem. Rev.* **2013**, *113* (5), 3407–3424.
- (140) Morozov, S.; Novoselov, K.; Katsnelson, M.; Schedin, F.; Elias, D.; Jaszczak, J.; Geim, A. Giant Intrinsic Carrier Mobilities in Graphene and Its Bilayer. *Phys. Rev. Lett.* **2008**, *100* (1), 016602.
- (141) Lee, C.; Wei, X.; Kysar, J. W.; Hone, J. Measurement of the Elastic Properties and Intrinsic Strength of Monolayer Graphene. *Science* **2008**, *321* (5887), 385–388.
- (142) Liu, F.; Ming, P.; Li, J. *Ab Initio* Calculation of Ideal Strength and Phonon Instability of Graphene under Tension. *Phys. Rev. B: Condens. Matter Mater. Phys.* **2007**, *76* (6), 064120.
- (143) Balandin, A. A. Thermal Properties of Graphene and Nanostructured Carbon Materials. *Nat. Mater.* **2011**, *10* (8), 569–581.
- (144) Nair, R. R.; Blake, P.; Grigorenko, A. N.; Novoselov, K. S.; Booth, T. J.; Stauber, T.; Peres, N. M. R.; Geim, A. K. Fine Structure Constant Defines Visual Transparency of Graphene. *Science* **2008**, *320* (5881), 1308.
- (145) Wang, H.; Kong, Q.; Wang, Y.; Deng, T.; Chen, C.; Hou, X.; Zhu, Y. Graphene Oxide Catalyzed Dehydration of Fructose into 5-Hydroxymethylfurfural with Isopropanol as Cosolvent. *ChemCatChem* **2014**, *6* (3), 728–732.
- (146) Wang, H.; Wang, Y.; Deng, T.; Chen, C.; Zhu, Y.; Hou, X. Carboxylate in Biorefinery: Selective Etherification of 5-Hydroxymethylfurfural to 5,5'-(Oxy-Bis(Methylene))Bis-2-Furfural over Graphene Oxide. *Catal. Commun.* **2015**, *59*, 127–130.
- (147) Dhakshinamoorthy, A.; Alvaro, M.; Concepcion, P.; Fornes, V.; Garcia, H. Graphene Oxide as an Acid Catalyst for the Room Temperature Ring Opening of Epoxides. *Chem. Commun.* **2012**, *48* (44), 5443–5445.
- (148) de Heer, W. A.; Berger, C.; Ruan, M.; Sprinkle, M.; Li, X.; Hu, Y.; Zhang, B.; Hankinson, J.; Conrad, E. Large Area and Structured Epitaxial Graphene Produced by Confinement Controlled Sublimation of Silicon Carbide. *Proc. Natl. Acad. Sci. U. S. A.* **2011**, *108* (41), 16900–16905.
- (149) Iacopi, F.; Mishra, N.; Cunniff, B. V.; Goding, D.; Dimitrijević, S.; Brock, R.; Dauskardt, R. H.; Wood, B.; Boeckl, J. A Catalytic Alloy Approach for Graphene on Epitaxial SiC on Silicon Wafers. *J. Mater. Res.* **2015**, *30* (05), 609–616.
- (150) Li, Z.; Wu, P.; Wang, C.; Fan, X.; Zhang, W.; Zhai, X.; Zeng, C.; Li, Z.; Yang, J.; Hou, J. Low-Temperature Growth of Graphene by Chemical Vapor Deposition Using Solid and Liquid Carbon Sources. *ACS Nano* **2011**, *5* (4), 3385–3390.
- (151) Zhu, Y.; Murali, S.; Stoller, M. D.; Ganesh, K. J.; Cai, W.; Ferreira, P. J.; Pirkle, A.; Wallace, R. M.; Cychosz, K. A.; Thommes, M.; Su, D.; Stach, E. A.; Ruoff, R. S. Carbon-Based Supercapacitors Produced by Activation of Graphene. *Science* **2011**, *332* (6037), 1537–1541.
- (152) Delamoreanu, A.; Rabot, C.; Vallee, C.; Zenasni, A. Wafer Scale Catalytic Growth of Graphene on Nickel by Solid Carbon Source. *Carbon* **2014**, *66*, 48–56.
- (153) Somekh, M.; Shawat, E.; Nessim, G. D. Fully Reproducible, Low-Temperature Synthesis of High-Quality, Few-Layer Graphene on Nickel Via Preheating of Gas Precursors Using Atmospheric Pressure Chemical Vapor Deposition. *J. Mater. Chem. A* **2014**, *2* (46), 19750–19758.
- (154) Babenko, V.; Murdock, A. T.; Koos, A. A.; Britton, J.; Crossley, A.; Holdway, P.; Moffat, J.; Huang, J.; Alexander-Webber, J. A.; Nicholas, R. J.; Grobert, N. Rapid Epitaxy-Free Graphene Synthesis on Silicidated Polycrystalline Platinum. *Nat. Commun.* **2015**, *6*, 7536.
- (155) Lee, J.-H.; Lee, E. K.; Joo, W.-J.; Jang, Y.; Kim, B.-S.; Lim, J. Y.; Choi, S.-H.; Ahn, S. J.; Ahn, J. R.; Park, M.-H.; Yang, C.-W.; Choi, B. L.; Hwang, S.-W.; Whang, D. Wafer-Scale Growth of Single-Crystal Monolayer Graphene on Reusable Hydrogen-Terminated Germanium. *Science* **2014**, *344* (6181), 286–289.
- (156) Gan, X.; Zhou, H.; Zhu, B.; Yu, X.; Jia, Y.; Sun, B.; Zhang, M.; Huang, X.; Liu, J.; Luo, T. A Simple Method to Synthesize Graphene at 633K by Dechlorination of Hexachlorobenzene on Cu Foils. *Carbon* **2012**, *50* (1), 306–310.
- (157) Yin, S.; Niu, Z.; Chen, X. Assembly of Graphene Sheets into 3d Macroscopic Structures. *Small* **2012**, *8* (16), 2458–2463.
- (158) Wang, D.; Kou, R.; Choi, D.; Yang, Z.; Nie, Z.; Li, J.; Saraf, L. V.; Hu, D.; Zhang, J.; Graff, G. L.; Liu, J.; Pope, M. A.; Aksay, I. A. Ternary Self-Assembly of Ordered Metal Oxide–Graphene Nanocomposites for Electrochemical Energy Storage. *ACS Nano* **2010**, *4* (3), 1587–1595.
- (159) Nandamuri, G.; Roumimov, S.; Solanki, R. Remote Plasma Assisted Growth of Graphene Films. *Appl. Phys. Lett.* **2010**, *96* (15), 154101.
- (160) Lin, Y.-C.; Lin, C.-Y.; Chiu, P.-W. Controllable Graphene N-Doping with Ammonia Plasma. *Appl. Phys. Lett.* **2010**, *96* (13), 133110.
- (161) Li, N.; Wang, Z.; Zhao, K.; Shi, Z.; Gu, Z.; Xu, S. Large Scale Synthesis of N-Doped Multi-Layered Graphene Sheets by Simple Arc-Discharge Method. *Carbon* **2010**, *48* (1), 255–259.
- (162) Wu, J.; Xie, L.; Li, Y.; Wang, H.; Ouyang, Y.; Guo, J.; Dai, H. Controlled Chlorine Plasma Reaction for Noninvasive Graphene Doping. *J. Am. Chem. Soc.* **2011**, *133* (49), 19668–19671.
- (163) Nourbakhsh, A.; Cantoro, M.; Vosch, T.; Pourtois, G.; Clemente, F.; van der Veen, M. H.; Hofkens, J.; Heyns, M. M.; De Gendt, S.; Sels, B. F. Bandgap Opening in Oxygen Plasma-Treated Graphene. *Nanotechnology* **2010**, *21* (43), 435203.
- (164) Gokus, T.; Nair, R. R.; Bonetti, A.; Böhmeler, M.; Lombardo, A.; Novoselov, K. S.; Geim, A. K.; Ferrari, A. C.; Hartschuh, A. Making Graphene Luminescent by Oxygen Plasma Treatment. *ACS Nano* **2009**, *3* (12), 3963–3968.
- (165) Lim, Y.-D.; Lee, D.-Y.; Shen, T.-Z.; Ra, C.-H.; Choi, J.-Y.; Yoo, W. J. Si-Compatible Cleaning Process for Graphene Using Low-Density Inductively Coupled Plasma. *ACS Nano* **2012**, *6* (5), 4410–4417.
- (166) Diankov, G.; Neumann, M.; Goldhaber-Gordon, D. Extreme Monolayer-Selectivity of Hydrogen-Plasma Reactions with Graphene. *ACS Nano* **2013**, *7* (2), 1324–1332.
- (167) Luo, Z.; Yu, T.; Kim, K.-j.; Ni, Z.; You, Y.; Lim, S.; Shen, Z.; Wang, S.; Lin, J. Thickness-Dependent Reversible Hydrogenation of Graphene Layers. *ACS Nano* **2009**, *3* (7), 1781–1788.
- (168) Yang, R.; Zhang, L.; Wang, Y.; Shi, Z.; Shi, D.; Gao, H.; Wang, E.; Zhang, G. An Anisotropic Etching Effect in the Graphene Basal Plane. *Adv. Mater.* **2010**, *22* (36), 4014–4019.
- (169) Shi, Z.; Yang, R.; Zhang, L.; Wang, Y.; Liu, D.; Shi, D.; Wang, E.; Zhang, G. Patterning Graphene with Zigzag Edges by Self-Aligned Anisotropic Etching. *Adv. Mater.* **2011**, *23* (27), 3061–3065.
- (170) Cheng, M.; Yang, R.; Zhang, L.; Shi, Z.; Yang, W.; Wang, D.; Xie, G.; Shi, D.; Zhang, G. Restoration of Graphene from Graphene Oxide by Defect Repair. *Carbon* **2012**, *50* (7), 2581–2587.
- (171) Lee, S. W.; Mattevi, C.; Chhowalla, M.; Sankaran, R. M. Plasma-Assisted Reduction of Graphene Oxide at Low Temperature and Atmospheric Pressure for Flexible Conductor Applications. *J. Phys. Chem. Lett.* **2012**, *3* (6), 772–777.
- (172) Jiao, L.; Zhang, L.; Wang, X.; Diankov, G.; Dai, H. Narrow Graphene Nanoribbons from Carbon Nanotubes. *Nature* **2009**, *458* (7240), 877–880.
- (173) Li, X.; Wang, X.; Zhang, L.; Lee, S.; Dai, H. Chemically Derived, Ultrasoft Graphene Nanoribbon Semiconductors. *Science* **2008**, *319* (5867), 1229–1232.



- (174) Wang, X.; Ouyang, Y.; Li, X.; Wang, H.; Guo, J.; Dai, H. Room-Temperature All-Semiconducting Sub-10-Nm Graphene Nanoribbon Field-Effect Transistors. *Phys. Rev. Lett.* **2008**, *100* (20), 206803.
- (175) Kato, T.; Hatakeyama, R. Site- and Alignment-Controlled Growth of Graphene Nanoribbons from Nickel Nanobars. *Nat. Nanotechnol.* **2012**, *7* (10), 651–656.
- (176) Sun, Z.; Yan, Z.; Yao, J.; Beitler, E.; Zhu, Y.; Tour, J. M. Growth of Graphene from Solid Carbon Sources. *Nature* **2010**, *468* (7323), 549–552.
- (177) Ruiz-Hitzky, E.; Darder, M.; Fernandes, F. M.; Zatile, E.; Palomares, F. J.; Aranda, P. Supported Graphene from Natural Resources: Easy Preparation and Applications. *Adv. Mater.* **2011**, *23* (44), 5250–5255.
- (178) Pan, F.; Jin, J.; Fu, X.; Liu, Q.; Zhang, J. Advanced Oxygen Reduction Electrocatalyst Based on Nitrogen-Doped Graphene Derived from Edible Sugar and Urea. *ACS Appl. Mater. Interfaces* **2013**, *5* (21), 11108–11114.
- (179) Li, X.-H.; Kurasch, S.; Kaiser, U.; Antonietti, M. Synthesis of Monolayer-Patched Graphene from Glucose. *Angew. Chem., Int. Ed.* **2012**, *51* (38), 9689–9692.
- (180) Ruan, G.; Sun, Z.; Peng, Z.; Tour, J. M. Growth of Graphene from Food, Insects, and Waste. *ACS Nano* **2011**, *5* (9), 7601–7607.
- (181) Gong, J.; Liu, J.; Wen, X.; Jiang, Z.; Chen, X.; Mijowska, E.; Tang, T. Upcycling Waste Polypropylene into Graphene Flakes on Organically Modified Montmorillonite. *Ind. Eng. Chem. Res.* **2014**, *53* (11), 4173–4181.
- (182) Müller, F.; Grandthyll, S.; Gsell, S.; Weinl, M.; Schreck, M.; Jacobs, K. Graphene from Fingerprints: Exhausting the Performance of Liquid Precursor Deposition. *Langmuir* **2014**, *30* (21), 6114–6119.
- (183) Dato, A.; Lee, Z.; Jeon, K.-J.; Erni, R.; Radmilovic, V.; Richardson, T. J.; Frenklach, M. Clean and Highly Ordered Graphene Synthesized in the Gas Phase. *Chem. Commun.* **2009**, *40*, 6095–6097.
- (184) Dato, A.; Frenklach, M. Substrate-Free Microwave Synthesis of Graphene: Experimental Conditions and Hydrocarbon Precursors. *New J. Phys.* **2010**, *12* (12), 125013.
- (185) Seo, D. H.; Yick, S.; Han, Z. J.; Fang, J. H.; Ostrikov, K. Synergistic Fusion of Vertical Graphene Nanosheets and Carbon Nanotubes for High-Performance Supercapacitor Electrodes. *ChemSusChem* **2014**, *7* (8), 2317–2324.
- (186) Bo, Z.; Mao, S.; Han, Z. J.; Cen, K.; Chen, J.; Ostrikov, K. Emerging Energy and Environmental Applications of Vertically-Oriented Graphenes. *Chem. Soc. Rev.* **2015**, *44*, 2108–2121.
- (187) Yick, S.; Han, Z. J.; Ostrikov, K. Atmospheric Microplasma-Functionalized 3d Microfluidic Strips within Dense Carbon Nanotube Arrays Confine Au Nanodots for SERS Sensing. *Chem. Commun.* **2013**, *49* (28), 2861–2863.
- (188) Seo, D. H.; Kumar, S.; Rider, A. E.; Han, Z.; Ostrikov, K. Deterministic Control of Structural and Optical Properties of Plasma-Grown Vertical Graphene Nanosheet Networks Via Nitrogen Gas Variation. *Opt. Mater. Express* **2012**, *2* (6), 700–707.
- (189) Yue, Z. J.; Seo, D. H.; Ostrikov, K.; Wang, X. L. Defects Induced Ferromagnetism in Plasma-Enabled Graphene Nanopetals. *Appl. Phys. Lett.* **2014**, *104* (9), 092417.
- (190) Seo, D.; Yue, Z.; Wang, X.; Levchenko, I.; Kumar, S.; Dou, S.; Ostrikov, K. Tuning of Magnetization in Vertical Graphenes by Plasma-Enabled Chemical Conversion of Organic Precursors with Different Oxygen Content. *Chem. Commun.* **2013**, *49* (99), 11635–11637.
- (191) Elias, D. C.; Nair, R. R.; Mohiuddin, T. M. G.; Morozov, S. V.; Blake, P.; Halsall, M. P.; Ferrari, A. C.; Boukhvalov, D. W.; Katsnelson, M. I.; Geim, A. K.; Novoselov, K. S. Control of Graphene's Properties by Reversible Hydrogenation: Evidence for Graphane. *Science* **2009**, *323* (5914), 610–613.
- (192) Ranjbar, A.; Bahramy, M. S.; Khazaei, M.; Mizuseki, H.; Kawazoe, Y. First-Principles Study of Structural Stability, Magnetism, and Hyperfine Coupling in Hydrogen Clusters Adsorbed on Graphene. *Phys. Rev. B: Condens. Matter Mater. Phys.* **2010**, *82* (16), 165446.
- (193) Son, Y.-W.; Cohen, M. L.; Louie, S. G. Half-Metallic Graphene Nanoribbons. *Nature* **2006**, *444* (7117), 347–349.
- (194) Xiao, L.; Wu, D.; Han, S.; Huang, Y.; Li, S.; He, M.; Zhang, F.; Feng, X. Self-Assembled Fe<sub>2</sub>O<sub>3</sub>/Graphene Aerogel with High Lithium Storage Performance. *ACS Appl. Mater. Interfaces* **2013**, *5* (9), 3764–3769.
- (195) Liang, Y.; Schwab, M. G.; Zhi, L.; Mugnaioli, E.; Kolb, U.; Feng, X.; Müllen, K. Direct Access to Metal or Metal Oxide Nanocrystals Integrated with One-Dimensional Nanoporous Carbons for Electrochemical Energy Storage. *J. Am. Chem. Soc.* **2010**, *132* (42), 15030–15037.
- (196) You, B.; Li, N.; Zhu, H.; Zhu, X.; Yang, J. Graphene Oxide-Dispersed Pristine Cnts Support for MnO<sub>2</sub> Nanorods as High Performance Supercapacitor Electrodes. *ChemSusChem* **2013**, *6* (3), 474–480.
- (197) Ahmad, I.; Khan, U.; Gun'ko, Y. K. Graphene, Carbon Nanotube and Ionic Liquid Mixtures: Towards New Quasi-Solid State Electrolytes for Dye Sensitized Solar Cells. *J. Mater. Chem.* **2011**, *21* (42), 16990–16996.
- (198) Ji, D.; Jiang, L.; Cai, X.; Dong, H.; Meng, Q.; Tian, G.; Wu, D.; Li, J.; Hu, W. Large Scale, Flexible Organic Transistor Arrays and Circuits Based on Polyimide Materials. *Org. Electron.* **2013**, *14* (10), 2528–2533.
- (199) Miller, J. R.; Outlaw, R. A.; Holloway, B. C. Graphene Double-Layer Capacitor with Ac Line-Filtering Performance. *Science* **2010**, *329* (5999), 1637–1639.
- (200) Woszczyzna, M.; Winter, A.; Grothe, M.; Willunat, A.; Wundrack, S.; Stosch, R.; Weimann, T.; Ahlers, F.; Turchanin, A. All-Carbon Vertical Van Der Waals Heterostructures: Non-Destructive Functionalization of Graphene for Electronic Applications. *Adv. Mater.* **2014**, *26* (28), 4831–4837.
- (201) Gui, X.; Wei, J.; Wang, K.; Cao, A.; Zhu, H.; Jia, Y.; Shu, Q.; Wu, D. Carbon Nanotube Sponges. *Adv. Mater.* **2010**, *22* (5), 617–621.
- (202) Xu, M.; Futaba, D. N.; Yamada, T.; Yumura, M.; Hata, K. Carbon Nanotubes with Temperature-Invariant Viscoelasticity from –196° to 1000°C. *Science* **2010**, *330* (6009), 1364–1368.
- (203) Dutta, S.; Bhaumik, A.; Wu, K. C. W. Hierarchically Porous Carbon Derived from Polymers and Biomass: Effect of Interconnected Pores on Energy Applications. *Energy Environ. Sci.* **2014**, *7* (11), 3574–3592.
- (204) Hashim, D. P.; Narayanan, N. T.; Romo-Herrera, J. M.; Cullen, D. A.; Hahm, M. G.; Lezzi, P.; Suttle, J. R.; Kelkhoff, D.; Muñoz-Sandoval, E.; Ganguli, S.; Roy, A. K.; Smith, D. J.; Vajtai, R.; Sumpter, B. G.; Meunier, V.; Terrones, H.; Terrones, M.; Ajayan, P. M. Covalently Bonded Three-Dimensional Carbon Nanotube Solids Via Boron Induced Nanojunctions. *Sci. Rep.* **2012**, *2*, 363.
- (205) Lalwani, G.; Kwaczala, A. T.; Kanakia, S.; Patel, S. C.; Judex, S.; Sitharaman, B. Fabrication and Characterization of Three-Dimensional Macroscopic All-Carbon Scaffolds. *Carbon* **2013**, *53*, 90–100.
- (206) Wang, H.; Xu, Z.; Kohandehghan, A.; Li, Z.; Cui, K.; Tan, X.; Stephenson, T. J.; King'andu, C. K.; Holt, C. M. B.; Olsen, B. C.; Tak, J. K.; Harfield, D.; Anyia, A. O.; Mitlin, D. Interconnected Carbon Nanosheets Derived from Hemp for Ultrafast Supercapacitors with High Energy. *ACS Nano* **2013**, *7* (6), 5131–5141.
- (207) Gong, J.; Michalkiewicz, B.; Chen, X.; Mijowska, E.; Liu, J.; Jiang, Z.; Wen, X.; Tang, T. Sustainable Conversion of Mixed Plastics into Porous Carbon Nanosheets with High Performances in Uptake of Carbon Dioxide and Storage of Hydrogen. *ACS Sustainable Chem. Eng.* **2014**, *2* (12), 2837–2844.
- (208) Gómez-Avilés, A.; Darder, M.; Aranda, P.; Ruiz-Hitzky, E. Functionalized Carbon–Silicates from Caramel–Sepiolite Nanocomposites. *Angew. Chem., Int. Ed.* **2007**, *46* (6), 923–925.
- (209) Gómez-Avilés, A.; Darder, M.; Aranda, P.; Ruiz-Hitzky, E. Multifunctional Materials Based on Graphene-Like/Sepiolite Nanocomposites. *Appl. Clay Sci.* **2010**, *47* (3–4), 203–211.
- (210) Titirici, M.-M.; Antonietti, M.; Baccile, N. Hydrothermal Carbon from Biomass: A Comparison of the Local Structure from

- Poly- to Monosaccharides and Pentoses/Hexoses. *Green Chem.* **2008**, *10* (11), 1204–1212.
- (211) Titirici, M.-M.; Antonietti, M. Chemistry and Materials Options of Sustainable Carbon Materials Made by Hydrothermal Carbonization. *Chem. Soc. Rev.* **2010**, *39* (1), 103–116.
- (212) Biswal, M.; Banerjee, A.; Deo, M.; Ogale, S. From Dead Leaves to High Energy Density Supercapacitors. *Energy Environ. Sci.* **2013**, *6* (4), 1249–1259.
- (213) Zhang, L.; Wang, Y.; Peng, B.; Yu, W.; Wang, H.; Wang, T.; Deng, B.; Chai, L.; Zhang, K.; Wang, J. Preparation of a Macroscopic, Robust Carbon-Fiber Monolith from Filamentous Fungi and Its Application in Li-S Batteries. *Green Chem.* **2014**, *16* (8), 3926–3934.
- (214) Raymundo-Piñero, E.; Leroux, F.; Béguin, F. A High-Performance Carbon for Supercapacitors Obtained by Carbonization of a Seaweed Biopolymer. *Adv. Mater.* **2006**, *18* (14), 1877–1882.
- (215) Guo, Y.; Qi, J.; Jiang, Y.; Yang, S.; Wang, Z.; Xu, H. Performance of Electrical Double Layer Capacitors with Porous Carbons Derived from Rice Husk. *Mater. Chem. Phys.* **2003**, *80* (3), 704–709.
- (216) Sun, L.; Tian, C.; Li, M.; Meng, X.; Wang, L.; Wang, R.; Yin, J.; Fu, H. From Coconut Shell to Porous Graphene-Like Nanosheets for High-Power Supercapacitors. *J. Mater. Chem. A* **2013**, *1* (21), 6462–6470.
- (217) Wu, F.-C.; Tseng, R.-L.; Hu, C.-C.; Wang, C.-C. Physical and Electrochemical Characterization of Activated Carbons Prepared from Firwoods for Supercapacitors. *J. Power Sources* **2004**, *138* (1–2), 351–359.
- (218) Wu, F.-C.; Tseng, R.-L.; Hu, C.-C.; Wang, C.-C. Effects of Pore Structure and Electrolyte on the Capacitive Characteristics of Steam- and Koh-Activated Carbons for Supercapacitors. *J. Power Sources* **2005**, *144* (1), 302–309.
- (219) Liu, M.-C.; Kong, L.-B.; Zhang, P.; Luo, Y.-C.; Kang, L. Porous Wood Carbon Monolith for High-Performance Supercapacitors. *Electrochim. Acta* **2012**, *60*, 443–448.
- (220) Lin, G.-F.; Jiang, J.-C.; Wu, K.-J.; Sun, K. Preparation and Characterization of Bamboo-Based Activated Carbon by Phosphoric Acid Activation. *Carbon* **2014**, *70*, 321.
- (221) Subramanian, V.; Luo, C.; Stephan, A. M.; Nahm, K. S.; Thomas, S.; Wei, B. Supercapacitors from Activated Carbon Derived from Banana Fibers. *J. Phys. Chem. C* **2007**, *111* (20), 7527–7531.
- (222) Balathanigaimani, M. S.; Shim, W.-G.; Lee, M.-J.; Kim, C.; Lee, J.-W.; Moon, H. Highly Porous Electrodes from Novel Corn Grains-Based Activated Carbons for Electrical Double Layer Capacitors. *Electrochem. Commun.* **2008**, *10* (6), 868–871.
- (223) Rufford, T. E.; Hulicova-Jurcakova, D.; Zhu, Z.; Lu, G. Q. Nanoporous Carbon Electrode from Waste Coffee Beans for High Performance Supercapacitors. *Electrochem. Commun.* **2008**, *10* (10), 1594–1597.
- (224) Kalpana, D.; Cho, S. H.; Lee, S. B.; Lee, Y. S.; Misra, R.; Renganathan, N. G. Recycled Waste Paper—a New Source of Raw Material for Electric Double-Layer Capacitors. *J. Power Sources* **2009**, *190* (2), 587–591.
- (225) Xu, D.; Xie, Y.; Song, Y.-J.; Deng, W.-Q. A Green and Facile Method toward Synthesis of Waste Paper-Derived 3d Functional Porous Graphene Via in Situ Activation of Cobalt(II). *J. Mater. Chem. A* **2015**, *3* (31), 16072–16078.
- (226) Chang, B.; Guo, Y.; Li, Y.; Yang, B. Hierarchical Porous Carbon Derived from Recycled Waste Filter Paper as High-Performance Supercapacitor Electrodes. *RSC Adv.* **2015**, *5* (88), 72019–72027.
- (227) Raymundo-Piñero, E.; Cadek, M.; Béguin, F. Tuning Carbon Materials for Supercapacitors by Direct Pyrolysis of Seaweeds. *Adv. Funct. Mater.* **2009**, *19* (7), 1032–1039.
- (228) Rufford, T. E.; Hulicova-Jurcakova, D.; Khosla, K.; Zhu, Z.; Lu, G. Q. Microstructure and Electrochemical Double-Layer Capacitance of Carbon Electrodes Prepared by Zinc Chloride Activation of Sugar Cane Bagasse. *J. Power Sources* **2010**, *195* (3), 912–918.
- (229) Ismanto, A. E.; Wang, S.; Soetaredjo, F. E.; Ismadji, S. Preparation of Capacitor's Electrode from Cassava Peel Waste. *Bioresour. Technol.* **2010**, *101* (10), 3534–3540.
- (230) Li, X.; Xing, W.; Zhuo, S.; Zhou, J.; Li, F.; Qiao, S.-Z.; Lu, G.-Q. Preparation of Capacitor's Electrode from Sunflower Seed Shell. *Bioresour. Technol.* **2011**, *102* (2), 1118–1123.
- (231) Elmouwahidi, A.; Zapata-Benabith, Z.; Carrasco-Marín, F.; Moreno-Castilla, C. Activated Carbons from Koh-Activation of Argan (*Argania Spinosa*) Seed Shells as Supercapacitor Electrodes. *Bioresour. Technol.* **2012**, *111*, 185–190.
- (232) Wang, X.; Gao, Z.; Chang, J.; Wu, D.; Wang, X.; Xu, F.; Guo, Y.; Jiang, K. Electrochemical Energy Storage and Adsorptive Dye Removal of Platanus Fruit-Derived Porous Carbon. *RSC Adv.* **2015**, *5* (21), 15969–15976.
- (233) Luan, Y.; Wang, L.; Guo, S.; Jiang, B.; Zhao, D.; Yan, H.; Tian, C.; Fu, H. A Hierarchical Porous Carbon Material from a Loofah Sponge Network for High Performance Supercapacitors. *RSC Adv.* **2015**, *5* (53), 42430–42437.
- (234) Bichat, M. P.; Raymundo-Piñero, E.; Béguin, F. High Voltage Supercapacitor Built with Seaweed Carbons in Neutral Aqueous Electrolyte. *Carbon* **2010**, *48* (15), 4351–4361.
- (235) Wu, M.; Li, P.; Li, Y.; Liu, J.; Wang, Y. Enteromorpha Based Porous Carbons Activated by Zinc Chloride for Supercapacitors with High Capacity Retention. *RSC Adv.* **2015**, *5* (21), 16575–16581.
- (236) Sugime, H.; Esconjauregui, S.; Yang, J.; D'Arsié, L.; Oliver, R. A.; Bhardwaj, S.; Cepek, C.; Robertson, J. Low Temperature Growth of Ultra-High Mass Density Carbon Nanotube Forests on Conductive Supports. *Appl. Phys. Lett.* **2013**, *103* (7), 073116.
- (237) Baughman, R. H.; Zakhidov, A. A.; de Heer, W. A. Carbon Nanotubes—the Route toward Applications. *Science* **2002**, *297* (5582), 787–792.
- (238) Yu, D.; Goh, K.; Wang, H.; Wei, L.; Jiang, W.; Zhang, Q.; Dai, L.; Chen, Y. Scalable Synthesis of Hierarchically Structured Carbon Nanotube-Graphene Fibres for Capacitive Energy Storage. *Nat. Nanotechnol.* **2014**, *9* (7), 555–562.
- (239) Lenert, A.; Bierman, D. M.; Nam, Y.; Chan, W. R.; Celanovic, I.; Soljacic, M.; Wang, E. N. A Nanophotonic Solar Thermophotovoltaic Device. *Nat. Nanotechnol.* **2014**, *9* (2), 126–130.
- (240) Selvakumar, N.; Krupanidhi, S. B.; Barshilia, H. C. Carbon Nanotube-Based Tandem Absorber with Tunable Spectral Selectivity: Transition from near-Perfect Blackbody Absorber to Solar Selective Absorber. *Adv. Mater.* **2014**, *26* (16), 2552–2557.
- (241) Awano, Y.; Sato, S.; Nihei, M.; Sakai, T.; Ohno, Y.; Mizutani, T. Carbon Nanotubes for Vlsi: Interconnect and Transistor Applications. *Proc. IEEE* **2010**, *98* (12), 2015–2031.
- (242) Robertson, J.; Zhong, G.; Esconjauregui, C. S.; Bayer, B. C.; Zhang, C.; Fouquet, M.; Hofmann, S. Applications of Carbon Nanotubes Grown by Chemical Vapor Deposition. *Jpn. J. Appl. Phys.* **2012**, *51* (1S), 01AH01.
- (243) Kreupl, F.; Graham, A. P.; Duesberg, G. S.; Steinhögl, W.; Liebau, M.; Unger, E.; Hönlein, W. Carbon Nanotubes in Interconnect Applications. *Microelectron. Eng.* **2002**, *64* (1–4), 399–408.
- (244) Sridhar, S.; Tiwary, C.; Vinod, S.; Taha-Tijerina, J. J.; Sridhar, S.; Kalaga, K.; Sirota, B.; Hart, A. H. C.; Ozden, S.; Sinha, R. K.; Harsh; Vajtai, R.; Choi, W.; Kordás, K.; Ajayan, P. M. Field Emission with Ultralow Turn on Voltage from Metal Decorated Carbon Nanotubes. *ACS Nano* **2014**, *8* (8), 7763–7770.
- (245) Xu, F.; Wu, M.-Y.; Safron, N. S.; Roy, S. S.; Jacobberger, R. M.; Bindl, D. J.; Seo, J.-H.; Chang, T.-H.; Ma, Z.; Arnold, M. S. Highly Stretchable Carbon Nanotube Transistors with Ion Gel Gate Dielectrics. *Nano Lett.* **2014**, *14* (2), 682–686.
- (246) Chae, S. H.; Yu, W. J.; Bae, J. J.; Duong, D. L.; Perello, D.; Jeong, H. Y.; Ta, Q. H.; Ly, T. H.; Vu, Q. A.; Yun, M.; Duan, X.; Lee, Y. H. Transferred Wrinkled Al<sub>2</sub>O<sub>3</sub> for Highly Stretchable and Transparent Graphene–Carbon Nanotube Transistors. *Nat. Mater.* **2013**, *12* (5), 403–409.
- (247) Javey, A.; Guo, J.; Wang, Q.; Lundstrom, M.; Dai, H. Ballistic Carbon Nanotube Field-Effect Transistors. *Nature* **2003**, *424* (6949), 654–657.



- (248) Shulaker, M. M.; Hills, G.; Patil, N.; Wei, H.; Chen, H.-Y.; Wong, H. S. P.; Mitra, S. Carbon Nanotube Computer. *Nature* **2013**, 501 (7468), 526–530.
- (249) Zhang, Q.; Huang, J.-Q.; Zhao, M.-Q.; Qian, W.-Z.; Wei, F. Carbon Nanotube Mass Production: Principles and Processes. *ChemSusChem* **2011**, 4 (7), 864–889.
- (250) Dresselhaus, M. S.; Dresselhaus, G.; Saito, R. Physics of Carbon Nanotubes. *Carbon* **1995**, 33 (7), 883–891.
- (251) Page, A. J.; Ding, F.; Irlé, S.; Morokuma, K. Insights into Carbon Nanotube and Graphene Formation Mechanisms from Molecular Simulations: A Review. *Rep. Prog. Phys.* **2015**, 78 (3), 036501.
- (252) Hofmann, S.; Csányi, G.; Ferrari, A. C.; Payne, M. C.; Robertson, J. Surface Diffusion: The Low Activation Energy Path for Nanotube Growth. *Phys. Rev. Lett.* **2005**, 95 (3), 036101.
- (253) Meyyappan, M. A Review of Plasma Enhanced Chemical Vapour Deposition of Carbon Nanotubes. *J. Phys. D: Appl. Phys.* **2009**, 42 (21), 213001.
- (254) Gohier, A.; Minea, T. M.; Djouadi, A. M.; Granier, A.; Dubosc, M. Limits of the Pecvd Process for Single Wall Carbon Nanotubes Growth. *Chem. Phys. Lett.* **2006**, 421 (1–3), 242–245.
- (255) Kumar, S.; Mehdipour, H.; Ostrikov, K. Plasma-Enabled Graded Nanotube Biosensing Arrays on a Si Nanodevice Platform: Catalyst-Free Integration and in Situ Detection of Nucleation Events. *Adv. Mater.* **2013**, 25 (1), 69–74.
- (256) Shaikjee, A.; Coville, N. J. The Role of the Hydrocarbon Source on the Growth of Carbon Materials. *Carbon* **2012**, 50 (10), 3376–3398.
- (257) Druzhinina, T.; Hoeppener, S.; Schubert, U. S. On the Synthesis of Carbon Nanofibers and Nanotubes by Microwave Irradiation: Parameters, Catalysts, and Substrates. *Adv. Funct. Mater.* **2009**, 19 (17), 2819–2825.
- (258) Futaba, D. N.; Goto, J.; Yasuda, S.; Yamada, T.; Yumura, M.; Hata, K. General Rules Governing the Highly Efficient Growth of Carbon Nanotubes. *Adv. Mater.* **2009**, 21 (47), 4811–4815.
- (259) Li, Q.; Yan, H.; Zhang, J.; Liu, Z. Effect of Hydrocarbons Precursors on the Formation of Carbon Nanotubes in Chemical Vapor Deposition. *Carbon* **2004**, 42 (4), 829–835.
- (260) Otsuka, K.; Ogihara, H.; Takenaka, S. Decomposition of Methane over Ni Catalysts Supported on Carbon Fibers Formed from Different Hydrocarbons. *Carbon* **2003**, 41 (2), 223–233.
- (261) Chesnokov, V. V.; Buyanov, R. A.; Mishakov, I. V.; Zaikovskii, V. I. Effect of Zinc Added to the Co/Al<sub>2</sub>O<sub>3</sub> Catalyst on the Formation of Carbon Nanofilaments from Methane and Butadiene-1,3. *Kinet. Catal.* **2006**, 47 (3), 445–450.
- (262) Reilly, P. T. A.; Whitten, W. B. The Role of Free Radical Condensates in the Production of Carbon Nanotubes During the Hydrocarbon Cvd Process. *Carbon* **2006**, 44 (9), 1653–1660.
- (263) Hernadi, K.; Fonseca, A.; Nagy, J. B.; Siska, A.; Kiricsi, I. Production of Nanotubes by the Catalytic Decomposition of Different Carbon-Containing Compounds. *Appl. Catal., A* **2000**, 199 (2), 245–255.
- (264) Hernadi, K. Catalytic Synthesis of Multiwall Carbon Nanotubes from Methylacetylene. *Chem. Phys. Lett.* **2002**, 363 (1–2), 169–174.
- (265) Koprinarov, N.; Konstantinova, M. Preparation of Carbon Spheres by Low-Temperature Pyrolysis of Cyclic Hydrocarbons. *J. Mater. Sci.* **2011**, 46 (5), 1494–1501.
- (266) Lee, W. J.; Li, C.-Z. Opposite Effects of Gas Flow Rate on the Rate of Formation of Carbon During the Pyrolysis of Ethane and Acetylene on a Nickel Mesh Catalyst. *Carbon* **2008**, 46 (9), 1208–1217.
- (267) Nessim, G. D.; Seita, M.; Plata, D. L.; O'Brien, K. P.; John Hart, A.; Meshot, E. R.; Reddy, C. M.; Gschwend, P. M.; Thompson, C. V. Precursor Gas Chemistry Determines the Crystallinity of Carbon Nanotubes Synthesized at Low Temperature. *Carbon* **2011**, 49 (3), 804–810.
- (268) Nieto-Márquez, A.; Valverde, J. L.; Keane, M. A. Selective Low Temperature Synthesis of Carbon Nanospheres Via the Catalytic Decomposition of Trichloroethylene. *Appl. Catal., A* **2009**, 352 (1–2), 159–170.
- (269) Tian, Y.; Hu, Z.; Yang, Y.; Chen, X.; Ji, W.; Chen, Y. Thermal Analysis–Mass Spectroscopy Coupling as a Powerful Technique to Study the Growth of Carbon Nanotubes from Benzene. *Chem. Phys. Lett.* **2004**, 388 (4–6), 259–262.
- (270) Tian, Y.; Hu, Z.; Yang, Y.; Wang, X.; Chen, X.; Xu, H.; Wu, Q.; Ji, W.; Chen, Y. In Situ Ta–Ms Study of the Six-Membered-Ring-Based Growth of Carbon Nanotubes with Benzene Precursor. *J. Am. Chem. Soc.* **2004**, 126 (4), 1180–1183.
- (271) Su, D. S. The Use of Natural Materials in Nanocarbon Synthesis. *ChemSusChem* **2009**, 2 (11), 1009–1020.
- (272) Wang, Z.; Zhao, Z.; Qiu, J. In Situ Synthesis of Super-Long Cu Nanowires inside Carbon Nanotubes with Coal as Carbon Source. *Carbon* **2006**, 44 (9), 1845–1847.
- (273) Wang, Z.; Zhao, Z.; Qiu, J. Synthesis of Branched Carbon Nanotubes from Coal. *Carbon* **2006**, 44 (7), 1321–1324.
- (274) Qiu, J.; Wang, Z.; Zhao, Z.; Wang, T. Synthesis of Double-Walled Carbon Nanotubes from Coal in Hydrogen-Free Atmosphere. *Fuel* **2007**, 86 (1–2), 282–286.
- (275) Endo, M.; Takeuchi, K.; Kim, Y. A.; Park, K. C.; Ichiki, T.; Hayashi, T.; Fukuyo, T.; Iino, S.; Su, D. S.; Terrones, M.; Dresselhaus, M. S. Simple Synthesis of Multiwalled Carbon Nanotubes from Natural Resources. *ChemSusChem* **2008**, 1 (10), 820–822.
- (276) Huang, J.; Zhang, Q.; Wei, F.; Qian, W.; Wang, D.; Hu, L. Liquefied Petroleum Gas Containing Sulfur as the Carbon Source for Carbon Nanotube Forests. *Carbon* **2008**, 46 (2), 291–296.
- (277) Qian, W.; Yu, H.; Wei, F.; Zhang, Q.; Wang, Z. Synthesis of Carbon Nanotubes from Liquefied Petroleum Gas Containing Sulfur. *Carbon* **2002**, 40 (15), 2968–2970.
- (278) Zhang, Q.; Huang, J.; Wei, F.; Xu, G.; Wang, Y.; Qian, W.; Wang, D. Large Scale Production of Carbon Nanotube Arrays on the Sphere Surface from Liquefied Petroleum Gas at Low Cost. *Chin. Sci. Bull.* **2007**, 52 (21), 2896–2902.
- (279) Yang, Y.; Liu, X.; Xu, B.; Li, T. Preparation of Vapor-Grown Carbon Fibers from Deoiled Asphalt. *Carbon* **2006**, 44 (9), 1661–1664.
- (280) Kidena, K.; Kamiyama, Y.; Nomura, M. A Possibility of the Production of Carbon Nanotubes from Heavy Hydrocarbons. *Fuel Process. Technol.* **2008**, 89 (4), 449–454.
- (281) Krishnarao, R. V.; Godkhindi, M. M.; Chakraborty, M.; Mukunda, P. G. Formation of Sic Whiskers from Compacts of Raw Rice Husks. *J. Mater. Sci.* **1994**, 29 (10), 2741–2744.
- (282) Zhu, J.; Jia, J.; Kwong, F. L.; Ng, D. H. L. Synthesis of 6h-Sic Nanowires on Bamboo Leaves by Carbothermal Method. *Diamond Relat. Mater.* **2013**, 33, 5–11.
- (283) Kumar, M.; Ando, Y. Carbon Nanotubes from Camphor: An Environment-Friendly Nanotechnology. *J. Phys.: Conf. Ser.* **2007**, 61, 643.
- (284) Kumar, M.; Ando, Y. Single-Wall and Multi-Wall Carbon Nanotubes from Camphor—a Botanical Hydrocarbon. *Diamond Relat. Mater.* **2003**, 12 (10–11), 1845–1850.
- (285) Kumar, M.; Okazaki, T.; Hiramatsu, M.; Ando, Y. The Use of Camphor-Grown Carbon Nanotube Array as an Efficient Field Emitter. *Carbon* **2007**, 45 (9), 1899–1904.
- (286) Kumar, M.; Ando, Y. A Simple Method of Producing Aligned Carbon Nanotubes from an Unconventional Precursor – Camphor. *Chem. Phys. Lett.* **2003**, 374 (5–6), 521–526.
- (287) Kumar, M.; Ando, Y. Controlling the Diameter Distribution of Carbon Nanotubes Grown from Camphor on a Zeolite Support. *Carbon* **2005**, 43 (3), 533–540.
- (288) Kumar, M.; Ando, Y. Camphor—a Botanical Precursor Producing Garden of Carbon Nanotubes. *Diamond Relat. Mater.* **2003**, 12 (3–7), 998–1002.
- (289) Kumar, M.; Zhao, X.; Ando, Y.; Iijima, S.; Sharon, M.; Hirahara, K. Carbon Nanotubes from Camphor by Catalytic Cvd. *Mol. Cryst. Liq. Cryst.* **2002**, 387 (1), 117–121.



- (290) Kumar, R.; Tiwari, R.; Srivastava, O. Scalable Synthesis of Aligned Carbon Nanotubes Bundles Using Green Natural Precursor: Neem Oil. *Nanoscale Res. Lett.* **2011**, *6* (1), 92.
- (291) Ghosh, P.; Afre, R. A.; Soga, T.; Jimbo, T. A Simple Method of Producing Single-Walled Carbon Nanotubes from a Natural Precursor: Eucalyptus Oil. *Mater. Lett.* **2007**, *61* (17), 3768–3770.
- (292) Afre, R. A.; Soga, T.; Jimbo, T.; Kumar, M.; Ando, Y.; Sharon, M. Vertically Aligned Carbon Nanotubes at Different Temperatures by Spray Pyrolysis Techniques. *Int. J. Mod. Phys. B* **2006**, *20* (29), 4965–4972.
- (293) Ghosh, P.; Soga, T.; Tanemura, M.; Zamri, M.; Jimbo, T.; Katoh, R.; Sumiyama, K. Vertically Aligned Carbon Nanotubes from Natural Precursors By spray Pyrolysis Method and Their Field Electron Emission Properties. *Appl. Phys. A: Mater. Sci. Process.* **2009**, *94* (1), 51–56.
- (294) Balasubramanian, K.; Burghard, M. Chemically Functionalized Carbon Nanotubes. *Small* **2005**, *1* (2), 180–192.
- (295) Awasthi, K.; Kumar, R.; Raghubanshi, H.; Awasthi, S.; Pandey, R.; Singh, D.; Yadav, T. P.; Srivastava, O. N. Synthesis of Nano-Carbon (Nanotubes, Nanofibres, Graphene) Materials. *Bull. Mater. Sci.* **2011**, *34* (4), 607–614.
- (296) Kang, Z.; Wang, E.; Mao, B.; Su, Z.; Chen, Li; Xu, L. Obtaining Carbon Nanotubes from Grass. *Nanotechnology* **2005**, *16* (8), 1192.
- (297) Setlur, A. A.; Doherty, S. P.; Dai, J. Y.; Chang, R. P. H. A Promising Pathway to Make Multiwalled Carbon Nanotubes. *Appl. Phys. Lett.* **2000**, *76* (21), 3008–3010.
- (298) Abdel-Fattah, T.; Siochi, E. J.; Crooks, R. E. Pyrolytic Synthesis of Carbon Nanotubes from Sucrose on a Mesoporous Silicate. *Fullerenes, Nanotubes, Carbon Nanostruct.* **2006**, *14* (4), 585–594.
- (299) Datta, A.; Dutta, P.; Sadhu, A.; Maiti, S.; Bhattacharyya, S. Single-Step Scalable Conversion of Waste Natural Oils to Carbon Nanowhiskers and Their Interaction with Mammalian Cells. *J. Nanopart. Res.* **2013**, *15* (7), 1808.
- (300) Suriani, A. B.; Md Nor, R.; Rusop, M. Vertically Aligned Carbon Nanotubes Synthesized from Waste Cooking Palm Oil. *J. Ceram. Soc. Jpn.* **2010**, *118* (1382), 963–968.
- (301) Pol, V. G.; Thiagarajan, P. Remediating Plastic Waste into Carbon Nanotubes. *J. Environ. Monit.* **2010**, *12* (2), 455–459.
- (302) Pol, S. V.; Pol, V. G.; Sherman, D.; Gedanken, A. A Solvent Free Process for the Generation of Strong, Conducting Carbon Spheres by the Thermal Degradation of Waste Polyethylene Terephthalate. *Green Chem.* **2009**, *11* (4), 448–451.
- (303) Yang, Z.; Zhang, Q.; Luo, G.; Huang, J.-Q.; Zhao, M.-Q.; Wei, F. Coupled Process of Plastics Pyrolysis and Chemical Vapor Deposition for Controllable Synthesis of Vertically Aligned Carbon Nanotube Arrays. *Appl. Phys. A: Mater. Sci. Process.* **2010**, *100* (2), 533–540.
- (304) Zhang, Q.; Huang, J.-Q.; Qian, W.-Z.; Zhang, Y.-Y.; Wei, F. The Road for Nanomaterials Industry: A Review of Carbon Nanotube Production, Post-Treatment, and Bulk Applications for Composites and Energy Storage. *Small* **2013**, *9* (8), 1237–1265.
- (305) Su, D. S.; Chen, X.-W. Natural Lavas as Catalysts for Efficient Production of Carbon Nanotubes and Nanofibers. *Angew. Chem.* **2007**, *119* (11), 1855–1856.
- (306) Su, D. S.; Rinaldi, A.; Frandsen, W.; Weinberg, G. Nanocarbons: Efficient Synthesis Using Natural Lava as Supported Catalyst. *Phys. Status Solidi B* **2007**, *244* (11), 3916–3919.
- (307) Rinaldi, A.; Zhang, J.; Mizera, J.; Girgsdies, F.; Wang, N.; Hamid, S. B. A.; Schlögl, R.; Su, D. S. Facile Synthesis of Carbon Nanotube/Natural Bentonite Composites as a Stable Catalyst for Styrene Synthesis. *Chem. Commun.* **2008**, *48*, 6528–6530.
- (308) Nie, J. Q.; Zhang, Q.; Zhao, M. Q.; Huang, J. Q.; Wen, Q.; Cui, Y.; Qian, W. Z.; Wei, F. Synthesis of High Quality Single-Walled Carbon Nanotubes on Natural Sepiolite and Their Use for Phenol Absorption. *Carbon* **2011**, *49* (5), 1568–1580.
- (309) Zhao, M. Q.; Zhang, Q.; Huang, J. Q.; Nie, J. Q.; Wei, F. Advanced Materials from Natural Materials: Synthesis of Aligned Carbon Nanotubes on Wollastonites. *ChemSusChem* **2010**, *3* (4), 453–459.
- (310) Chen, X.-W.; Timpe, O.; Hamid, S. B. A.; Schlögl, R.; Su, D. S. Direct Synthesis of Carbon Nanofibers on Modified Biomass-Derived Activated Carbon. *Carbon* **2009**, *47* (1), 340–343.
- (311) Zhu, J.; Jia, J.; Kwong, F. L.; Ng, D. H. L.; Tjong, S. C. Synthesis of Multiwalled Carbon Nanotubes from Bamboo Charcoal and the Roles of Minerals on Their Growth. *Biomass Bioenergy* **2012**, *36*, 12–19.
- (312) Bradbury, W. L.; Olevsky, E. A. Production of SiC–C Composites by Free-Pressureless Spark Plasma Sintering (Fpsps). *Scr. Mater.* **2010**, *63* (1), 77–80.
- (313) Eftekhari, A.; Jafarkhani, P.; Moztaaradeh, F. High-Yield Synthesis of Carbon Nanotubes Using a Water-Soluble Catalyst Support in Catalytic Chemical Vapor Deposition. *Carbon* **2006**, *44* (7), 1343–1345.
- (314) Irimia-Vladu, M.; Glowacki, E.; Sariciftci, N. S.; Bauer, S. Natural Materials for Organic Electronics. In *Small Organic Molecules on Surfaces*; Sitter, H., Draxl, C., Ramsey, M., Eds.; Springer: Berlin, 2013; Vol. 173, pp 295–318.
- (315) Irimia-Vladu, M.; Troshin, P. A.; Reisinger, M.; Shmygleva, L.; Kanbur, Y.; Schwabegger, G.; Bodea, M.; Schwödiauer, R.; Mumyatov, A.; Fergus, J. W.; Razumov, V. F.; Sitter, H.; Sariciftci, N. S.; Bauer, S. Biocompatible and Biodegradable Materials for Organic Field-Effect Transistors. *Adv. Funct. Mater.* **2010**, *20* (23), 4069–4076.
- (316) Lin, Y.; Wang, Y.; Wang, J.; Hou, J.; Li, Y.; Zhu, D.; Zhan, X. A Star-Shaped Perylene Diimide Electron Acceptor for High-Performance Organic Solar Cells. *Adv. Mater.* **2014**, *26* (30), 5137–5142.
- (317) Meredith, P.; Tandy, K.; Mostert, A. B. A Hybrid Ionic–Electronic Conductor: Melanin, the First Organic Amorphous Semiconductor? In *Organic Electronics*; Wiley-VCH Verlag GmbH & Co. KGaA: 2013; pp 91–111.
- (318) Glowacki, E. D.; Voss, G.; Leonat, L.; Irimia-Vladu, M.; Bauer, S.; Sariciftci, N. S. Indigo and Tyrian Purple – from Ancient Natural Dyes to Modern Organic Semiconductors. *Isr. J. Chem.* **2012**, *52* (6), 540–551.
- (319) Pan, J.; Xu, Y.; Sun, L.; Sundström, V.; Polívka, T. Carotenoid and Pheophytin on Semiconductor Surface: Self-Assembly and Photoinduced Electron Transfer. *J. Am. Chem. Soc.* **2004**, *126* (10), 3066–3067.
- (320) Mostert, A. B.; Powell, B. J.; Pratt, F. L.; Hanson, G. R.; Sarna, T.; Gentle, I. R.; Meredith, P. Role of Semiconductivity and Ion Transport in the Electrical Conduction of Melanin. *Proc. Natl. Acad. Sci. U. S. A.* **2012**, *109* (23), 8943–8947.
- (321) Kushwaha, R.; Srivastava, P.; Bahadur, L. Natural Pigments from Plants Used as Sensitizers for TiO<sub>2</sub> Based Dye-Sensitized Solar Cells. *J. Energy* **2013**, *2013*, 654953.
- (322) Burch, R. R.; Dong, Y.-H.; Fincher, C.; Goldfinger, M.; Rouviere, P. E. Electrical Properties of Polyunsaturated Natural Products: Field Effect Mobility of Carotenoid Polyenes. *Synth. Met.* **2004**, *146* (1), 43–46.
- (323) Selvaraju, S.; Niradha Sachinthan, K. A.; Hopson, R. A.; McFarland, F. M.; Guo, S.; Rheingold, A. L.; Nelson, T. L. Eumelanin-Inspired Core Derived from Vanillin: A New Building Block for Organic Semiconductors. *Chem. Commun.* **2015**, *51*, 2957.
- (324) Kim, Y. J.; Wu, W.; Chun, S.-E.; Whitacre, J. F.; Bettinger, C. J. Biologically Derived Melanin Electrodes in Aqueous Sodium-Ion Energy Storage Devices. *Proc. Natl. Acad. Sci. U. S. A.* **2013**, *110* (52), 20912–20917.
- (325) Yun, H.-J.; Kang, S.-J.; Xu, Y.; Kim, S. O.; Kim, Y.-H.; Noh, Y.-Y.; Kwon, S.-K. Dramatic Inversion of Charge Polarity in Diketopyrrolopyrrole-Based Organic Field-Effect Transistors Via a Simple Nitrile Group Substitution. *Adv. Mater.* **2014**, *26* (43), 7300–7307.
- (326) Klimovich, I. V.; Leshanskaya, L. I.; Troyanov, S. I.; Anokhin, D. V.; Novikov, D. V.; Pirayev, A. A.; Ivanov, D. A.; Dremova, N. N.; Troshin, P. A. Design of Indigo Derivatives as Environment-Friendly Organic Semiconductors for Sustainable Organic Electronics. *J. Mater. Chem. C* **2014**, *2* (36), 7621–7631.
- (327) Glowacki, E. D.; Romanazzi, G.; Yumusak, C.; Coskun, H.; Monkowius, U.; Voss, G.; Burian, M.; Lechner, R. T.; Demitri, N.;

- Redhammer, G. J.; Sünger, N.; Suranna, G. P.; Sariciftci, S. Epindolidiones—Versatile and Stable Hydrogen-Bonded Pigments for Organic Field-Effect Transistors and Light-Emitting Diodes. *Adv. Funct. Mater.* **2015**, *25* (5), 776–787.
- (328) Irimia-Vladu, M.; Glowacki, E. D.; Voss, G.; Bauer, S.; Sariciftci, N. S. Green and Biodegradable Electronics. *Mater. Today* **2012**, *15* (7–8), 340–346.
- (329) Meager, I.; Nikolka, M.; Schroeder, B. C.; Nielsen, C. B.; Planells, M.; Bronstein, H.; Rumer, J. W.; James, D. I.; Ashraf, R. S.; Sadhanala, A.; Hayoz, P.; Flores, J.-C.; Sirringhaus, H.; McCulloch, I. Thieno[3,2-b]Thiophene Flanked Isoindigo Polymers for High Performance Ambipolar OFET Applications. *Adv. Funct. Mater.* **2014**, *24* (45), 7109–7115.
- (330) Xu, S.; Ai, N.; Zheng, J.; Zhao, N.; Lan, Z.; Wen, L.; Wang, X.; Pei, J.; Wan, X. Extended Isoindigo Core: Synthesis and Applications as Solution-Processable N-Ofet Materials in Ambient Conditions. *RSC Adv.* **2015**, *5* (11), 8340–8344.
- (331) He, B.; Pun, A. B.; Zhrebetskyy, D.; Liu, Y.; Liu, F.; Klivansky, L. M.; McGough, A. M.; Zhang, B. A.; Lo, K.; Russell, T. P.; Wang, L.; Liu, Y. New Form of an Old Natural Dye: Bay-Annulated Indigo (Bai) as an Excellent Electron Accepting Unit for High Performance Organic Semiconductors. *J. Am. Chem. Soc.* **2014**, *136* (42), 15093–15101.
- (332) Irimia-Vladu, M.; Glowacki, E. D.; Troshin, P. A.; Schwabegger, G.; Leonat, L.; Susarova, D. K.; Krystal, O.; Ullah, M.; Kanbur, Y.; Bodea, M. A.; Razumov, V. F.; Sitter, H.; Bauer, S.; Sariciftci, N. S. Indigo – from Jeans to Semiconductors: Indigo - a Natural Pigment for High Performance Ambipolar Organic Field Effect Transistors and Circuits (Adv. Mater. 3/2012). *Adv. Mater.* **2012**, *24* (3), 321–321.
- (333) Mei, J.; Graham, K. R.; Stalder, R.; Reynolds, J. R. Synthesis of Isoindigo-Based Oligothiophenes for Molecular Bulk Heterojunction Solar Cells. *Org. Lett.* **2010**, *12* (4), 660–663.
- (334) Wang, E.; Ma, Z.; Zhang, Z.; Vandewal, K.; Henriksson, P.; Inganäs, O.; Zhang, F.; Andersson, M. R. An Easily Accessible Isoindigo-Based Polymer for High-Performance Polymer Solar Cells. *J. Am. Chem. Soc.* **2011**, *133* (36), 14244–14247.
- (335) Sharenko, A.; Proctor, C. M.; van der Poll, T. S.; Henson, Z. B.; Nguyen, T.-Q.; Bazan, G. C. A High-Performing Solution-Processed Small Molecule:Perylene Diimide Bulk Heterojunction Solar Cell. *Adv. Mater.* **2013**, *25* (32), 4403–4406.
- (336) Zhong, Y.; Trinh, M. T.; Chen, R.; Wang, W.; Khlyabich, P. P.; Kumar, B.; Xu, Q.; Nam, C.-Y.; Sfeir, M. Y.; Black, C.; Steigerwald, M. L.; Loo, Y.-L.; Xiao, S.; Ng, F.; Zhu, X. Y.; Nuckolls, C. Efficient Organic Solar Cells with Helical Perylene Diimide Electron Acceptors. *J. Am. Chem. Soc.* **2014**, *136* (43), 15215–15221.
- (337) Huang, C.; Barlow, S.; Marder, S. R. Perylene-3,4,9,10-Tetracarboxylic Acid Diimides: Synthesis, Physical Properties, and Use in Organic Electronics. *J. Org. Chem.* **2011**, *76* (8), 2386–2407.
- (338) Wang, C.; Chen, D.; Chen, W.; Chen, S.; Ye, K.; Zhang, H.; Zhang, J.; Wang, Y. Polymorph, Assembly, Luminescence and Semiconductor Properties of a Quinacridone Derivative with Extended [Small Pi]-Conjugated Framework. *J. Mater. Chem. C* **2013**, *1* (35), 5548–5556.
- (339) Daniel Glowacki, E.; Leonat, L.; Irimia-Vladu, M.; Schwödiauer, R.; Ullah, M.; Sitter, H.; Bauer, S.; Serdar Sariciftci, N. Intermolecular Hydrogen-Bonded Organic Semiconductors—Quinacridone Versus Pentacene. *Appl. Phys. Lett.* **2012**, *101* (2), 023305.
- (340) Qu, S.; Tian, H. Diketopyrrolopyrrole (Dpp)-Based Materials for Organic Photovoltaics. *Chem. Commun.* **2012**, *48* (25), 3039–3051.
- (341) Glowacki, E. D.; Coskun, H.; Blood-Forsythe, M. A.; Monkowius, U.; Leonat, L.; Grzybowski, M.; Gryko, D.; White, M. S.; Aspuru-Guzik, A.; Sariciftci, N. S. Hydrogen-Bonded Diketopyrrolopyrrole (Dpp) Pigments as Organic Semiconductors. *Org. Electron.* **2014**, *15* (12), 3521–3528.
- (342) Burke, D. J.; Lipomi, D. J. Green Chemistry for Organic Solar Cells. *Energy Environ. Sci.* **2013**, *6* (7), 2053–2066.
- (343) Li, Y.; Sonar, P.; Murphy, L.; Hong, W. High Mobility Diketopyrrolopyrrole (Dpp)-Based Organic Semiconductor Materials for Organic Thin Film Transistors and Photovoltaics. *Energy Environ. Sci.* **2013**, *6* (6), 1684–1710.
- (344) Li, W.; Roelofs, W. S. C.; Turbiez, M.; Wienk, M. M.; Janssen, R. A. J. Polymer Solar Cells with Diketopyrrolopyrrole Conjugated Polymers as the Electron Donor and Electron Acceptor. *Adv. Mater.* **2014**, *26* (20), 3304–3309.
- (345) Suginta, W.; Khunkaewla, P.; Schulte, A. Electrochemical Biosensor Applications of Polysaccharides Chitin and Chitosan. *Chem. Rev.* **2013**, *113* (7), 5458–5479.
- (346) Kim, D.-H.; Viventi, J.; Amsden, J. J.; Xiao, J.; Vigeland, L.; Kim, Y.-S.; Blanco, J. A.; Panilaitis, B.; Frechette, E. S.; Contreras, D.; Kaplan, D. L.; Omenetto, F. G.; Huang, Y.; Hwang, K.-C.; Zakin, M. R.; Litt, B.; Rogers, J. A. Dissolvable Films of Silk Fibroin for Ultrathin Conformal Bio-Integrated Electronics. *Nat. Mater.* **2010**, *9* (6), 511–517.
- (347) Tao, H.; Hwang, S.-W.; Marelli, B.; An, B.; Moreau, J. E.; Yang, M.; Brenckle, M. A.; Kim, S.; Kaplan, D. L.; Rogers, J. A.; Omenetto, F. G. Silk-Based Resorbable Electronic Devices for Remotely Controlled Therapy and in Vivo Infection Abatement. *Proc. Natl. Acad. Sci. U. S. A.* **2014**, *111* (49), 17385–17389.
- (348) Vepari, C.; Kaplan, D. L. Silk as a Biomaterial. *Prog. Polym. Sci.* **2007**, *32* (8–9), 991–1007.
- (349) Zhang, X.; Reagan, M. R.; Kaplan, D. L. Electrospun Silk Biomaterial Scaffolds for Regenerative Medicine. *Adv. Drug Delivery Rev.* **2009**, *61* (12), 988–1006.
- (350) Lu, S.; Wang, X.; Lu, Q.; Hu, X.; Uppal, N.; Omenetto, F. G.; Kaplan, D. L. Stabilization of Enzymes in Silk Films. *Biomacromolecules* **2009**, *10* (5), 1032–1042.
- (351) Omenetto, F. G.; Kaplan, D. L. New Opportunities for an Ancient Material. *Science* **2010**, *329* (5991), 528–531.
- (352) Barr, M. C.; Rowehl, J. A.; Lunt, R. R.; Xu, J.; Wang, A.; Boyce, C. M.; Im, S. G.; Bulović, V.; Gleason, K. K. Direct Monolithic Integration of Organic Photovoltaic Circuits on Unmodified Paper. *Adv. Mater.* **2011**, *23* (31), 3500–3505.
- (353) Martins, R.; Nathan, A.; Barros, R.; Pereira, L.; Barquinha, P.; Correia, N.; Costa, R.; Ahnood, A.; Ferreira, I.; Fortunato, E. Complementary Metal Oxide Semiconductor Technology with and on Paper. *Adv. Mater.* **2011**, *23* (39), 4491–4496.
- (354) Russo, A.; Ahn, B. Y.; Adams, J. J.; Duoss, E. B.; Bernhard, J. T.; Lewis, J. A. Pen-on-Paper Flexible Electronics. *Adv. Mater.* **2011**, *23* (30), 3426–3430.
- (355) Irimia-Vladu, M.; Sariciftci, N. S.; Bauer, S. Exotic Materials for Bio-Organic Electronics. *J. Mater. Chem.* **2011**, *21* (5), 1350–1361.
- (356) Lendlein, A.; Langer, R. Biodegradable, Elastic Shape-Memory Polymers for Potential Biomedical Applications. *Science* **2002**, *296* (5573), 1673–1676.
- (357) Jeon, D.-B.; Bak, J.-Y.; Yoon, S.-M. Oxide Thin-Film Transistors Fabricated Using Biodegradable Gate Dielectric Layer of Chicken Albumen. *Jpn. J. Appl. Phys.* **2013**, *52* (12R), 128002.
- (358) Chang, J.-W.; Wang, C.-G.; Huang, C.-Y.; Tsai, T.-D.; Guo, T.-F.; Wen, T.-C. Chicken Albumen Dielectrics in Organic Field-Effect Transistors. *Adv. Mater.* **2011**, *23* (35), 4077–4081.
- (359) Wang, C.-H.; Hsieh, C.-Y.; Hwang, J.-C. Flexible Organic Thin-Film Transistors with Silk Fibroin as the Gate Dielectric. *Adv. Mater.* **2011**, *23* (14), 1630–1634.
- (360) Kwon, Y.-W.; Lee, C. H.; Choi, D.-H.; Jin, J.-I. Materials Science of DNA. *J. Mater. Chem.* **2009**, *19* (10), 1353–1380.
- (361) Sönmezoglu, S.; Ateş Sönmezoglu, Ö. Optical and Dielectric Properties of Double Helix DNA Thin Films. *Mater. Sci. Eng., C* **2011**, *31* (8), 1619–1624.
- (362) Cuervo, A.; Dans, P. D.; Carrascosa, J. L.; Orozco, M.; Gomila, G.; Fumagalli, L. Direct Measurement of the Dielectric Polarization Properties of DNA. *Proc. Natl. Acad. Sci. U. S. A.* **2014**, *111* (35), E3624–E3630.
- (363) Holzel, R. Dielectric and Dielectrophoretic Properties of DNA. *IET Nanobiotechnol.* **2009**, *3* (2), 28–45.
- (364) Virkar, A. Organic Semiconductor Growth and Transistor Performance as a Function of the Density of the Octadecylsilane Dielectric Modification Layer. In *Investigating the Nucleation, Growth,*



and Energy Levels of Organic Semiconductors for High Performance Plastic Electronics; Springer: New York, 2012; pp 27–49.

(365) Bazaka, K.; Jacob, M. V. Synthesis of Radio Frequency Plasma Polymerized Non-Synthetic Terpinen-4-ol Thin Films. *Mater. Lett.* **2009**, *63* (18–19), 1594–1597.

(366) Yasuda, H. *Plasma Polymerization*; Academic Press: 1985.

(367) Michelmores, A.; Gross-Kosche, P.; Al-Bataineh, S. A.; Whittle, J. D.; Short, R. D. On the Effect of Monomer Chemistry on Growth Mechanisms of Nonfouling Peg-Like Plasma Polymers. *Langmuir* **2013**, *29* (8), 2595–2601.

(368) Wood, T. J.; Hurst, G. A.; Schofield, W. C. E.; Thompson, R. L.; Oswald, G.; Evans, J. S. O.; Sharples, G. J.; Pearson, C.; Petty, M. C.; Badyal, J. P. S. Electroless Deposition of Multi-Functional Zinc Oxide Surfaces Displaying Photoconductive, Superhydrophobic, Photowetting, and Antibacterial Properties. *J. Mater. Chem.* **2012**, *22* (9), 3859–3867.

(369) Wells, G. P.; Estrada-Raygoza, I. C.; Thamban, P. L. S.; Nelson, C. T.; Chung, C.-W.; Overzet, L. J.; Goeckner, M. J. Understanding the Synthesis of Ethylene Glycol Pulsed Plasma Discharges. *Plasma Processes Polym.* **2013**, *10* (2), 119–135.

(370) Kwok, D. T. K.; Tong, L.; Yeung, C. Y.; Remedios, C. G. d.; Chu, P. K. Hybrid Plasma Surface Modification and Ion Implantation of Biopolymers. *Surf. Coat. Technol.* **2010**, *204* (18–19), 2892–2897.

(371) Denis, L.; Marsal, P.; Olivier, Y.; Godfroid, T.; Lazzaroni, R.; Hecq, M.; Cornil, J.; Snyders, R. Deposition of Functional Organic Thin Films by Pulsed Plasma Polymerization: A Joint Theoretical and Experimental Study. *Plasma Processes Polym.* **2010**, *7* (2), 172–181.

(372) Manakhov, A.; Moreno-Couranjou, M.; Boscher, N. D.; Rogé, V.; Choquet, P.; Pireaux, J.-J. Atmospheric Pressure Pulsed Plasma Copolymerisation of Maleic Anhydride and Vinyltrimethoxysilane: Influence of Electrical Parameters on Chemistry, Morphology and Deposition Rate of the Coatings. *Plasma Processes Polym.* **2012**, *9* (4), 435–445.

(373) Duran, H.; Yameen, B.; Khan, H. U.; Förch, R.; Knoll, W. Surface-Initiated Ring Opening Polymerization of N-Carboxy Anhydride of Benzyl-L-Glutamate Monomers on Soft Flexible Substrates. *React. Funct. Polym.* **2013**, *73* (3), 606–612.

(374) Duque, L.; Menges, B.; Borros, S.; Förch, R. Immobilization of Biomolecules to Plasma Polymerized Pentafluorophenyl Methacrylate. *Biomacromolecules* **2010**, *11* (10), 2818–2823.

(375) Fahmy, A.; Schönhals, A.; Friedrich, J. Reaction of Water with (Radicals in) Plasma Polymerized Allyl Alcohol (and Formation of Oh-Rich Polymer Layers). *J. Phys. Chem. B* **2013**, *117* (36), 10603–10611.

(376) Shearer, J. C.; Fisher, E. R. Enhancing Surface Functionality of Supported Fe<sub>2</sub>O<sub>3</sub> Nanoparticles Using Pulsed Plasma Deposition of Allyl Alcohol. *Nanosci. Nanotechnol. Lett.* **2012**, *4* (3), 358–363.

(377) Tarducci, C.; Schofield, W. C. E.; Badyal, J. P. S.; Brewer, S. A.; Willis, C. Monomolecular Functionalization of Pulsed Plasma Deposited Poly(2-Hydroxyethyl Methacrylate) Surfaces. *Chem. Mater.* **2002**, *14* (6), 2541–2545.

(378) Wood, T. J.; Badyal, J. P. S. Pulsed Plasmachemical Deposition of Highly Proton Conducting Composite Sulfonic Acid–Carboxylic Acid Films. *ACS Appl. Mater. Interfaces* **2012**, *4* (3), 1675–1682.

(379) Chen, J.-P.; Kuo, C.-Y.; Lee, W.-L. Thermo-Responsive Wound Dressings by Grafting Chitosan and Poly(N-Isopropylacrylamide) to Plasma-Induced Graft Polymerization Modified Non-Woven Fabrics. *Appl. Surf. Sci.* **2012**, *262*, 95–101.

(380) Anderson, K. D.; Young, S. L.; Jiang, H.; Jakubiak, R.; Bunning, T. J.; Naik, R. R.; Tsukruk, V. V. Plasma-Enhanced Copolymerization of Amino Acid and Synthetic Monomers. *Langmuir* **2012**, *28* (3), 1833–1845.

(381) Tarducci, C.; Schofield, W. C. E.; Badyal, J. P. S.; Brewer, S. A.; Willis, C. Cyano-Functionalized Solid Surfaces. *Chem. Mater.* **2001**, *13* (5), 1800–1803.

(382) Tarducci, C.; Kinmond, E. J.; Badyal, J. P. S.; Brewer, S. A.; Willis, C. Epoxide-Functionalized Solid Surfaces. *Chem. Mater.* **2000**, *12* (7), 1884–1889.

(383) Teare, D. O. H.; Barwick, D. C.; Schofield, W. C. E.; Garrod, R. P.; Ward, L. J.; Badyal, J. P. S. Substrate-Independent Approach for Polymer Brush Growth by Surface Atom Transfer Radical Polymerization. *Langmuir* **2005**, *21* (24), 11425–11430.

(384) Thiry, D.; Britun, N.; Konstantinidis, S.; Dauchot, J.-P.; Guillaume, M.; Cornil, J.; Snyders, R. Experimental and Theoretical Study of the Effect of the Inductive-to-Capacitive Transition in Propanethiol Plasma Polymer Chemistry. *J. Phys. Chem. C* **2013**, *117* (19), 9843–9851.

(385) Çökeliler, D.; Göktas, H.; Tosun, P. D.; Mutlu, S. Infection Free Titanium Alloys by Stable Thiol Based Nanocoating. *J. Nanosci. Nanotechnol.* **2010**, *10* (4), 2583–2589.

(386) Tarducci, C.; Badyal, J. P. S.; Brewer, S. A.; Willis, C. Diels-Alder Chemistry at Furan Ring Functionalized Solid Surfaces. *Chem. Commun.* **2005**, *3*, 406–408.

(387) Anokhin, D. V.; Leshanskaya, L. I.; Piryazev, A. A.; Susarova, D. K.; Dremova, N. N.; Shcheglov, E. V.; Ivanov, D. A.; Razumov, V. F.; Troshin, P. A. Towards Understanding the Behavior of Indigo Thin Films in Organic Field-Effect Transistors: A Template Effect of the Aliphatic Hydrocarbon Dielectric on the Crystal Structure and Electrical Performance of the Semiconductor. *Chem. Commun.* **2014**, *50* (57), 7639–7641.

(388) Yang, S. Y.; Shin, K.; Park, C. E. The Effect of Gate-Dielectric Surface Energy on Pentacene Morphology and Organic Field-Effect Transistor Characteristics. *Adv. Funct. Mater.* **2005**, *15* (11), 1806–1814.

(389) Yang, H.; Yang, C.; Kim, S. H.; Jang, M.; Park, C. E. Dependence of Pentacene Crystal Growth on Dielectric Roughness for Fabrication of Flexible Field-Effect Transistors. *ACS Appl. Mater. Interfaces* **2010**, *2* (2), 391–396.

(390) Bao, X.; Zhu, Q.; Wang, T.; Guo, J.; Yang, C.; Yu, D.; Wang, N.; Chen, W.; Yang, R. Simple O<sub>2</sub> Plasma-Processed V<sub>2</sub>O<sub>5</sub> as an Anode Buffer Layer for High-Performance Polymer Solar Cells. *ACS Appl. Mater. Interfaces* **2015**, *7*, 7613.

(391) Jacob, M. V.; Easton, C. D.; Woods, G. S.; Berndt, C. C. Fabrication of a Novel Organic Polymer Thin Film. *Thin Solid Films* **2008**, *516* (12), 3884–3887.

(392) Kumar, D. S.; Nakamura, K.; Nishiyama, S.; Noguchi, H.; Ishii, S.; Kashiwagi, K.; Yoshida, Y. Electrical and Optical Properties of Plasma Polymerized Eucalyptus Oil Films. *J. Appl. Polym. Sci.* **2003**, *90* (4), 1102–1107.

(393) Kumar, D. S.; Krishna Pillai, M. G. Conduction Mechanism in Plasma Polymerized Lemongrass Oil Films. *Thin Solid Films* **1999**, *353* (1–2), 249–253.

(394) Ahmad, J.; Bazaka, K.; Jacob, M. Optical and Surface Characterization of Radio Frequency Plasma Polymerized 1-Isopropyl-4-Methyl-1,4-Cyclohexadiene Thin Films. *Electronics* **2014**, *3* (2), 266–281.

(395) Anderson, L. J.; Jacob, M. V. Effect of Rf Power on the Optical and Morphological Properties of Rf Plasma Polymerised Linalyl Acetate Thin Films. *Appl. Surf. Sci.* **2010**, *256* (10), 3293–3298.

(396) Jacob, M. V.; Bazaka, K.; Weis, M.; Taguchi, D.; Manaka, T.; Iwamoto, M. Fabrication and Characterization of Polyterpenol as an Insulating Layer and Incorporated Organic Field Effect Transistor. *Thin Solid Films* **2010**, *518* (21), 6123–6129.

(397) Taguchi, D.; Manaka, T.; Iwamoto, M.; Bazaka, K.; Jacob, M. V. Analyzing Hysteresis Behavior of Capacitance–Voltage Characteristics of Izo/C60/Pentacene/Au Diodes with a Hole-Transport Electron-Blocking Polyterpenol Layer by Electric-Field-Induced Optical Second-Harmonic Generation Measurement. *Chem. Phys. Lett.* **2013**, *572*, 150–153.

(398) Jacob, M. V.; Bazaka, K.; Taguchi, D.; Manaka, T.; Iwamoto, M. Electron-Blocking Hole-Transport Polyterpenol Thin Films. *Chem. Phys. Lett.* **2012**, *528*, 26–28.

(399) Bazaka, K.; Jacob, M. V.; Taguchi, D.; Manaka, T.; Iwamoto, M. Investigation of Interfacial Charging and Discharging in Double-Layer Pentacene-Based Metal-Insulator-Metal Device with Polyterpenol Blocking Layer Using Electric Field Induced Second Harmonic Generation. *Chem. Phys. Lett.* **2011**, *503* (1–3), 105–111.



- (400) Taguchi, D.; Manaka, T.; Iwamoto, M.; Anderson, L. J.; Jacob, M. V. Study of Carrier Blocking Property of Poly-Linalyl Acetate Thin Layer by Electric-Field-Induced Optical Second-Harmonic Generation Measurement. *Chem. Phys. Lett.* **2014**, 593, 69–71.
- (401) Ahmad, J.; Bazaka, K.; Anderson, L. J.; White, R. D.; Jacob, M. V. Materials and Methods for Encapsulation of Opv: A Review. *Renewable Sustainable Energy Rev.* **2013**, 27, 104–117.
- (402) Bazaka, K.; Jacob, M. V. Post-Deposition Ageing Reactions of Plasma Derived Polyterpenol Thin Films. *Polym. Degrad. Stab.* **2010**, 95 (6), 1123–1128.
- (403) Bazaka, K.; Jacob, M. V.; Bowden, B. F. Optical and Chemical Properties of Polyterpenol Thin Films Deposited Via Plasma-Enhanced Chemical Vapor Deposition. *J. Mater. Res.* **2011**, 26 (08), 1018–1025.
- (404) Jacob, M. V.; Olsen, N. S.; Anderson, L. J.; Bazaka, K.; Shanks, R. A. Plasma Polymerised Thin Films for Flexible Electronic Applications. *Thin Solid Films* **2013**, 546, 167–170.
- (405) Easton, C. D.; Jacob, M. V.; Shanks, R. A. Fabrication and Characterisation of Polymer Thin-Films Derived from Cineole Using Radio Frequency Plasma Polymerisation. *Polymer* **2009**, 50 (15), 3465–3469.
- (406) Ahmad, J.; Bazaka, K.; Vasilev, K.; Jacob, M. V. Electrical Conduction in Plasma Polymerized Thin Films of  $\gamma$ -Terpinene. *J. Appl. Polym. Sci.* **2015**, 132 (30), 42318.
- (407) Ahmad, J.; Bazaka, K.; Oelgemöller, M.; Jacob, M. Wetting, Solubility and Chemical Characteristics of Plasma-Polymerized 1-Isopropyl-4-Methyl-1,4-Cyclohexadiene Thin Films. *Coatings* **2014**, 4 (3), 527–552.
- (408) Bazaka, K.; Jacob, M. V. Solubility and Surface Interactions of Rf Plasma Polymerized Polyterpenol Thin Films. *Mater. Express* **2012**, 2 (4), 285–293.
- (409) Bazaka, K.; Jacob, M. V. Nanotribological and Nanomechanical Properties of Plasma-Polymerized Polyterpenol Thin Films. *J. Mater. Res.* **2011**, 26 (23), 2952–2961.
- (410) Anderson, L.; Di Girolamo, F.; Barra, M.; Cassinese, A.; Jacob, M. V. Optical Properties of Thermally Evaporated Pdi-8cn2 Thin Films. *Phys. Procedia* **2011**, 14, 29–33.
- (411) Ding, H.; Zhong, M.; Kim, Y. J.; Pholpabu, P.; Balasubramanian, A.; Hui, C. M.; He, H.; Yang, H.; Matyjaszewski, K.; Bettinger, C. J. Biologically Derived Soft Conducting Hydrogels Using Heparin-Doped Polymer Networks. *ACS Nano* **2014**, 8 (5), 4348–4357.
- (412) Glowacki, E. D.; Irimia-Vladu, M. Natural and Nature-Inspired Materials in Organic Electronics. *SPIE Newsroom* **2012**, DOI: 10.1117/2.1201201.004054.
- (413) Hwang, S.-W.; Tao, H.; Kim, D.-H.; Cheng, H.; Song, J.-K.; Rill, E.; Brenckle, M. A.; Panilaitis, B.; Won, S. M.; Kim, Y.-S.; Song, Y. M.; Yu, K. J.; Ameen, A.; Li, R.; Su, Y.; Yang, M.; Kaplan, D. L.; Zakin, M. R.; Slepian, M. J.; Huang, Y.; Omenetto, F. G.; Rogers, J. A. A Physically Transient Form of Silicon Electronics. *Science* **2012**, 337 (6102), 1640–1644.
- (414) Hwang, S.-W.; Kang, S.-K.; Huang, X.; Brenckle, M. A.; Omenetto, F. G.; Rogers, J. A. Materials for Programmed, Functional Transformation in Transient Electronic Systems. *Adv. Mater.* **2015**, 27 (1), 47–52.
- (415) Jia, X.; Yang, Y.; Wang, C.; Zhao, C.; Vijayaraghavan, R.; MacFarlane, D. R.; Forsyth, M.; Wallace, G. G. Biocompatible Ionic Liquid–Biopolymer Electrolyte-Enabled Thin and Compact Magnesium–Air Batteries. *ACS Appl. Mater. Interfaces* **2014**, 6 (23), 21110–21117.
- (416) Zheng, Y. F.; Gu, X. N.; Witte, F. Biodegradable Metals. *Mater. Sci. Eng., R* **2014**, 77, 1–34.
- (417) Kang, S.-K.; Hwang, S.-W.; Cheng, H.; Yu, S.; Kim, B. H.; Kim, J.-H.; Huang, Y.; Rogers, J. A. Dissolution Behaviors and Applications of Silicon Oxides and Nitrides in Transient Electronics. *Adv. Funct. Mater.* **2014**, 24 (28), 4427–4434.
- (418) Kim, Y. J.; Chun, S.-E.; Whitacre, J.; Bettinger, C. J. Self-Deployable Current Sources Fabricated from Edible Materials. *J. Mater. Chem. B* **2013**, 1 (31), 3781–3788.
- (419) Fortner, J. D.; Lyon, D. Y.; Sayes, C. M.; Boyd, A. M.; Falkner, J. C.; Hotze, E. M.; Alemany, L. B.; Tao, Y. J.; Guo, W.; Ausman, K. D.; Colvin, V. L.; Hughes, J. B. C60 in Water: Nanocrystal Formation and Microbial Response. *Environ. Sci. Technol.* **2005**, 39 (11), 4307–4316.
- (420) Fortner, J. D.; Kim, D.-I.; Boyd, A. M.; Falkner, J. C.; Moran, S.; Colvin, V. L.; Hughes, J. B.; Kim, J.-H. Reaction of Water-Stable C60 Aggregates with Ozone. *Environ. Sci. Technol.* **2007**, 41 (21), 7497–7502.
- (421) Wu, J.; Goodwin, D. G.; Peter, K.; Benoit, D.; Li, W.; Fairbrother, D. H.; Fortner, J. D. Photo-Oxidation of Hydrogenated Fullerene (Fullerane) in Water. *Environ. Sci. Technol. Lett.* **2014**, 1 (12), 490–494.
- (422) Schreiner, K. M.; Filley, T. R.; Blanchette, R. A.; Bowen, B. B.; Bolskar, R. D.; Hockaday, W. C.; Masiello, C. A.; Raebiger, J. W. White-Rot Basidiomycete-Mediated Decomposition of C60 Fullerol. *Environ. Sci. Technol.* **2009**, 43 (9), 3162–3168.
- (423) Pérez, S.; Farré, M. I.; Barceló, D. Analysis, Behavior and Ecotoxicity of Carbon-Based Nanomaterials in the Aquatic Environment. *TrAC, Trends Anal. Chem.* **2009**, 28 (6), 820–832.
- (424) Blanchette, R. A. Delignification by Wood-Decay Fungi. *Annu. Rev. Phytopathol.* **1991**, 29 (1), 381–403.
- (425) da Silva, M.; Cerniglia, C.; Pothuluri, J.; Canhos, V.; Esposito, E. Screening Filamentous Fungi Isolated from Estuarine Sediments for the Ability to Oxidize Polycyclic Aromatic Hydrocarbons. *World J. Microbiol. Biotechnol.* **2003**, 19 (4), 399–405.
- (426) Dean-Ross, D.; Moody, J.; Cerniglia, C. E. Utilization of Mixtures of Polycyclic Aromatic Hydrocarbons by Bacteria Isolated from Contaminated Sediment. *FEMS Microbiol. Ecol.* **2002**, 41 (1), 1–7.
- (427) Tuor, U.; Winterhalter, K.; Fiechter, A. Enzymes of White-Rot Fungi Involved in Lignin Degradation and Ecological Determinants for Wood Decay. *J. Biotechnol.* **1995**, 41 (1), 1–17.
- (428) Leonowicz, A.; Cho, N.; Luterek, J.; Wilkolazka, A.; Wojtas-Wasilewska, M.; Matuszewska, A.; Hofrichter, M.; Wesenberg, D.; Rogalski, J. Fungal Laccase: Properties and Activity on Lignin. *J. Basic Microbiol.* **2001**, 41 (3–4), 185–227.
- (429) Sayes, C. M.; Fortner, J. D.; Guo, W.; Lyon, D.; Boyd, A. M.; Ausman, K. D.; Tao, Y. J.; Sitharaman, B.; Wilson, L. J.; Hughes, J. B.; West, J. L.; Colvin, V. L. The Differential Cytotoxicity of Water-Soluble Fullerenes. *Nano Lett.* **2004**, 4 (10), 1881–1887.
- (430) Oh, W.-K.; Kim, S.; Yoon, H.; Jang, J. Shape-Dependent Cytotoxicity and Proinflammatory Response of Poly(3,4-Ethyleneedioxythiophene) Nanomaterials. *Small* **2010**, 6 (7), 872–879.
- (431) Rothen-Rutishauser, B.; Brown, D. M.; Pfaller-Boyles, M.; Kinloch, I. A.; Windle, A. H.; Gehr, P.; Stone, V. Relating the Physicochemical Characteristics and Dispersion of Multiwalled Carbon Nanotubes in Different Suspension Media to Their Oxidative Reactivity in Vitro and Inflammation in Vivo. *Nanotoxicology* **2010**, 4 (3), 331–342.
- (432) Bianco, A.; Kostarelos, K.; Prato, M. Making Carbon Nanotubes Biocompatible and Biodegradable. *Chem. Commun.* **2011**, 47 (37), 10182–10188.
- (433) Sayes, C. M.; Liang, F.; Hudson, J. L.; Mendez, J.; Guo, W.; Beach, J. M.; Moore, V. C.; Doyle, C. D.; West, J. L.; Billups, W. E.; Ausman, K. D.; Colvin, V. L. Functionalization Density Dependence of Single-Walled Carbon Nanotubes Cytotoxicity in Vitro. *Toxicol. Lett.* **2006**, 161 (2), 135–142.
- (434) Lacerda, L.; Ali-Boucetta, H.; Herrero, M. A.; Pastorin, G.; Bianco, A.; Prato, M.; Kostarelos, K. Tissue Histology and Physiology Following Intravenous Administration of Different Types of Functionalized Multiwalled Carbon Nanotubes. *Nanomedicine* **2008**, 3 (2), 149–161.
- (435) Battigelli, A.; Ménard-Moyon, C.; Da Ros, T.; Prato, M.; Bianco, A. Endowing Carbon Nanotubes with Biological and Biomedical Properties by Chemical Modifications. *Adv. Drug Delivery Rev.* **2013**, 65 (15), 1899–1920.
- (436) Sato, Y.; Yokoyama, A.; Nodasaka, Y.; Kohgo, T.; Motomiya, K.; Matsumoto, H.; Nakazawa, E.; Numata, T.; Zhang, M.; Yudasaka,

- M.; Hara, H.; Araki, R.; Tsukamoto, O.; Saito, H.; Kamino, T.; Watari, F.; Tohji, K. Long-Term Biopersistence of Tangled Oxidized Carbon Nanotubes inside and Outside Macrophages in Rat Subcutaneous Tissue. *Sci. Rep.* **2013**, *3*, 2516.
- (437) Nunes, A.; Bussy, C.; Gherardini, L.; Meneghetti, M.; Herrero, M. A.; Bianco, A.; Prato, M.; Pizzorusso, T.; Al-Jamal, K. T.; Kostarelos, K. In Vivo Degradation of Functionalized Carbon Nanotubes after Stereotactic Administration in the Brain Cortex. *Nanomedicine* **2012**, *7* (10), 1485–1494.
- (438) Liu, X.; Hurt, R. H.; Kane, A. B. Biodurability of Single-Walled Carbon Nanotubes Depends on Surface Functionalization. *Carbon* **2010**, *48* (7), 1961–1969.
- (439) Girish, C. M.; Sasidharan, A.; Gowd, G. S.; Nair, S.; Koyakutty, M. Confocal Raman Imaging Study Showing Macrophage Mediated Biodegradation of Graphene in Vivo. *Adv. Healthcare Mater.* **2013**, *2* (11), 1489–1500.
- (440) Peet, J.; Heeger, A. J.; Bazan, G. C. Plastic Solar Cells: Self-Assembly of Bulk Heterojunction Nanomaterials by Spontaneous Phase Separation. *Acc. Chem. Res.* **2009**, *42* (11), 1700–1708.
- (441) Peet, J.; Kim, J. Y.; Coates, N. E.; Ma, W. L.; Moses, D.; Heeger, A. J.; Bazan, G. C. Efficiency Enhancement in Low-Bandgap Polymer Solar Cells by Processing with Alkane Dithiols. *Nat. Mater.* **2007**, *6* (7), 497–500.
- (442) Graham, K. R.; Mei, J.; Stalder, R.; Shim, J. W.; Cheun, H.; Steffy, F.; So, F.; Kippelen, B.; Reynolds, J. R. Polydimethylsiloxane as a Macromolecular Additive for Enhanced Performance of Molecular Bulk Heterojunction Organic Solar Cells. *ACS Appl. Mater. Interfaces* **2011**, *3* (4), 1210–1215.
- (443) Andrievsky, G.; Klochov, V.; Derevyanchenko, L. Is the C60 Fullerene Molecule Toxic? *Fullerenes, Nanotubes, Carbon Nanostruct.* **2005**, *13* (4), 363–376.
- (444) Adón, F. T.; Kapralov, A. A.; Yanamala, N.; Feng, W.; Baygan, A.; Chambers, B. J.; Hultenby, K.; Ye, F.; Toprak, M. S.; Brandner, B. D.; Fornara, A.; Klein-Seetharaman, J.; Kotchey, G. P.; Star, A.; Shvedova, A. A.; Fadeel, B.; Kagan, V. E. Biodegradation of Single-Walled Carbon Nanotubes by Eosinophil Peroxidase. *Small* **2013**, *9* (16), 2721–2729.
- (445) Kotchey, G. P.; Hasan, S. A.; Kapralov, A. A.; Ha, S. H.; Kim, K.; Shvedova, A. A.; Kagan, V. E.; Star, A. A Natural Vanishing Act: The Enzyme-Catalyzed Degradation of Carbon Nanomaterials. *Acc. Chem. Res.* **2012**, *45* (10), 1770–1781.
- (446) Kotchey, G. P.; Gaugler, J. A.; Kapralov, A. A.; Kagan, V. E.; Star, A. Effect of Antioxidants on Enzyme-Catalyzed Biodegradation of Carbon Nanotubes. *J. Mater. Chem. B* **2013**, *1* (3), 302–309.
- (447) Davies, M. J.; Hawkins, C. L.; Pattison, D. I.; Rees, M. D. Mammalian Heme Peroxidases: From Molecular Mechanisms to Health Implications. *Antioxid. Redox Signaling* **2008**, *10* (7), 1199–1234.
- (448) Kagan, V. E.; Konduru, N. V.; Feng, W.; Allen, B. L.; Conroy, J.; Volkov, Y.; Vlasova, I. I.; Belikova, N. A.; Yanamala, N.; Kapralov, A.; Tyurina, Y. Y.; Shi, J.; Kisin, E. R.; Murray, A. R.; Franks, J.; Stolz, D.; Gou, P.; Klein-Seetharaman, J.; Fadeel, B.; Star, A.; Shvedova, A. A. Carbon Nanotubes Degraded by Neutrophil Myeloperoxidase Induce Less Pulmonary Inflammation. *Nat. Nanotechnol.* **2010**, *5* (5), 354–359.
- (449) Allen, B. L.; Kichambare, P. D.; Gou, P.; Vlasova, I. I.; Kapralov, A. A.; Konduru, N.; Kagan, V. E.; Star, A. Biodegradation of Single-Walled Carbon Nanotubes through Enzymatic Catalysis. *Nano Lett.* **2008**, *8* (11), 3899–3903.
- (450) Vlasova, I. I.; Vakhrusheva, T. V.; Sokolov, A. V.; Kostevich, V. A.; Gusev, A. A.; Gusev, S. A.; Melnikova, V. I.; Lobach, A. S. Pegylated Single-Walled Carbon Nanotubes Activate Neutrophils to Increase Production of Hypochlorous Acid, the Oxidant Capable of Degrading Nanotubes. *Toxicol. Appl. Pharmacol.* **2012**, *264* (1), 131–142.
- (451) Allen, B. L.; Kotchey, G. P.; Chen, Y.; Yanamala, N. V. K.; Klein-Seetharaman, J.; Kagan, V. E.; Star, A. Mechanistic Investigations of Horseradish Peroxidase-Catalyzed Degradation of Single-Walled Carbon Nanotubes. *J. Am. Chem. Soc.* **2009**, *131* (47), 17194–17205.
- (452) Russier, J.; Menard-Moyon, C.; Venturelli, E.; Gravel, E.; Marcolongo, G.; Meneghetti, M.; Doris, E.; Bianco, A. Oxidative Biodegradation of Single- and Multi-Walled Carbon Nanotubes. *Nanoscale* **2011**, *3* (3), 893–896.
- (453) Hernandez, H. L.; Kang, S.-K.; Lee, O. P.; Hwang, S.-W.; Kaitz, J. A.; Inci, B.; Park, C. W.; Chung, S.; Sottos, N. R.; Moore, J. S.; Rogers, J. A.; White, S. R. Triggered Transience of Metastable Poly(Phthalaldehyde) for Transient Electronics. *Adv. Mater.* **2014**, *26* (45), 7637–7642.
- (454) Kotchey, G. P.; Zhao, Y.; Kagan, V. E.; Star, A. Peroxidase-Mediated Biodegradation of Carbon Nanotubes in Vitro and in Vivo. *Adv. Drug Delivery Rev.* **2013**, *65* (15), 1921–1932.
- (455) Kotchey, G. P.; Allen, B. L.; Vedala, H.; Yanamala, N.; Kapralov, A. A.; Tyurina, Y. Y.; Klein-Seetharaman, J.; Kagan, V. E.; Star, A. The Enzymatic Oxidation of Graphene Oxide. *ACS Nano* **2011**, *5* (3), 2098–2108.
- (456) Penetrante, B. M.; Brusasco, R. M.; Merritt, B. T.; Vogtlin, G. E. Environmental Applications of Low-Temperature Plasmas. *Pure Appl. Chem.* **1999**, *71* (10), 1829–1835.
- (457) Pekárek, S.; Pospíšil, M.; Krýsa, J. Non-Thermal Plasma and TiO<sub>2</sub>-Assisted N-Heptane Decomposition. *Plasma Processes Polym.* **2006**, *3* (3), 308–315.
- (458) Nasonova, A.; Pham, H. C.; Kim, D.-J.; Kim, K.-S. No and So<sub>2</sub> Removal in Non-Thermal Plasma Reactor Packed with Glass Beads-TiO<sub>2</sub> Thin Film Coated by Pcvd Process. *Chem. Eng. J.* **2010**, *156* (3), 557–561.
- (459) Allwood, J. M.; Ashby, M. F.; Gutowski, T. G.; Worrell, E. Material Efficiency: A White Paper. *Resources, Conservation and Recycling* **2011**, *55* (3), 362–381.
- (460) Marwede, M.; Reller, A. Estimation of Life Cycle Material Costs of Cadmium Telluride- and Copper Indium Gallium Diselenide-Photovoltaic Absorber Materials Based on Life Cycle Material Flows. *J. Ind. Ecol.* **2014**, *18* (2), 254–267.
- (461) Candelise, C.; Winkler, M.; Gross, R. Implications for Cdte and Cigs Technologies Production Costs of Indium and Tellurium Scarcity. *Prog. Photovoltaics* **2012**, *20* (6), 816–831.
- (462) Peiró, L. T.; Méndez, G. V.; Ayres, R. U. Material Flow Analysis of Scarce Metals: Sources, Functions, End-Uses and Aspects for Future Supply. *Environ. Sci. Technol.* **2013**, *47* (6), 2939–2947.
- (463) Woodhouse, M.; Goodrich, A.; Margolis, R.; James, T. L.; Lokanc, M.; Eggert, R. Supply-Chain Dynamics of Tellurium, Indium, and Gallium within the Context of Pv Manufacturing Costs. *Photovoltaics, IEEE Journal of* **2013**, *3* (2), 833–837.
- (464) Barba-Gutiérrez, Y.; Adenso-Díaz, B.; Hopp, M. An Analysis of Some Environmental Consequences of European Electrical and Electronic Waste Regulation. *Resources, Conservation and Recycling* **2008**, *52* (3), 481–495.
- (465) Stone, R. Confronting a Toxic Blowback from the Electronics Trade. *Science* **2009**, *325* (5944), 1055.
- (466) Lai, K.-h.; Wong, C. W. Y.; Venus Lun, Y. H. The Role of Customer Integration in Extended Producer Responsibility: A Study of Chinese Export Manufacturers. *Int. J. Prod. Econ.* **2014**, *147B*, 284–293.
- (467) Lu, C.; Zhang, L.; Zhong, Y.; Ren, W.; Tobias, M.; Mu, Z.; Ma, Z.; Geng, Y.; Xue, B. An Overview of E-Waste Management in China. *J. Mater. Cycles Waste Manage.* **2015**, *17*, 1–12.